Role of peroxisomes in granulosa cells, follicular development and steroidogenesis in the mouse ovary

Inaugural Dissertation

submitted to the

Faculty of Medicine

in partial fulfillment of the requirements

for the PhD-Degree

of the Faculties of Veterinary Medicine and Medicine

of the Justus Liebig University Giessen

by

Wang, Shan

of

ChengDu, China

Gießen (2017)

From the Institute for Anatomy and Cell Biology,

Division of Medical Cell Biology

Director/Chairperson: Prof. Dr. Eveline Baumgart-Vogt

Faculty of Medicine of Justus Liebig University Giessen

First Supervisor: Prof. Dr. Eveline Baumgart-Vogt

Second Supervisor: Prof. Dr. Christiane Herden

Declaration

“I declare that I have completed this dissertation single-handedly without the unauthorized help of a second party and only with the assistance acknowledged therein. I have appropriately acknowledged and referenced all text passages that are derived literally from or are based on the content of published or unpublished work of others, and all information that relates to verbal communications. I have abided by the principles of good scientific conduct laid down in the charter of the Justus Liebig University of Giessen in carrying out the investigations described in the dissertation.”

Shan, Wang

November 27th 2017

Giessen,Germany

Table of Contents

1 Introduction

1.1 Peroxisomal morphology, biogenesis, and metabolic function

1.1.1 Morphology of peroxisomes

Peroxisomes are ubiquitous cell organelles, which participate in many important metabolic functions in different organisms and are widely distributed in variety of tissues and organs. They contain enzymes that are involved in oxidative metabolic reactions and lipid metabolism, but their size, number, proteome and metabolic function vary in different cell types.

Peroxisomes were first discovered in the 1950s by Rhodin as spherical structures with a diameter of 0.3-1.0 µm using routine transmission electron microscopy [2]. Morphological studies of the mouse kidney by Rhodin revealed that peroxisomes contain a fine granular matrix and are surrounded by a single membrane. Peroxisomes were first named 'microbodies' and only later in 1966, acquired the name peroxisomes when Christian de Duve and Pierre Baudhuin demonstrated that this organelle could produce and degrade hydrogen peroxide (H_2O_2) [3]. They also showed that in rat hepatocytes, peroxisomes typically contain a crystalloid core consisting of xanthine oxidase and urate oxidase, which is absent in humans [4-6].

In 1973, scientists discovered that the cells isolated from patients suffering from Zellweger syndrome lacked peroxisomes [7]. In spite of this, the significance of peroxisomes as important organelles involved in many biochemical reactions was not elucidated until the mid-1980s. For the past two decades, scientists have been intensively studying peroxisomes with the goal to understand its function in the context of human metabolism. Studies are underway on the analysis of inherited peroxisomal diseases such as Zellweger's syndrome, adrenoleukodystrophy, rhizomelic chondrodysplasia punctate, and Refsum disease as well as the analysis of peroxisomal deficiency in model organisms and cell culture researchers were producing increasing evidence relating peroxisomal deficiency with different diseases such as metabolic syndrome, diabetes or neurodegeneration due to their central role in lipid metabolism and oxidative stress management [8-10].

1.1.2 Biogenesis of peroxisomes

1.1.2.1 Peroxins

Conceptually, the biogenesis of peroxisomes takes place in three steps: (1) Formation of the peroxisomal membrane; (2) Import of peroxisomal matrix proteins; (3) Peroxisome fission and proliferation. For peroxisome biogenesis, inheritance and proliferation different proteins belonging to the peroxin family are required. Nowadays more than 30 PEX genes numbered according to their date of discovery have been identified by genetic and biochemical methods [11, 12].

Peroxins can be divided into different groups according to their functions in peroxisomal biosynthesis. For example, PEX3, PEX16 and PEX19 are involved in peroxisome membrane formation; PEX5, PEX7 are involved in matrix protein import, PEX13, PEX14, PEX17 serves as docking complex for the import of peroxisomal matrix proteins [11-13].

1.1.2.2 The origin of peroxisomes

Two hypotheses concerning the origin of the organelle have been proposed and controversially debated. The first one suggests peroxisomes arise by growth and division from pre-existing peroxisomes by posttranslational import of additional membrane and matrix proteins [14]. This hypothesis has been further supported by both *in vivo* and *in vitro* studies (Figure 1) [15-18]. Recently, this model has been challenged by many researchers suggesting that peroxisomes might arise *de novo*. In this case, peroxisomes have been suggested to arise from the endoplasmic reticulum (ER) or other endomembrane systems in which early peroxisomal biogenesis peroxins such as PEX3p or PEX19p accumulate. From here pre-peroxisomal vesicles bud off and peroxisomal membrane proteins (PMPs) are first integrated with the help of PEX3p or PEX19p, followed by the import of the matrix proteins and maturation of the peroxisomes (Figure 1) [19, 20].

These two-way models might happen simultaneously, but the contribution of each model to the establishment and maintenance of the peroxisome pool is still not fully clarified to date.

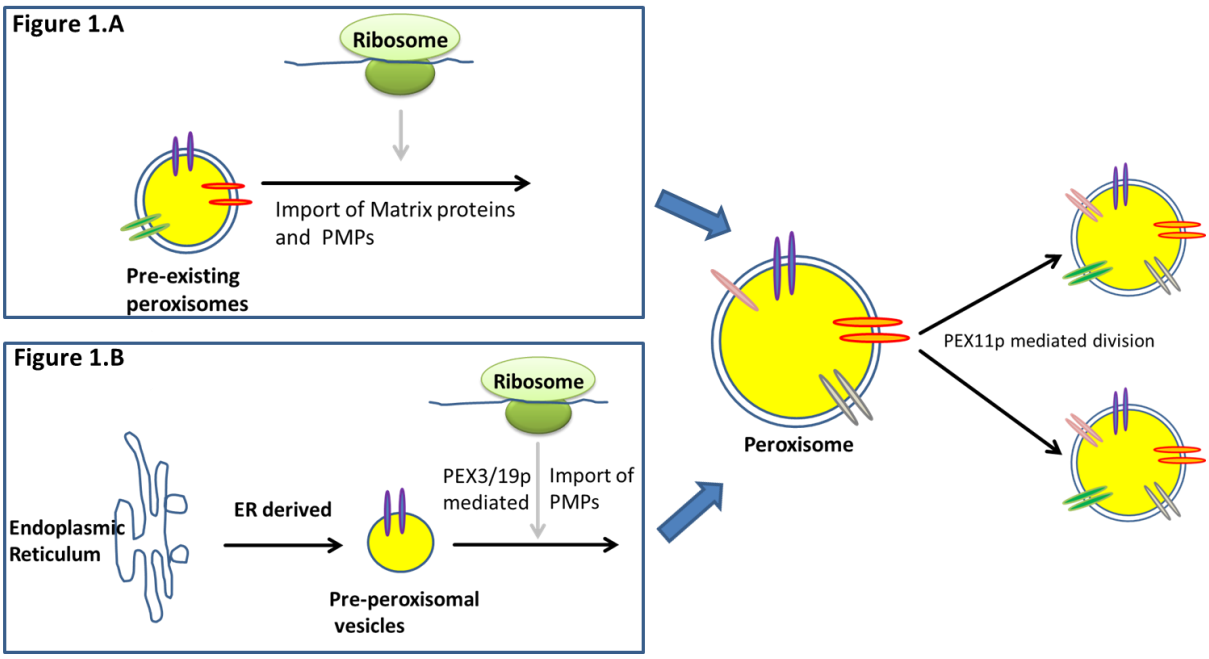

Figure 1. Two-way model for the origin of peroxisomes. Figure 1A. Classic model. New peroxisomes are generated by fusion and fission of mature peroxisomes or preperoxisomes. **Figure 1B. *De novo* model.** Pre-peroxisomal vesicles originate from the endomembrane system such as the ER.

1.1.2.3 Import of peroxisomal membrane proteins

The import of peroxisomal membrane protein follows other routes than the one of matrix proteins. A set of evidences proved that the targeting of most PMPs occurs directly and posttranslationally from the cytosol to the peroxisomes aided by PEX19p [21-24].

According to the review from Eckert and Erdmann in 2003 [19], PMPs are sorted into three groups:

(1) Type I PMPs (e.g., PMP34) are recognized and targeted by PEX19p to a docking site on the peroxisomal membrane where PEX3p is located and aids the insertion of the membrane proteins.

(2) In this case, PEX19p acts as a chaperone for the translocation targeting sequence. Type II PMPs bound to PEX19p form a complex and are then delivered to the peroxisomal membrane under the help of PEX19p. PEX3p may contribute to target this complex to the peroxisomal membrane and then the PMPs can be

released from the complex and inserted [19]. After insertion of the PMPs, PEX19p is recycled back to the cytosol.

(3) The third type of PMPs is proposed to be targeted to peroxisomes completely independent of PEX19p.

1.1.2.4 Import of peroxisomal matrix proteins

Peroxisomal matrix proteins are synthesized on free ribosomes in the cytosol and then post-translationally translocated into the matrix of the organelle [14].

Peroxisomal targeting signals (PTS1 and PTS2) are directing peroxisomal proteins from the cytosol to the peroxisomes. The sequence PTS1 is located at the carboxyl-terminus of proteins while the PTS2 is located at the amino-terminus. PTS1 contains the consensus sequence (S/C/A)(K/R/H)(L/M) and PTS2 has the consensus sequence (R/K)(L/V/I)(X)5(H/Q)(L/A) [25-28]. PEX5p and PEX7p are cytosolic PTS receptors that recognize PTS1 and PTS2 respectively [29-32]. They recognize and bind to their cargo proteins in the cytosol and deliver them to a docking complex on the peroxisome membrane, which then translocate the proteins to the matrix. After the cargo is released, the receptors are shuttled back to the cytosol. Figure 2 depicts the peroxins involved in the translocation of peroxisomal matrix proteins into the organelle.

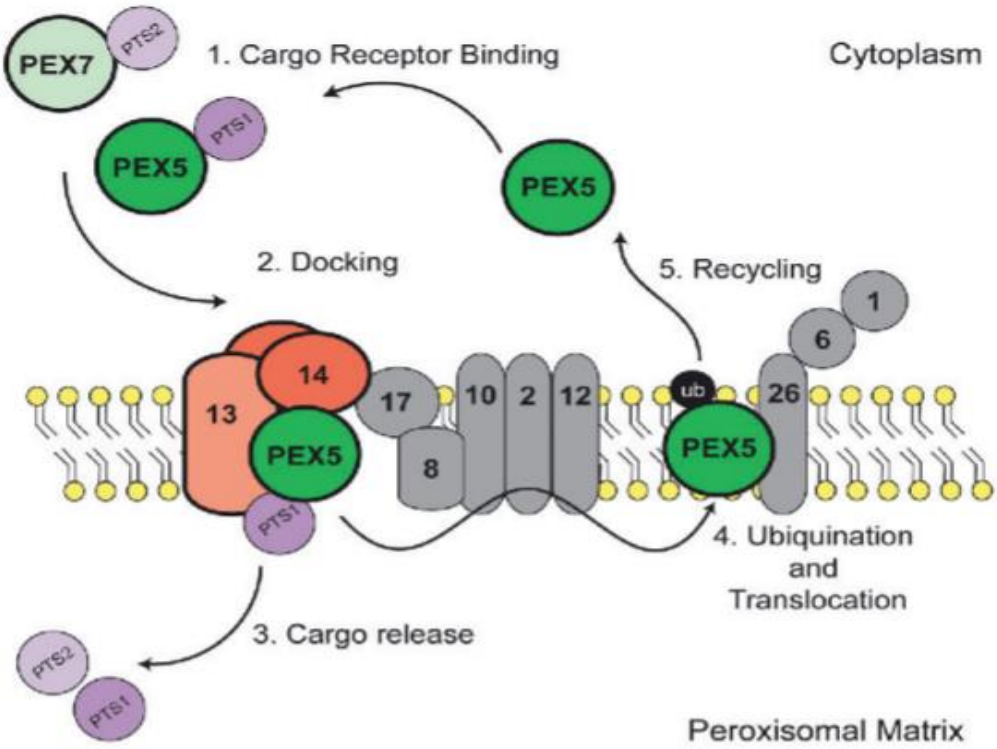

Figure 2. Schematic representation of peroxisomal matrix protein import [33]. The import of peroxisomal matrix proteins can be considered to take place in three steps [34-36]: (1) Step 1. Recognition and Translocation. PEX5p and PEX7p bind to the cargo protein, which contains PTS1 and PTS2 respectively, to form a complex in the cytosol. This complex will be transported to the peroxisomal membrane**.** (2) Step 2. Docking. Three peroxins PEX13p, PEX14p and PEX17p, which are located in the peroxisomal membrane are involved in the docking systems and contain PEX5p and PEX7p docking sites. PEX13p is a transmembrane protein and its N-terminal domain was shown to have the ability for binding PEX7p. Both termini of PEX13p are located in the cytosol and are capable of directing both PTS1 and PTS2 protein import. The C-terminal domain of PEX13p can bind to PEX5p and PEX14p. (3) Step 3. Release. After the receptor-cargo complexes have docked to the peroxisomal membrane, the receptor is released from the cargo and recycled to the cytosol for the next translocation process.

1.1.2.5 Peroxisome proliferation

Plenty of genes were investigated and proposed to be involved in peroxisome proliferation, among all the genes and proteins which were investigated, PEX11p as a member of the PEX family are widely accepted to coordinate the peroxisome proliferation and to contribute to control their size and abundance (Figure 1) [37-42].

1.1.3 Peroxisomal metabolic functions

The morphology of peroxisomes and their metabolic functions significantly vary among different tissues and species [43]. They usually participate in lipid metabolism, reactive oxygen species (ROS) metabolism, biosynthesis of ether phospholipids

(plasmalogens), cholesterol and bile acids. Furthermore, they are involved in amino acid and retinoid metabolism.

1.1.3.1 Peroxisomal fatty acid β-oxidation

Through β-oxidation, peroxisomes can degrade many kinds of fatty acids, some of which is unable to be degraded in mitochondria. These include long-chain and very-long-chain fatty acyl-coenzyme (CoAs), 2-methyl-branched fatty acyl-CoAs, long-chain dicarboxylyl-CoAs and the CoA esters of the bile acid intermediates di- and trihydroxycoprostanoic acids. A large amount of H_2O_2 is generated during the degradation process of these fatty acids [44, 45].

Fatty acids must be activated to their CoA derivatives before they can be β-oxidized by peroxisomes or mitochondria. Long chain and very long chain fatty acids are activated by long-chain and very-long-chain acyl-CoA synthetases separately [46], long-chain acyl-CoA synthetases can also activate isoprenoid-derived branched-chain fatty acids [47]. These two enzymes are located on the peroxisome membrane [46].

Dicarboxylic acids, prostaglandins, and the C27 bile acid intermediates are activated in the ER [48, 49]. The import of fatty acids into the peroxisomal membrane is catalyzed by peroxisomal ATP-binding cassette transporters (ABCD). The ABCD protein family contains a transmembrane domain and a conserved ATP binding site. To date, four ABCD proteins have been described in mammals: the adrenoleukodystrophy protein (ALDP) / (ABCD1), the adrenoleukodystrophy-related protein (ALDRP) / (ABCD2), the peroxisomal membrane protein (PMP70) / (ABCD3) and the PMP70-related protein (P70R) / (ABCD4) [50-53].

After that, peroxisomal fatty acid β-oxidation takes place in four steps: (1) Oxidation. Acyl-CoA is first desaturated to 2-trans-enoyl-CoA. (2) Hydration. In this step enoyl-CoA is converted to 3-hydroxyacyl-CoA. (3) Dehydrogenation. The hydroxyacyl intermediate is dehydrogenated to a 3-ketoacyl-CoA. (4) Thiolytic cleavage. An acetyl-CoA will be released together with an acyl-CoA, which is two carbon atoms shorter than the original acyl-CoA and then enter the next round of β-oxidation [44, 45, 54]. The detailed peroxisomal fatty acid β-oxidation process is described as follows:

- **First Step: Oxidation, catalyzed by Acyl-CoA oxidases (ACOX enzyme)**

During the first reaction of peroxisomal β-oxidation, three different types of ACOX genes (ACOX1, ACOX2 and ACOX3) were described in mammals with different substrates. VLCFA is degraded by Palmitoyl-CoA oxidase (ACOX1) specifically. In humans, ACOX2 participates in the degradation of branched fatty acids, pristanic acid and bile acid intermediates [55]. In rodents, bile acid intermediates are catalyzed by trihydroxycoprostanoyl-CoA oxidase (ACOX2) and branched-chain fatty acids are catalyzed by pristanoyl-CoA oxidase (ACOX3) respectively [48, 56, 57]. During this process, H_2O_2 is generated by donating electrons directly to molecular oxygen under catalysis by FAD-containing oxidases [45, 54].

- **Second and third step: Hydration and dehydrogenation, catalyzed by two different multifunctional proteins (MFPs)**

The first oxidation step is followed by the hydration of the enoyl-CoAs to 3-hydroxyacyl-CoAs, which is then dehydrogenated to generate 3-ketoacyl-CoAs [44, 45, 48, 54]. A protein called multifunctional protein (MFPs) contains both enoyl-CoA hydratase and 3 hydroxyacyl-CoA dehydrogenase activities and catalyzes both hydration and dehydrogenation [45, 58, 59]. There are two types of MFPs: MFP1 and MFP2. Substrates for MFP2 include bile acid intermediates and pristanic acid, which contain the 2-methyl branch in the carbon chain. Substrates with a straight carbon chain can be degraded by either MFP1 or MFP2 [60].

- **Last step: Thiolytic cleavage, catalyzed by thiolase and sterol carrier proteins (SCPx)**

During the last step, 3-ketoacyl-CoAs are cleaved into chain-shortened acyl-CoAs and acetyl-CoA or propionyl-CoA [45, 48, 61, 62] by 3-ketoacyl-CoA thiolase and the SCPx as recently discovered. Thiolase contributes to the classic straight-chain β-oxidation spiral, while SCPx is involved in the non-inducible branched-chain β-oxidation system [45, 61-63]. SCPx is a recently discovered protein, its N-terminal domain has 3-ketoacyl-CoA thiolase activity while its C-terminal domain, functions as a lipid carrier or transfer protein [45]. Compared with thiolase, SCPx has much broader substrate spectrum degrading not only branched-chain fatty acids and bile acid intermediates, but also 3-ketoacyl-CoAs of straight-chain fatty acids [45, 48, 53].

1.1.3.2 Peroxisomes and ether phospholipid synthesis

The etherphospholipid biosynthesis takes place in three steps: the first two steps occur inside the peroxisomes and the last step is present in both peroxisomes and ER [64, 65]. The first step is catalyzed by glycerone phosphate acyl transferase (GNPAT). This enzyme is involved in the conversion from glycerone phosphate to acyl-glycerone phosphate (acyl-GNP). The formed acyl-GNP will be then converted to alkyl-glycerone phosphate (alkyl-GNP) by alkylglycerone phosphate synthase (AGPS) [65]. The last step of ether phospholipid synthesis is catalyzed by the enzyme alkyl/acyl-GNP NAD(P)H oxidoreductase to produce alkylglycerol-3-phosphate (alkyl-G-3P), which is then transported to ER to for plasmalogen synthesis [66]. Patients who lack either GNPAT or AGPs have display a deficiency in ether phospholipid synthesis and possess a therefore reduced plasmalogen content [66]. Plasmalogens are important ether phospholipids that play a role not only in cells membrane dynamics but also in ROS trapping to protect the cells against the damage resulted from lipid peroxidation [66, 67].

1.1.3.3 Peroxisome and cholesterol synthesis

The rate-limiting step for cholesterol synthesis is catalyzed by 3-hydroxy-3-methylglutaryl coenzyme A (HMG-CoA) reductase. Firstly, it was believed that HMG-CoA is solely expressed in the ER but later this enzyme was discovered also in peroxisomes [68]. Further experiments provided more evidences that the peroxisomes is associated with cholesterol biosynthesis [69]. Accumulating evidence has shown that all of the enzymes required for the generation of farnesyl diphosphate (FPP) from acetyl-CoA are localized in peroxisomes [70]. For instance, enzymes like isopentenyl diphosphate delta isomerase (IDI1), mevalonate kinase (MVK), phosphomevalonate kinase (PMVK) and mevalonate pyrophosphate decarboxylase (MPD), which convert mevalonate to farnesyl diphosphate (FPP) are all located inside the peroxisomal matrix [70, 71]. Moreover, Kovacs *et al* proved that peroxisomes contribute to the maintenance of the homeostasis of cholesterol [72].

1.1.3.4 Peroxisome and oxidative stress

Peroxisomes were first proposed to participate in the metabolism of oxygen metabolites after discovering catalase and H_2O_2-generating oxidases inside their matrix [3, 73-75]. In the past decade, peroxisomes have been proven to be a major source of ROS and at the same time a major site for degradation of ROS [76].

Reactive oxygen species (ROS) include several radical species, e.g., the hydroxyl radical ($^{\cdot}OH$) or the superoxide anion ($O2^{\cdot-}$). The hydroxyl radical ($^{\cdot}OH$) is reported to be the most highly reactive and toxic form of oxygen. Hydrogen peroxide (H_2O_2) despite it does not possess unpaired electrons is also considered as ROS. Besides ROS, Reactive nitrogen species (RNS) have similar effects on cells and it includes radical species such as primary nitric oxide ($^{\cdot}NO$).

A significant increase in the intracellular concentration of ROS and RNS will lead to oxidative stress. ROS and RNS exert a particularly toxic effect on DNA, proteins, and lipids, which can induce the accumulation of oxidative damage in distinct cellular locations, redox-sensitive signaling pathways and metabolic reactions. However, in addition to their detrimental effects, ROS and RNS play a mediator role in a variety of important cellular processes and cell signaling pathways, such as their pivotal role in apoptosis [77, 78].

Catalase is the classical marker enzyme of peroxisomes that degrades not only H_2O_2 but at the same time metabolites also a large variety of substrates such as methanol, ethanol, phenol and nitrites due to its peroxidatic activity [79]. This enzyme is targeted to peroxisomes via a modified PTS1 [80]. It is the main detoxifying enzyme that prevents an accumulation of H_2O_2 in peroxisomes [81]. The inhibition of catalase activity in rat liver suppressed peroxisomal β-oxidation activity [82] while the overexpression of catalase in transgenic mice led to an extension of their life span [83]. In tumors of liver and other organs, the amount of catalase was found significantly reduced [84, 85]. Under some pathological conditions such as ischemia–reperfusion injury, catalase activity was also reported to be decreased [86]. In addition to catalase, peroxisomes harbor a variety of other defense mechanisms and antioxidant enzymes to against ROS. Peroxiredoxin I and V, SOD1, epoxide hydrolase and glutathione S-transferase are all able to degrade ROS [76, 87].

1.2 Peroxisome biogenesis disorder

1.2.1 Peroxisome related human disease

Peroxisomes are crucial to normal cellular function and therefore peroxisomal deficiency leads to serious biochemical abnormalities resulting in various clinical symptoms and even death. Until now, twenty five peroxisomal disorders have been described, which can be categorized into two types: (1) peroxisome biogenesis disorder (PBD); (2) single peroxisomal metabolic enzymes related disorder [88]. As mentioned in the sections above, peroxin (Pex) genes are responsible for peroxisomal membrane protein and matrix protein biogenesis. Mutations in any of these genes can lead to PBDs [9, 11]. According to the clinical manifestations, PBDs were divided into two groups: (a) the Zellweger spectrum disorders, (b) rhizomelic chondrodysplasia punctate (RCDP) [70]. The Zellweger spectrum includes the severe Zellweger cerebro-hepato-renal syndrome (ZS), the less severe phenotypes neonatal adrenoleukodystrophy (NALD), and infantile Refsum disease (IRD) [9, 89]. Table 1 lists known peroxisomal disorders [70]. The most famous and severe disease caused by peroxisomal deficiency, called Zellweger syndrome (ZS), manifests itself with severe hypotonia of the body, embryological malformations in the central nervous system and in the kidney as well as adrenal deficiency caused by adrenal cortex degeneration. Children who suffer from ZS usually cannot survive more than one year after birth. Until now, no effective clinical treatment has been available [9, 65, 89-92]. Compared with ZS, NALD and IRD patients display less severe clinical phenotypes. Patients with NALD can survive more than ten years and many IRD patients are expected to survive up to their third decade [93]. RCDP patients usually demonstrate skeletal abnormalities, and the reason for RCDP is either mutations of enzymes involved in plasmalogen biosynthesis or PTS-2-specific protein import problems [91, 93]. The variety of clinical symptoms caused by peroxisomal disorder is summarized in Table 2 [70].

Table 1. Peroxisomal disorders. Modified from Kovacs *et.al* [70].

Peroxisome biogenesis disorders	Single peroxisomal enzyme deficiencies
Zellweger spectrum disorders:	Adrenoleukodystrophya/Adrenomyeloneuropathy
Zellweger syndrome (ZS)	Acyl-CoA oxidase deficiency
Neonatal adrenoleukodystrophy (NALD)	3-Ketoacyl-CoA thiolase deficiency
Infantile Refsum disease (IRD)	D-Bifunctional enzyme deficiency
Rhizomelic chondrodysplasia punctata (RCDP)	Classical adult Refsum disease
Hyperpipecolic acidemia	Dihydroxyacetonephosphate (DHAP) deficiency
	acyltransferase deficiency
	Alkyl-GNP synthase deficiency
	Mevalonate kinase deficiency
	a-Methylacyl-CoA racemase deficiency
	Acatalasemia
	Glutaric aciduria type III
	Hyperoxaluria type I

Table 2. Features of disorders of peroxisome assembly. Modified from Kovacs *et.al* [70].

Biochemical abnormalities
Accumulation of very long chain fatty acids (VLCFA)
Accumulation of phytanic acid, pristanic acid and pipecolic acid
Depletion of plasmalogens
Accumulation of abnormal bile acids
Accumulation of bioactive compounds like eicosanoids, retinoids
Depletion of docosahexaenoic acid (DHA)
Hypocholesterolemia

Clinical Features
Dysmorphic features: high forehead, large fontanelles, epicanthus, hypertelorism, low nasal ridge, abnormal ears
Hypoplastic supraorbital ridges
Hypotonia
Hepatomegaly
Renal cysts
Retinopathy
Cataracts
Impaired hearing
Chondrodysplasia punctata
Psychomotor delay
Neonatal seizures

Neurological abnormalities
Abnormal neuronal migration: Neocortex Cerebral hemispheres Cerebellum Inferior olivary complex
Abnormal Purkinje cells
dendritic arborization
Abnormal white matter: Demyelination Hypomyelination Dysmyelination
Postdevelopmental
Neuronal degeneration
Microgyration

1.2.2 Mouse model with peroxisomal deficiency

In order to investigate the pathological consequences and the mechanisms for PBDs, scientists established *Pex* gene knock-out animal models. *Pex5* [94] and *Pex*2 [95] knock-out models were first created in 1997 by different groups. Both *Pex2* and *Pex5* knock-out mice have incomplete peroxisomal structures and exhibit biochemical abnormalities and pathological defects of ZS patients [94, 95]. Moreover, *Pex11β* [96] and the *Pex13* [97] gene knock-out mouse models were also established and exhibited organ abnormalities of typical ZS, including intrauterine growth retardation, hypotonia and neonatal lethality. A *Pex13* knock-out mouse model was generated by the deletion of exon2 in embryonic stem cells (ES) via the Cre/LoxP system. These animal models provide new prospects to study the pathogenesis of organ

malformations, and dysfunctions related to peroxisome dysfunction and improve the search for new therapeutic strategies.

1.2.3 Peroxisomal disorders and human fertility

Zellweger syndrome patients exhibiting either cryptorchism in boys or clitoromegaly in girls suggest a problem in the development of genital organs and dysfunction in regulation of the androgen-estrogen balance. Peroxisomal metabolism is essential for normal functions of steroid synthesizing organs and peroxisomal biogenesis defects can lead to adreno cortical insufficiency and spermatogenesis defects or even complete testicular degeneration [98]. Patients with peroxisomal single enzyme deficiencies, such as X-linked adrenoleukodystrophy (X-ALD) or adrenomyeloneuropathy (a milder phenotype of X-ALD) exhibit an adreno-testiculo-leukomyelo-neuropathic complex of symptoms [98, 99].

Several mouse models for peroxisomal knock-out proteins show the critical role of this organelle in male reproductive health. For example, a GNPAT knock-out mouse exhibited atrophic testis and arrest of spermatogenesis [100]. The ACOX1-deficient mice exhibited reduced amount of spermatids and Leydig cells [101]. Moreover, Huyghe and colleagues have shown that MFP2 knock-out mice develop male infertility [102]. The knock-out of MFP2 caused fatty acids accumulation in the seminiferous tubules and sertoli cells, a reduction of elongated spermatids and an incomplete germinal epithelium. In our laboratory, a sertoli cell specific *Pex13* knock-out mouse model was used to investigate peroxisomal functions in the testis [103], exhibiting “Sertoli cell only” syndrome (SCO). Additionally, strong accumulation of neutral lipids and peroxisome-metabolized fatty acids (VLCFA, pristanic and phytanic acid) were observed in the testis and sertoli cells in seminiferous tubules contained large intratubular vacuoles [103].

In contrast to the peroxisomal insufficiency associated pathologies known from male patients, almost no reports are available in the literature on associated pathological alterations in the ovary of female patients. Whether peroxisomal defects might lead to failure in steroid biosynthesis has also not been elucidated yet. There are only two evidences can be found which described the impacts of peroxisomal deficiency in female reproduction. In the GNPAT knock-out mice a reduced ovary size could be observed displaying intact follicles in all stages. Nevertheless, the number of

secondary and tertiary follicles and of the corpora lutea was reduced, indicating female subfertility [100]. Another evidence showed that female ACOX knock-out mice were sterile with smaller ovaries [104].

1.3 Mouse ovary

The inner female reproductive system consists of the ovary, fallopian tubes, uterus, cervix, and vagina. Within this system, the ovary is the place where: (1) the differentiation and release of a mature oocyte for fertilization take place; (2) hormones, which are necessary for follicular development, menstrual cycle (estrous cycle) and keeping up of the function of the reproductive tract are synthesized and secreted [105, 106].

The ovary contains ovarian cortex in the outer layer and medulla in the innermost layer with blood vessels and lymphatics. In the ovarian cortex, there are ovarian follicles as well as the stroma in between them. A mature ovarian follicle is composed of an oocyte in the middle, surrounded by multiple layers of granulosa cells and enclosed by theca cells in the outer layer. Corpus luteum derived from the follicles can also be found in the cortex. The histology of mouse ovary from [1] is shown in Figure 3.

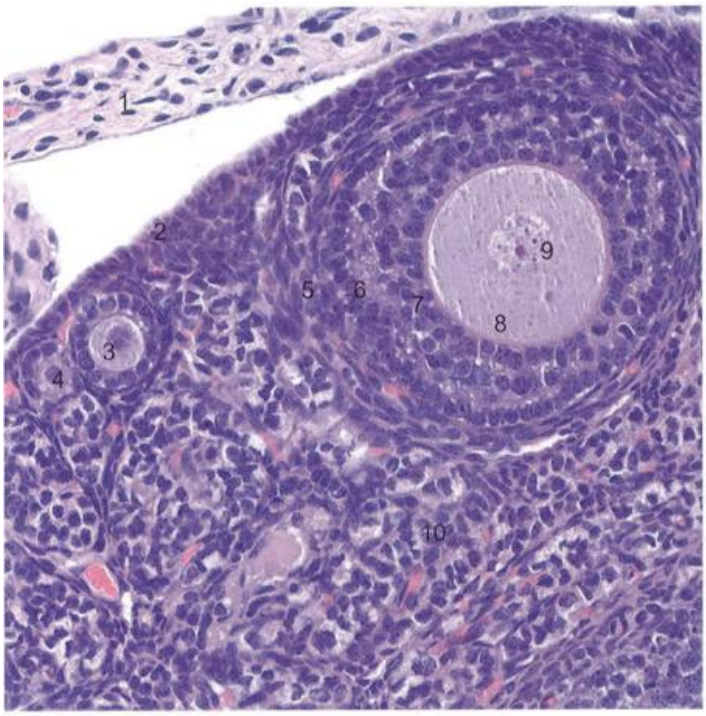

Figure 3. Histology of mouse ovary [1].

(1) Ovarian capsule.
(2) Epithelial layers
(3) Primary follicle.
(4) Primordial follicle.
(5) Theca layers.
(6) (7) granulosa layers.
(8) Oocyte.
(9) Chromosome.

1.3.1 Follicular development of mouse ovary

The process of the ovarian follicular development includes 5 stages in the mouse: primordial follicles, primary follicles, pre-antral follicles (secondary follicles), antral follicles (tertiary follicles), and pre-ovulatory follicles.

First, oogonia cease multiplication in the embryonic period around 13.5 days and enter meiosis to form oocytes. Theses oocytes are called germ cell nets due to that they are closely connected with each other [107, 108]. Shortly after birth, the germ cells break down and the surviving cells are separated by the somatic cells and primordial follicles are formed. The typical characteristic of this stage is a very small oocyte enclosed by an incomplete and fattened layer of epithelium cells [108]. After that the size of the oocyte increases and the epithelium cells continue to grow to cuboidal granulosa cells. This stage is named primary follicles [106]. One typical change in this stage is the appearance of zona pellucida, which surrounds the oocyte and exist until ovulation [109]. Following this, the granulosa cells start to proliferate to multiple layers to form pre-antral follicles and the outer layer of theca cells is building up. Extensive network of gap junctions are formed amongst granulosa cells in the end of this stage [106]. Then the follicles are developing to antral follicles with the formation of the antral cavity, a fluid-filled space. This cavity contains water, electrolytes, serum proteins and large amounts of steroid hormones secreted from the granulosa cells. During this stage, most of the antral follicles will undergo atresia and the remaining antral follicles will continue to grow to pre-ovulatory follicles under stimulation of FSH [106]. Pre-ovulatory stage is the last follicular stage. At this stage, oocyte is released for fertilization under the stimulation of luteinizing hormone (LH) [105]. During ovulation, the basement membrane of the follicles ruptures and the mature oocyte is released. The whole ovulation process is considered similar with an inflammatory response, since several inflammatory factors are up-regulated during ovulation [110]. After the oocyte is released for fertilization, the remaining granulosa and theca cells will differentiate to the corpus luteum (CL) [105, 106, 111]. CL is capable of producing large amounts of hormones for the maintenance of the early stage of pregnancy. The follicular development progress is shown in Figure 4.

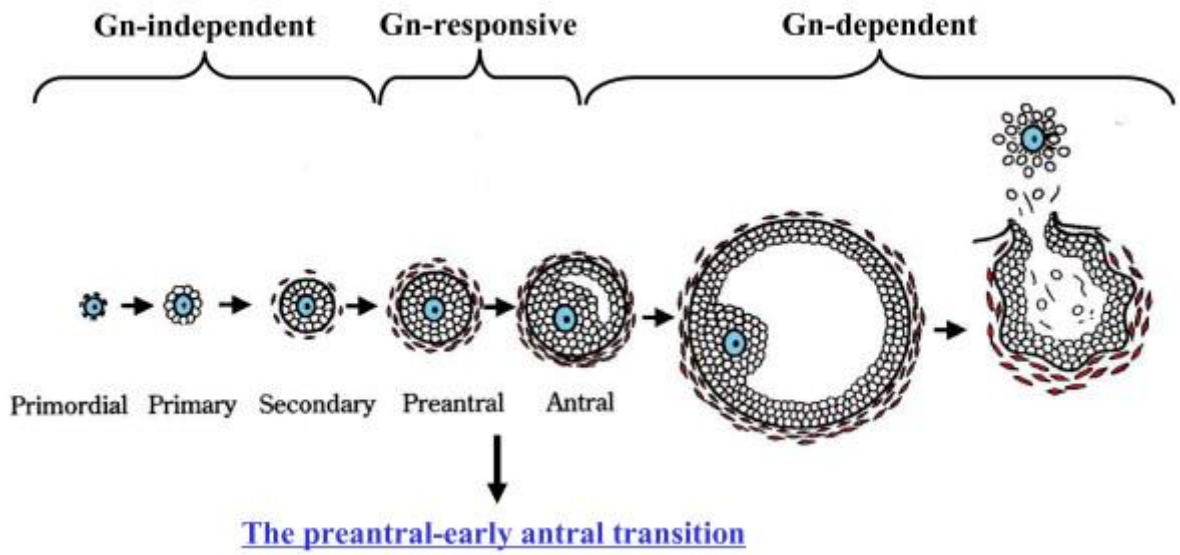

Figure 4. Schematic representation of the follicular development in mouse ovary [112]. Folliculogenesis starts with primordial follicles containing a small oocyte, enclosed by a flattened layer of epithelial cells. Primary follicles possess one cuboidal layer of granulosa cells. In early secondary follicles the zona pellucida is formed and the granulosa cells start to proliferate to multiple layers. In this stage follicles also acquire an outer layer of theca cells. Tertiary follicles are also called antral follicles, because a fluid-filled antral cavity appears, which contains water, electrolytes and steroids. After this stage, only a few antral follicles will develop into pre-ovulatory and ovulatory follicles. After stimulation with LH, the oocyte will be released for fertilization and the remaining parts of the ovulatory follicle will form the corpus luteum. The rest of the less developed follicles in the ovarian cycle will then enter apoptosis.

1.3.2 Estrous cycle in the mouse ovary

The mouse estrous cycle can be divided into four phases: proestrus, estrus, metestrus and diestrus. On average, one estrus cycle lasts for about 4-6 days. And the time period in different phases last normally, 18 h, 42 h, 12 h and 48-72 h respectively.

In the proestrus phase (Figure 5A), the follicles grow very rapidly and many developing follicles with cavity can be observed. CL are often degenerated, with central fibrous tissue formation, and the ovarian cells commonly contain cytoplasmic vacuoles. In estrus phase (Figure 5B), ovulation is spontaneous and occurs about 10 hours after the beginning of estrus. "Heat" lasts about 13 hours. Usually 10-20 eggs ovulate each time. Follicles with big cavities are visible and they are located in the superficial margin of the ovarian cortex. Degenerated ovarian CL are often present in the estrus phase. When entering the metestrus phase (Figure 5C), many CL are present in the ovary and the follicles with cavity are barely seen in this stage. During

diestrus phase (Figure 5D), small follicles and large CL from the previous ovulation in the ovary are present, which have attained their maximal size. Vacuoles are commonly present, particularly at the center of these large CL, indicative of active steroidogenesis. Early fibrous tissue formation may be seen in which place was previously the central, fluid-filled cavity.

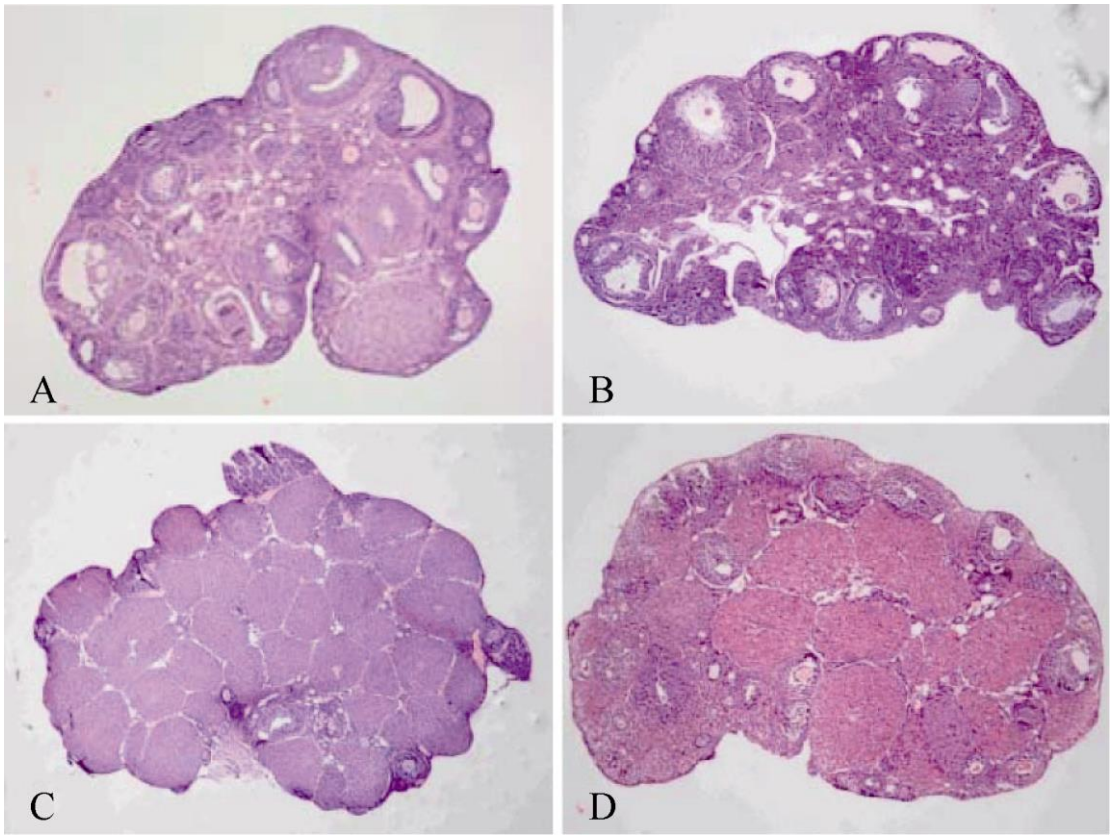

Figure 5. Histological sections of ovaries in different stages of the estrus cycle [113]. A) Proestrus; B) Estrus; C) Metestrus; D) Diestrus.

1.3.3 Steroid biosynthesis in the ovary

Steroids are synthesized from cholesterol in the adrenal gland and gonads in response to tissue-specific tropic hormones. For steroidogenesis, it is necessary to translocate cholesterol from the cytosol to mitochondria, where the cholesterol is converted to pregnenolone. Cholesterol can be obtained from at least four potential sources: 1) from plasma low-density lipoprotein (LDL) or high-density lipoprotein (HDL); 2) synthesized *de novo* from acetate; 3) derived from the hydrolysis of stored

cholesterol esters in the form of lipid droplets or; 4) interiorized from the plasma membrane.

1.3.3.1 Transport of mobilized cholesterol to the mitochondria

For the production of progesterone, cholesterol is first transported to the outer mitochondrial membrane (OMM). This transportation could either be done via the vesicular transport mechanism or through a non-vesicular transport process involving high-affinity cholesterol binding proteins [114-117]. Sterol carrier protein 2 (SCP2), a protein which was reported to mediate cholesterol transport to mitochondria for steroid synthesis [118] will be further discussed in section 1.5.

The second crucial step for steroid synthesis is the delivery of cholesterol from the outer mitochondrial membrane (OMM) to the inner mitochondrial membrane (IMM), where the cholesterol cytochrome P450 side chain cleavage (CYP450scc) enzyme is located. The conversion of cholesterol to pregnenolone is catalyzed by this enzyme [119-121]. Cholesterol transportation is considered as the rate limiting step for steroidogenesis and this step is conducted by a protein called steroidogenic acute regulatory protein (StAR) [122, 123]. The regulation of StAR protein will be further discussed in the following sections.

1.3.3.2 Steroidogenic pathway in the ovary

The steroidogenic pathway in the ovary is based on the “two cells theory”, because estrogen production occurs in two different cell types, the theca interna cells and the granulosa cells. LH stimulates the theca interna cells to produce androgen, which is then converted to estrogen in granulosa cells under the stimulation of FSH [124]. The steroidogenic pathway in the ovary is shown in Figure 6.

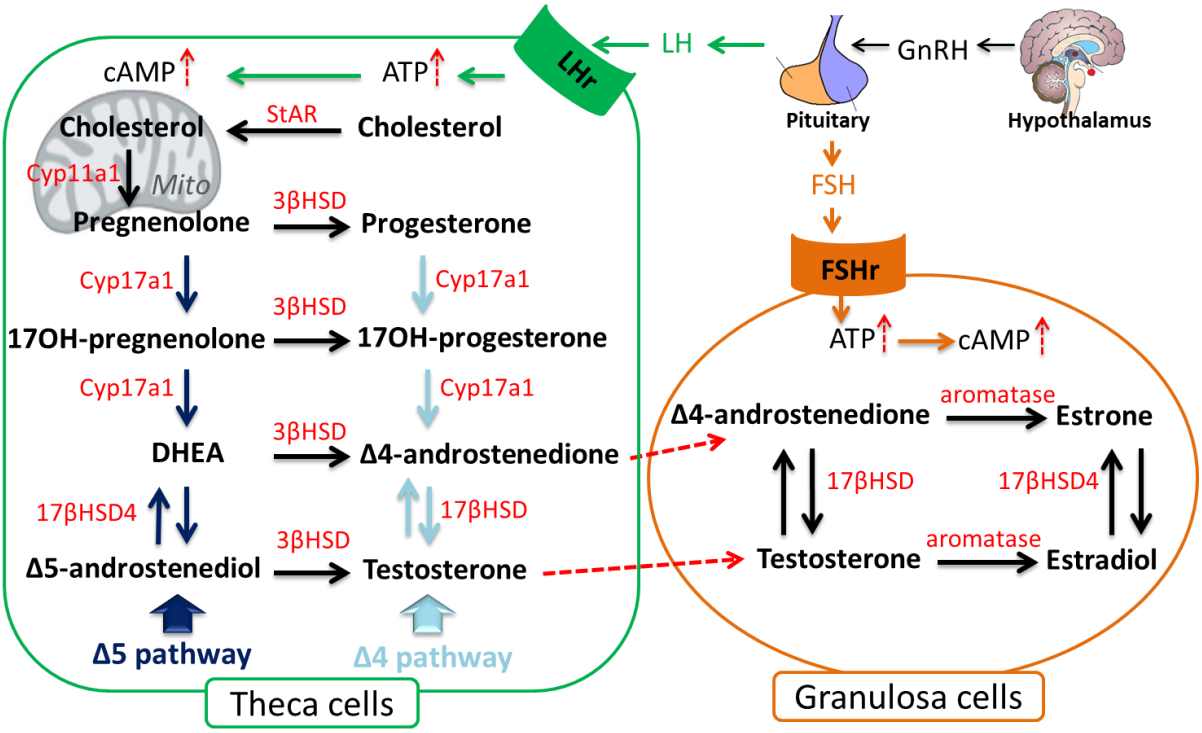

Figure 6. Steroidogenic pathway in the ovary before ovulation. Modified from Craig *et.al* [125].

Several different enzymes that are located in the theca cells are required for the steroidogenic pathway: cytochrome P450 side chain cleavage (CYP450scc)/ cytochrome P450C11 (CYP11A1), 3-beta-hydroxysteroid dehydrogenase (3β-HSD) and cytochrome P450C17 (CYP17A1). Both CYP11A1 and 3β-HSD can be detected in granulosa cells while CYP17A1 is exclusively expressed in theca cells. These enzymes are expressed in theca cells when the follicles start to develop an antrum cavity. At this stage, theca cells start to produce androgen, mainly in the form of androstenedione. The first enzymatic reaction is the conversion of cholesterol to pregnenolone by CYP11A1 [126-128]. Thereafter, pregnenolone is further converted to progesterone by the enzyme 3β-HSD. 3β-HSD catalyzes the dehydrogenation and isomeration of pregnonelone to progesterone, which converts a Δ5-3β-hydroxysteroid to another form of steroid hormones Δ4-ketosteroid. Due to this reaction, the steroidogenic pathway is bifurcated into two pathways: 1) Δ5-3β-hydroxysteroid pathway that starts with pregnenolone and 2) the Δ4-ketosteroid pathway that starts with progesterone. The final product of both pathways in the ovary is androgen. For the Δ5-3β-hydroxysteroid pathway, CYP17A1 initially catalyzes the conversion of pregnenolone to 17-hydroxypregnenolone, which is then converted to

dehydroepiandrosterone (DHEA) [128]. Thereafter, DHEA is converted to Δ4-androstenedione by 3β-HSD. In the Δ4-ketosteroid pathway, CYP17A1 converts progesterone to 17-hydroxyprogesterone, which is then converted to Δ4-androstenedione. During the above processes, 3β-HSD converts 17-hydroxypregnenolone to 17-hydroxyprogesterone and DHEA to Δ4-androstenedione respectively. Next, Δ4-androstenedione is transported to granulosa cells and aromatized to estrone by aromatase/CYP19A1 and further converted to estradiol by the 17β hydroxysteroid dehydrogenase (17β-HSD) [128]. 17β-HSD is constitutively expressed in granulosa cells from primary stage to pre-ovulatory Graafian follicles, whereas the expression of aromatase is stimulated by FSH until the dominant follicle stages.

CYP17A1 is expressed exclusively in theca interna cells while aromatase/CYP19A1 is specifically located in granulosa cells [129-132]. Thus, androgens can only be synthesized from theca interna cells and estrogen production in granulosa cells is dependent on androgen precursors supplied from theca interna. During follicular development, CYP11A1 expression is significantly enhanced in theca cells upon gonadotropin stimulation while in granulosa cells it can only be detected until the LH surge before ovulation. Moreover, the expression level of CYP11A1 in granulosa cells is much lower than that in theca cells during follicular development [133-135]. After ovulation, in the luteinized granulosa cells, CYP11A1 is greatly stimulated by FSH to produce large amounts of progesterone while CYP11A1 expression is reduced in luteinized theca cells [136]. Regarding to the 3β-HSD, it is unable to be detected in granulosa cells at any stage during follicular development while in corpus luteum, the 3β-HSD was detected in both luteinized theca and granulosa cells with equal intensity in both cell types [137]. The significant up-regulation of both CYP11A1 and 3β-HSD in the corpus luteum are responsible for the elevated demand for progesterone synthesis [130].

1.3.3.3 Regulation of the steroidogenic acute regulatory (StAR) protein

The steroidogenic acute regulatory (StAR) protein regulates the rate-limiting step in steroidogenesis by transferring cholesterol from the outer mitochondrial membrane to the inner membrane [138]. Although the StAR protein plays an indispensable role in

steroid metabolism, its function and regulation still remain unclear. The schematic representation of the regulation of StAR protein is illustrated in Figure 7.

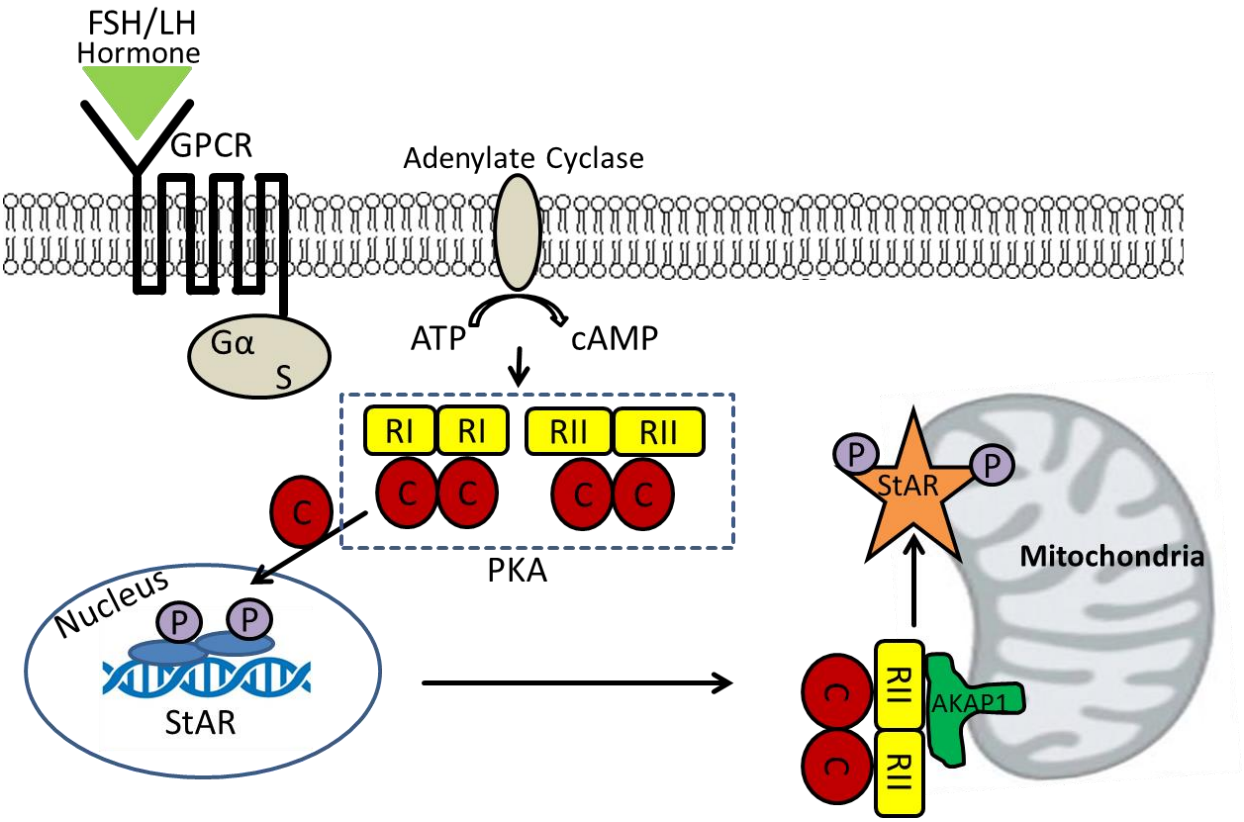

Figure 7. A schematic model describing cAMP-PKA signaling pathways in regulating transcription and translation of StAR.

In the gonads, StAR protein is regulated predominantly via cAMP-dependent mechanisms. It is widely acknowledge that LH binding to its G-protein-coupled receptor leads to the activation of the adenylate cyclase/cyclic-AMP (cAMP)/protein kinase A (PKA) signaling pathway [139-142]. LH stimulates progesterone synthesis primarily by enhancing intracellular cAMP levels, which leads to the activation of PKA, influencing the expression and activity of components in the steroidogenic pathway [143-145]. The PKA holoenzyme exists as a tetramer composed of two regulatory (R) and two catalytic (C) subunits. After cAMP stimulation, two binding sites on the R subunits are occupied by cAMP, and a conformational change occurs to lower their affinity to the C subunits. This results in the dissociation of the holoenzyme complex and renders the enzyme active [146]. Until now, four different regulatory subunits (RIα, RIβ, RIIα and RIIβ) and three potential catalytic subunits (Cα, Cβ and Cγ) have

been identified in mammalian tissues [146, 147]. PKA active catalytic subunits are able to phosphorylate specific target proteins as well as transcriptional factors including steroidogenic factor 1 (SF-1), GATA binding protein 4 (GATA-4), and cAMP response-element binding protein (CREB) that function to activate genes involved in steroidogenesis, including StAR [138, 148, 149].

As mentioned above, the hypothalamic-pituitary-ovary axis is regulated by gonadotropic hormones FSH and LH to maintain the normal ovarian function. Interestingly, cAMP-PKA-dependent signaling cascades initiated by FSH or LH are assumed to be regulated by “A-Kinase Anchoring Proteins” (AKAPs) due to their ability to bind PKA [150]. Specific AKAPs recruit PKA to discrete subcellular compartments that coordinate and focus PKA action with respect to its substrates, making PKA signaling more effective. A kinase anchoring protein 1 is also known as AKAP121 in mice or AKAP149 in human, as widely expressed in testis, ovary, heart, liver, kidney, skeletal muscle, and brain. AKAP1 binds to RI and RII of PKA and anchors them to the cytoplasmic face of the mitochondria. AKAP121, as the most prevalent isoform, is of particular interest since it is known to enhance cAMP signaling to the mitochondria as well as to target mRNAs to the mitochondria through its RNA-binding domain [151-157]. Studies have shown AKAP1 has a positive effect on StAR signaling pathways by recruiting StAR mRNA to the mitochondria [158].

1.4 Peroxisomes in the ovary

Peroxisomes in the ovary were first discovered in 1972. Catalase is an enzyme localized within the peroxisomal matrix that degrades H_2O_2, it was discovered in the mouse ovary with 3, 3’-diaminobenzidine (DAB) labelling and electron microscopic analysis [159]. Peroxisomes in the ovary are named microperoxisomes for their smaller size and lack of nucleoid in comparison with classical peroxisomes in the liver [160]. Compared to the liver, which is terminally differentiated, part of the cells in the ovary undergoes constant differentiation with each estrous cycle. Singh *et al* found the highest catalase activity in the metestrous and declined enzyme activity in the estrous and proestrous then was lowest in the diestrous cycle [161]. In 1992 Peterson and Stevenson demonstrated an increase in the specific activity of ovarian catalase during the development and differentiation of ovarian follicles [162]. Besides this, they found that after treatment with gonadotropins, a substantial increase of

catalase activity could be observed. Elevated catalase activity was also observed during the ovarian development and luteinization in rat granulosa and theca cells [163, 164]. In *vitro* study of goat ovary, Behl and Pandey found a three-fold increase of catalase activity in granulosa cells from large follicles compared with small and medium follicles [165]. Similar to in vivo studies by Peterson and Stevenson, they also found increased catalase activity after FSH treatment in vitro. These results indicate that catalase and most likely the entire peroxisome may play a central role in follicular maturation.

1.5 Up to date evidences for the involvement of peroxisomes in steroid hormone metabolism

On the basis of structural and biological differences, steroid hormones are classified into seven families in mammalian species: androgens (male sex steroids), estrogens (female sex steroids), progestins, mineralcorticoids, glucocorticoids, bile acids and vitamin D [166]. Compared with the peptide hormones, the synthesis of steroid hormones requires specific enzymes that convert cholesterol into the appropriate steroid. Cholesterol is a critical component of cell membranes and also an obligatory precursor for steroid biosynthesis that is obtained either from the diet or synthesized *de novo* from acetate in a complicated process involving almost 30 different enzymes. Interestingly, the pre-squalene segment of the cholesterol biosynthesis pathway is localized in peroxisomes. However, whether acetyl-CoA derived from peroxisomal β-oxidation is channeled to cholesterol synthesis inside the peroxisomes is still under debate [71, 167, 168]. According to this, the role of peroxisomes in cholesterol synthesis for further steroid production needs to be more clarified. Also, in PEX2 knock-out mice the cholesterol synthesis pathway and the overall cholesterol regulation is disturbed in the liver [70].

Apart from that, there are evidences that some peroxisomal enzymes are linked with steroid biosynthesis. A protein called sterol carrier protein 2 (SCP2) with a peroxisomal targeting signal sequence at the C-terminus [169], plays roles in bile acid formation from cholesterol and peroxisomal β-oxidation of branched-chain fatty acids [90]. Interestingly, this non-specific lipid transfer protein was indicated to be involved in steroid metabolism via conducting cholesterol to steroidogenic mitochondria [117, 118, 170]. Another enzyme connecting peroxisomes with

steroidogenesis is the peroxisomal 17β-hydroxysteroid dehydrogenase type 4 (17β-HSD4), called by the peroxisomal community MPF2 (gene name Hsd17b4) that participates not only in peroxisomal β-oxidation but also in steroid conversion, and is involved in the oxidation process of estradiol to estrone. 17β-HSD 4 is an 80 KDa protein with an N-terminally cleaved enzymatically active fragment of 32 kDa. Both the 80 kDa and the N-terminal 32 kDa protein are capable of conducting the dehydrogenase reaction not only with D-3-hydroxyacyl-coenzyme A (CoA) but also with steroids at the C17 position. This was the first observation of an enzyme, which contains dehydrogenase activity not only with 3-hydroxyacyl-CoA derivates of fatty acids but also with steroids [171-174]. MFP2/17βHSD4 therefore has been cloned also by groups coming from the two different directions [174]. Apart from these two evidences, changes of steroid levels were observed in testis homogenates of sertoli cell specific *Pex13* knock-out mice (scsPex13KO). The concentration of DHEA showed a dramatic increase in *Pex13* KO mice while the levels of other steroid precursors such as 17OH-Pregnenolone, 17OH-Progesterone and D4-Androstenedione were decreased in scs*Pex13*KO testis homogenates [103].

2 Aims of the study

Until now, the role of peroxisomal metabolism and biogenesis in normal ovarian physiology as well as the influences of peroxisomal metabolism on overall ovarian function in granulosa cells remain unclear. Therefore, this study was aimed to analyze the correlation of granulosa peroxisomal metabolism in follicular development and steroidogenesis, and to determine the pathological consequences of granulocytic steroid metabolism in peroxisomal dysfunction.

On the basis of this purpose, we first analyzed the distribution and regulation of peroxisome marker enzymes during mouse ovarian follicular development to explore whether peroxisomes have a function during follicular development. After that, the granular tumor cell line, KK-1, was used in our experiments. Peroxisomal compartments were analyzed after human chorionic gonadotropin (hCG) treatment in KK-1 cells to examine whether peroxisomes are involved in steroidogenesis. After this confirmation, peroxisomal biosynthesis gene *Pex13* was knocked down in KK-1 cells to detect the results of peroxisome dysfunction on steroid synthesis as well as steroidogenic enzymes. Finally, we investigated the possible mechanism of effects on steroidogenesis in the deficiency of peroxisomes. This study, for the first time, provides insights into the role of peroxisomes in the context of steroid biosynthesis and corresponding mechanisms.

3 Materials and methods

3.1 Materials

3.1.1 Chemicals for the general experiments

Chemicals for the general experiments are listed in Table 3.

Table 3. List of chemicals and drugs used in this project with corresponding suppliers.

Chemicals	Company
Acrylamide	Roth, Karlsruhe, Germany
Agarose LE	Roche, Grenzach-Wyhlen, Germany
Ascorbic acid	Sigma, Steinheim, Germany
Bradford reagent	Sigma, Steinheim, Germany
Dimethylsulfoxide (DMSO)	Sigma, Steinheim, Germany
Ethanol	Riedel-de-Haën, Seelze, Germany
Glycine	Roth, Karlsruhe, Germany
Glycerol	Sigma, Steinheim, Germany
β-Glycerolphosphate	Sigma, Steinheim, Germany
Mowiol 4-88	Polysciences, Eppelheim, Germany
N-Propyl-gallate	Sigma, Steinheim, Germany
Paraformaldehyde (PFA)	Sigma, Steinheim, Germany
Penicillin/Streptomycin	PAN Biotech, Aidenbach, Germany
Ponceau S	Serva, Heidelberg, Germany
Potassium dihydrogen phosphate	Merck, Darmstadt, Germany
Potassium hydroxide	Fluka, Neu-Ulm, Germany
Sodium chloride	Roth, Karlsruhe, Germany
Sodium hydroxide	Merck, Darmstadt, Germany
Sucrose	Merck, Darmstadt, Germany
Sodium dodecyl sulphate (SDS)	Sigma, Steinheim, Germany
Tetramethylethylenediamine (TEMED)	Roth, Karlsruhe, Germany
Trishydroxymethylaminomethane (Tris)	Merck, Darmstadt, Germany
Triton X-100	Sigma, Steinheim, Germany
Trypan blue	Sigma, Steinheim, Germany
Tween 20	Fluka, Steinheim, Germany
Xylene	Merck, Darmstadt, Germany

3.1.2 General Instruments used in the laboratory

Table 4. All general Instruments used in this project are listed in Table 4.

Instruments	Company
Biocell A10 water system	Milli Q-Millipore, Schwalbach, Germany
Bio-Rad electrophoresis apparatus (Sub Cell GT) system	Bio-Rad, Heidelberg, Germany
Dish washing machine (G 78 83 CD)	Miele, Gütersloh, Germany
Gel-Doc 2000 gel documentation system	Bio-Rad, Heidelberg, Germany
Hera cell 240 incubator	Heraeus, Hanau, Germany
Hera safe, clean bench KS-12	Heraeus, Hanau, Germany
Ice machine, Scotsman AF-100	Scotsman Ice Systems, Vernon Hills, IL,USA
i Cycler PCR machine MiQ2 optical module	Bio-Rad, Heidelberg, Germany
Leica DMRD fluorescence microscope	Leica, Bensheim, Germany
Leica DC 480 camera	Leica, Bensheim, Germany
Leica TP1020 embedding machine	Leica, Nussloch, Germany
Leica TCS SP2 confocal laser scanning microscope	Leica, Nussloch, Germany
Leica SM 2000R rotation microtome	Leica, Nussloch, Germany
Microwave oven MB-392445	LG, Willich, Germany
Microtome stretching water bathType 1003	Vieth Enno, Wiesmoor, Germany
Multifuge 3 SR centrifuge	Heraeus, Hanau, Germany
Oven HERAEUS T 5050 EKP	Heraeus, Hanau, Germany
pH meter E163649	IKA, Weilheim, Germany
Pipettes (2,20,200,1000µl)	Eppendorf, Hamburg, Germany
Potter-Elvehjem homogenizer 8533024	B.Braun, Melsungen, Germany
Power supply - 200, 300 and 3000 Xi	Bio-Rad, Heidelberg, Germany
Pressure/Vacuum Autoclave FVA/3	Fedegari, Albuzzano, Italy
Pump Drive PD 5001	Heidolph Instruments, Schwabach, Germany
Sorvall Evolution RC centrifuge	Kendro, NC, USA
SmartspecTM 3000 spectrophotometer	Bio-Rad, Heidelberg, Germany
T25 basic homogenizer	IKA, Staufen, Germany
Thermo plate HBT 130	Medax, Kiel, Germany
Thermo mixer HBT 130	HLC, BioTech, Bovenden, Germany
Trans-Blot SD semi dry transfer cell	Bio-Rad, Heidelberg, Germany
Vortex M10	VWR International, Darmstadt, Germany
Water bath shaker GFL 1083	GFL, Burgwedel, Germany

3.1.3 General materials used for cell culture

General materials and cell culture media used for KK-1 cell cultivation are listed in Table 5.

Table 5. General materials for cell culture listed with corresponding suppliers.

Materials for cell culture and treatment	Company name
Cover slips	Menzel-Gläser, Braunschweig, Germany
Culture dish (35 mm)	BD Biosciences, Heidelberg, Germany
Culture dish (60 mm)	BD Biosciences, Heidelberg, Germany
Fetal bovine serum (FBS)	Thermo Fisher Scientific, Schwerte, Germany
Filter tips and canules	Braun, Melsungen, Germany
Multi-well cell culture plates (6 wells)	BD Biosciences, Heidelberg, Germany
Multi-well cell culture plates (12 wells)	BD Biosciences, Heidelberg, Germany
Penicillin-Streptomycin	Life technology, Darmstadt, Germany

3.2 Methods

3.2.1 Morphological experiments

3.2.1.1 Animal experiments

Female C57Bl/6J mice (Charles River Laboratories, Sulzfeld, Germany) at the age of 4-6 months were used for experiments in order to characterize peroxisomes in the ovary. The animals were delivered two days before the experiments. The mice were housed under standard conditions with free access to standard laboratory food and water and a 12 h dark-/light-cycle. All experiments with laboratory mice were approved by the Government Commission of Animal Care Germany.

3.2.1.2 Hematoxylin and Eosin (H&E) staining

Paraffin sections of mouse ovaries (2 µm thick) were stained with Hematoxylin and Eosin. Paraffin sections were deparaffinized and rehydrated using the following steps: Xylene 3 times for 10 min, 100% ethanol 2 times for 5 min and then 96% ethanol, 80% ethanol, 70% ethanol, and aqua dest, each step for 5 min. The sections were then stained for 7 min in 10% Mayer's hematoxylin. The cytoplasm was stained for 5 min in 1% Eosin, containing 0.2% glacial acetic acid after washing 10 min under the tap water for revealing the nuclei. After that the slides were shortly washed with tap water and dehydrated in 70% ethanol, 80% ethanol, 2 times 96% ethanol, 3 times 100% ethanol, each time for 2 min, followed by 3 x 10 min in Xylene. The sections were analyzed by using a LEICA CMRD microscope equipped with a LEICA CD 480 camera.

3.2.1.3 Indirect immunofluorescence staining on paraformaldehyde-fixed, paraffin-embedded mouse ovaries

Sections containing mouse ovaries were deparaffinized and rehydrated as follows: Xylene 3 times for 10 min, 100% ethanol 2 times for 5 min, then 96% ethanol, 80% ethanol, 70% ethanol, and aqua dest, each step for 5 min at RT. Thereafter deparaffinized and rehydrated ovarian sections were subjected to digestion with trypsin in TBS for 9 min at 37°C in order to improve the retrieval of peroxisomal antigens and to increase the accessibility of epitopes. The silds were put thereafter in a microwave at 900 W in 10 mM citrate buffer at pH 6.0 for 15 min [175]. After incubation with 4% TBSA for 2 h at RT, the sections were incubated with primary antibodies in 1% BSA in TBST in a moist chamber overnight. In parallel, negative controls were incubated with PBS buffer only instead of the first antibodies. On the following day, the silds were washed with PBS 5 min for 3 times. Thereafter they were incubated with fluorochrome-conjugated secondary antibody for 2 h at RT. After incubation with the secondary antibody, nuclei were visualized with 1 µM TOTO-3 iodide (Molecular Probes/Invitrogen, Carlsbad, USA) together with Hoechst 33342 (1 µg/ml) (Molecular Probes/Invitrogen, Cat. no: 33342) for 10 min at RT . Finally all the samples were examined with a LEICA fluorescence microscope and the best preparations were used for confocal laser scanning microscopy (CLSM) using a LEICA TCS SP2. The solutions used in these experiments are described in Table 6. All the antibodies which were applied in the experiment are listed in Table 7.

Table 6. Solutions for immunofluorescence staining.

10X PBS	1.5 M NaCl, 131 mM K_2HPO_4, 50 mM KH_2PO_4, prior to use adjust to pH 7.4
Trypsin (0.1%)	0.1 g trypsin in 100 ml of 1x PBS buffer, freshly prepared
Glycine (1%)	1 g glycine in 100 ml of 1X PBS buffer
Glycin (1%) + Triton X-100 (0.1%)	1 g glycine in 100 ml of 1X PBS buffer + 0.1 ml Triton X-100
Blocking buffer-4% PBSA + 0,05% Tween 20	To 8 g BSA add 200 ml of 1x PBS and 100 µl of Tween 20
Dilution buffer- 1% PBSA + 0,05% Tween 20	To 2 g BSA add 200 ml of 1x PBS and 100 µl of Tween 20
Mowiol 4-88 solution	Overnight stirring of 16.7% Mowiol 4-88 (w/v) + 80 ml of 1x PBS, add 40 ml of glycerol, stirred overnight; centrifuge at 15,000 rpm/min for 1 h. The supernatant was collected and store at -20° C
Anti-fading agent (2.5%)	2.5 g N-propyl-gallate in 50 ml of PBS and 50 ml of glycerol
Mounting medium	Mowiol 4-88 mixed with anti-fading agent in a ratio of 3:1

Table 7. Antibodies used for immunofluorescence or Western blots.

Primary antibody	Species AB raised in	Dilution(WB)	Dilution(IF)	Supplier
Peroxisomal biogenesis and metabolic protein				
Catalase (CAT)	Rabbit, polyclonal	1:15,000	1:500	Gift from Denis I. Crane, School of Biomol. Biophys. Sci., Griffith Univ., Nathan, Brisbane, Australia
Peroxisomal biogenesis factor 13 (PEX13p)	Rabbit, polyclonal	1:1,000		
Peroxisomal biogenesis factor 14 (PEX14p)	Rabbit, polyclonal	1:5,000	1:2,000	
Glyceronephosphate acyltransferase (GNPAT)	Rabbit, polyclonal	1:500	1:500	Proteintech, Manchester, UK, Cat no: 14931-1-AP
Peroxisomal 2-keto-acyl-CoA thiolase	Rabbit, polyclonal	1:5,000		Gift from Nancy E. Bravermann; Depts. of Human Genetics and Pediatrics, McGill University-Montreal Montreal, QC, Canada
Anti-Hydroxysteroid (17-beta) dehydrogenase 4 (17bHSD4/MFP2)	Rabbit, polyclonal	1:1,500	1:250	Abcam, Cambridge, UK, Cat. No: ab97971
Peroxisomal membrane protein (ABCD3 / PMP70)	Rabbit, polyclonal		1:300	Abcam, Cambridge, UK, Cat. No: ab3421
Antioxidative enzymes from other cell compartments				
Mouse superoxide dismutase 1 (SOD1)	Rabbit, polyclonal	1:1,000		Research diagnostics, Flanders, New Jersey, Cat no: RDI-RTSODMabR
Mouse superoxide dismutase 2 (SOD2)	Rabbit, polyclonal	1:1,000	1:500	Abcam, Cambridge, UK, Cat. No: ab13533
Glutathione reductase (GR)	Rabbit, polyclonal	1:2,000	1:500	Biozol, Eching, Germany, Cat.No: ab16801
Steroidogenic enzymes and enzymes involved in steroidogenic pathway				
Mouse cytochrome P450 side chain cleavage enzyme (CYP11A1/CYP450scc)	Rabbit, polyclonal	1:1,000		Cell Signaling, Beverly, MA, USA, Cat. No: #14217
Steroidogenic acute regulatory protein (StAR)	Rabbit,monoclonal	1:1,000		Cell Signaling, Beverly, MA, USA, Cat. No: #8449
cAMP-dependant protein kinase A C-α subunit (PKA C-α)	Rabbit,monoclonal	1:1,000		Cell Signaling, Beverly, MA, USA, Cat. No: D38C6
Polypeptide protein tag				
myc-Tag	Mouse,monoclonal	1:1,000	1:1,500	Cell Signaling, Beverly, MA, USA, Cat. No: 9B11
Loading Control				
β-Actin	Mouse,monoclonal	1:3,000		Sigma, St Louis, USA, Cat. No: A5316
Secondary Antibodies	**Species AB raised in**	**Dilution(WB)**	**Dilution(IF)**	**Supplier**
anti-Rabbit-IgG alkaline phosphatase conjugate	Goat, polyclonal	1:10,000		Sigma Aldrich, Cat. no: A0545
anti-Mouse-IgG alkaline phosphatase conjugate	Goat, polyclonal	1:10,000		Sigma Aldrich, Cat. no: A3562
anti-Rabbit-IgG AlexaFluor488	Donkey		1:1,000	Molecular Probes/Invitrogen, Cat. no: A21206
anti-Mouse-IgG AlexaFluor555	Donkey		1:1,000	Molecular Probes/Invitrogen, Cat. no: A31570

3.2.1.4 Indirect immunofluorescence staining of KK-1 cells

The coverslips with growing KK-1 cells were rinsed 2 times with PBS (pH 7.4) and fixed with 4% paraformaldehyde (PFA) at RT for 20 min. After removal of the PFA, KK-1 cells were washed 3 times with PBS. The coverslips containing the cells were incubated in PBS containing 1% glycine for 10 min, followed by another 10 min incubation with PBS containing 1% glycine and 0.1% Triton X-100 for permeabilization. Subsequently, the cells were washed 3 times with PBS and incubated in PBS containing 1% BSA and 0.05% Tween 20 for 30 min to block nonspecific protein binding sites. Thereafter, the coverslips were incubated with primary antibodies at 4°C in a moist chamber overnight. The next day, the silds were washed with PBS 3 times for 5 min and then incubated with the secondary antibody for 1 h 30 min at RT. Nuclei were counterstained with Hoechst 33342 (1 µg/ml) (Molecular Probes/Invitrogen, Cat. no: 33342). The solutions used in these experiments are described in Table 6. All the antibodies which were applied in the experiment are listed in Table 7.

3.2.1.5 Dihydroethidium (DHE) staining for ROS detection

Dihydroethidium (DHE) staining was used to evaluate intracellular ROS levels. Dihydroethidium (DHE) is an oxidizable fluorescent dye. Growing KK-1 cells were treated according to the necessary experiment and grown for different time points. The DHE stock solution (Invitrogen, Cat. no: D-23107) was diluted to 10 µmol with normal KK-1 cell culture medium (the composition of KK-1 cell culture medium is described in section 3.2.2.1) and the medium was added to KK-1 cells growing on coverslips for 30 min incubation at 37°C. Thereafter, the cells were washed three times with PBS and fixed with 4% PFA for 20 min at RT. Nuclei were counterstained with Hoechst 33342 (1 µg/ml) (Molecular Probes/Invitrogen, Cat. no: 33342) for 10 min at RT. Images were taken with a LEICA TSC SP5 confocal microscope (CLSM) and the average values of fluorescence intensity were measured with the Image J software program.

3.2.2 Cell culture experiments

3.2.2.1 The granulosa tumor cell line---KK-1

KK-1 cells are immortalized murine granulosa tumor cells. They were established by Prof. Huhtaniemi and his colleagues by using transgenic mice expressing the SV40 T-antigen, driven by fragments of the inhibin-α subunit promoter (Hammersmith Campus, Imperial College, London,UK) [176]. KK-1 cells were reported to display LH and FSH receptor responsiveness and to express steroidogenic enzymes. Apart from that, this cell line exhibits a dose-dependent steroidogenic response when stimulated with hCG or FSH. The KK-1 cell line which was used in this study was kindly provided by Prof. Rahman (Department of Physiology, University of Turku, Turku, Finland). KK-1 cells were cultured in DMEM/F12 1:1 medium (life technologies, Germany, Cat. no: 31330-038), supplemented with 10% (heat inactivated) fetal bovine serum (FBS), containing 50 mIU/ml penicilin and 0.5 mg/ml streptomycin at 37° C in a humidified atmosphere of 95% air and 5% CO2. KK-1 cells are luteinized granulosa cells, thus they possess LH receptors but lose their FSH receptors gradually after passage 10 [176]. Therefore, cell passages used in this study for checking estrogen synthesis were all earlier than passage 10 and for detecting progesterone and pregnenolone synthesis, passages before 13 were used.

3.2.2.2 Freezing and thawing of KK-1 cells

KK-1 cells were rinsed with PBS (Sigma, Steinheim, Germany, Cat. no: D8537) first followed by trypsinizing action. The trypsin-EDTA buffer (0.25%) (Life technologies, Cat. no: 25200-056) was warmed up to 37°C before use. For a 10 cm plate 1 ml trypsin buffer was added to the cells and the plate was moved back into the incubator for 3 min. Thereafter the reaction was stopped by re-suspending the cells in 2 ml DMEM/F12 medium and centrifuged at RT with 900 g for 5 min. The supernatant was sucked away and the precipitate was re-suspended in freezing medium (70% KK-1 cell culture medium, 20%FBS, 10%DMSO). 1ml of re-suspended cells was added to each tube used for CRYO preservation. The number of cells was at least $5x10^6$ cells/ml. The tubes were frozen for 2 h in -20°C and moved to -80°C for 24 h, thereafter the cell stocks were transferred to liquid nitrogen container.

When new cells need to be thawed, CryoPure tubes were quickly removed from the liquid nitrogen container and placed into a 37°C water bath. The CryoPure tubes

were immediately disinfected with 70% ethanol after thawing. The cells suspension was transferred into a 15 ml falcon tube and the same amount of pre-warmed culture medium was added to the tube with the thawed cells. The diluted cell suspension was centrifuged at 350 g for 5 min at RT. After the centrifugation, KK-1 cells were gently resuspended in culture medium, and transferred into the appropriate culture vessel and placed into the recommended culture environment.

3.2.2.3 Passaging of KK-1 cell cultures

The splitting conditions for KK-1 cells were: 70% confluent bottle to 2X 9.6 cm Petri dishes. The doubling time for KK-1 cells are 18-22 h. The cell passaging protocol was the same as for KK-1 cell freezing until the step “resuspend the cells after trypsinizing action”. After centrifugation, the cells were resuspended with suitable culture medium thoroughly and the cell solution with medium was mixed up and down for 10-15 times. Thereafter, KK-1 cells were plated to a new petri dish plates.

3.2.2.4 Hydrogen peroxide (H_2O_2) treatment

KK-1 cells were grown in culture medium to around 80% confluency and were preincubated in serum-free medium for 1 h. After that, KK-1 cells were treated for 3 h in DMEM/F12 medium that contain 1,5 IE hCG plus increasing concentrations of H_2O_2 (0,100,150,250 and 350 µmol) (Merck Millipore,Darmstadt, Germany, Cat. no: 108597). 30% stock solution of H_2O_2 was used, and appropriate volumes were added to DMEM/F12 just before cells treatment. In the end of the time point, medium were collected for steroid measurement and proteins were collected for further examination.

3.2.3.5 MTT assay

The effect of H_2O_2 treatment on the viability of KK-1 cells was evaluated by the MTT assay (Sigma, Steinheim, Germany ,Cat. no: M5655) after treatment with H_2O_2 at different concentrations (0,100,150,250 and 350 µmol) for 3h. KK-1 cells were then washed and incubated with 0.5 mg/ml MTT in DMEM medium (without phenol red) for 1 to 2 h. The formazan crystals which were formed from the tetrazolium dye in viable cells were dissolved in dimethyl sulfoxide (DMSO) and the absorbance read at 570 nm using a spectrophotometer. The percentage of cell viability was calculated by

using the following formula: A570 of treated cells/A570 of non-treated cells X 100 [177].

3.2.3.6 Trypan Blue test

Cell viability of KK-1 cells after H_2O_2 treatment was also determined by the Trypan Blue test, which is the most common dye exclusion method for assessing cell viability. Firstly, the cell suspension was prepared at approximately $1x10^6$ cells/ml by trypsinizing and resuspending the cells in fresh warm KK-1 cell culture medium. The cells were gently pipetted up and down several times in order to break up cells clumps. Thereafter, 200 µl of the cell suspension was mixed with an equal volume of 0,4% filtrated Trpyan blue (Fluka Chemika) in 1xPBS. The mixture was gently mixed and incubated for 5 min at RT. A haemocytometer chamber was filled with 10 µl cell suspension and the number of cells was counted under an inverted phase contrast microscope. Both viable (unstained) and nonviable (stained) cells in each of the four corner quadrants were counted.The final calculation steps were shown as follows:

Number of cells (viable or nonviable) = (Average cell number of four corner quadrants counted) $x10^4$ x 2 x sample dilution.

Finally the percentage of viability was calculated by using the next equation:

%Viable cells = Number of viable cells/total cell number.

3.2.3.7 Tocopherol treatment

Pex13 siRNA transfected KK-1 cells were first treated with different concentrations of α-tocopherol (Sigma, Steinheim, Germany, Cat.no:T3251) to determine the best working concentration. 0 µmol, 5 µmol and 10 µmol α-tocopherol were added to *Pex13* knock-down (KD) cells as well as control group (scramble siRNA), ROS intensity were calculated to determine the best working concentration (10 µmol). After this, *Scr* siRNA groups with and without α-tocopherol as well as *Pex13* siRNA groups with and without α-tocopherol were incubated to determine the effects of tocopherol on steroid synthesis after the *Pex13* KD, α-Tocopherol was immediatly added to the cells at the same time as the transfection was done. The detalied transfection procedure is discribed in section 3.2.4.2.1. After 48 h, cells were treated with 1,5 IE

hCG for 8 h. At the end of the treatment period, protein and medium were collected for further investigations.

3.2.3 Biochemical experiments

3.2.3.1 Western bloting

All the solutions for proteins isolation, SDS-PAGE and Western blotting are listed in Table 8.

Table 8. Solutions for protein isolation, SDS-PAGE and Western blotting.

Cell lysis buffer (1X)	50 mM Tris +150 mM NaCl +1% Triton-X-100 (pH 7.4). Before use 10% protease inhibitor cocktail was added
Resolving gel buffer A	1.5 M Tris-HCl, pH 8.8 + 0.4% SDS
Stacking gel buffer B	0.5 M Tris-HCl, pH 6.8 + 0.4% SDS
Resolving gel (12%) (for 4 SDS-PAGE gels)	8 ml of 30% acrylamide + 10 ml of buffer A + 2 ml of ddH2O + 15 µl of tetramethylethylendiamin (TEMED) + 130 µl of 10% ammonium persulfate (APS)
Stacking gel (for 4 SDS-PAGE gels)	1.25 ml of 30% acrylamide + 5 ml of buffer B + 5 ml of ddH2O + 15 µl of TEMED + 130 µl of 10% APS
10X Sample buffer	3.55 ml ddH2O + 1.25 ml 0.5M Tris-HCl, pH 6.8 + 2.5 ml 50% (w/v) glycerol + 2.0 ml 10% (w/v) SDS + 0.05% Bromophenol Blue. Before use, add 50 ml β-mercaptoethanol
10X Electrophoresis buffer	250 mM Tris + 2 M glycine + 1% SDS
20X Transfer buffer	Bis-Tris-HCl buffer (pH 6.4) for transfer of proteins from polyacrylamide gel to PVDF membranes; NuPAGE transfer buffer, Invitrogen, Heidelberg, Germany
10X TBS	0.1 M Tris + 0.15 M NaCl in 1000 ml of ddH_2O, adjust to pH 8.0
10% Blocking buffer	10 g fat free milk powder in 100 ml of ddH_2O
5% BSA solution	5 g BSA in 100 ml 1X TBST +0.05% Tween 20, pH 8.0
1X Washing buffer (TBST)	10 mM Tris/HCl, 0.15M NaCl, 0.05% Tween 20, pH 8.0
Stripping buffer (500 ml)	62.5 mM Tris (pH 6.8), 0.2% SDS, 500 ml ddH2O – 42°C water bath for 35 min with additional 500 µl β-mercaptoethanol
Ponceau S solution	0.1% (w/v) Ponceau S in 5% (v/v) acetic acid

3.2.3.1.1 Isolation of whole cell lysates

One hundred µl cell lysis buffer was added to each 6-well plate after washing the cell cultures with 1x PBS, after that the cells were scraped thoroughly with a rubber policeman and transferred to Eppendorff tubes. Thereafter, the tubes were incubated on ice for 30min with vortexing at intervals. The tubes were then centrifuged at 2500 g for 10 min at 4°C. Thereafter, the supernatant was collected to a new tube and stored at -20°C for further application.

3.2.3.1.2 Western blotting

Protein concentration measurement of each sample was done by the Bradford Assay using bovine serum albumin (BSA) (Roth, Karlsruhe, Germany) as a standard [178]. 20-40 µg protein of each sample as well as 5 µl dual color precision plus protein Standards® (Nippon Genetics Europe GmbH, Dueren, Germany, Cat no: MWP02) were loaded into the slots of 8-12% SDS polyacrylamide gels.

Electrophoresis was done at stable voltage of 2.4 V/cm^2 and the finished gel was blotted onto polyvinylidene fluoride (PVDF) membranes (Millipore, Schwalbach, Germany) after the sample proteins were separated by SDS-PAGE. Blotting conditions were set at 90 mA constant current for 60 min for one gel with a Bio-Rad Trans-Blot® SD semidry transfer cell (Bio-Rad München, Germany). After blotting, PVDF membranes were blocked with Tris-buffered saline (TBS) containing 10% non-fat milk powder (Roth, Karlsruhe, Germany) and 0.05% Tween-20 (TBST) to block the non-specific protein binding sites for 1 h at RT. After blocking, the membrane was incubated with the specific primary antibody at 4°C overnight. The next morning, the membrane was washed 10 min for 3 times with 1X TBST solution in order to remove the primary antibody. Subsequently, the membrane was incubated with alkaline phosphatase-conjugated secondary antibodies at RT for 1 h 30min. All the primary and secondary antibodies used in Western blotting are listed in Table 7. Thereafter, Immun-StarTM AP substrate (Bio-Rad, Munchen, Germany) was used to detect the alkaline phosphatase activity. The blots were exposed to Kodak Biomax MR Films. To detect different target proteins, the membranes were reused several times by stripping and reincubation. The stripping condition is listed in Table 8. After stripping, the membrane was washed 3 times with TBST for 5min and re-blocked for 1 hour at

RT for another antibody detection. All the western blots were carried out 3 times to obtain reliable results.

3.2.3.2 Steroid measurements in KK-1 cell cultures

3.2.3.2.1 Cell treatment for stimulating steroid synthesis

For progesterone measurement, hCG (BREVACTID® 5000 I.E., Ferring, Kiel, Germany) was used as stimulus. hCG is a LH analogue and widely applied in clinical therapy. Before treatment, the serum-containing culture medium was removed from growing cells and washed with serum free DMEM/F12 medium. Thereafter KK-1 cells were treated with 1.5 IE hCG (diluted in serum-free medium) and incubated at 37°C for 8 h. Finally, the conditioned medium was collected and stored at −20°C for progesterone Enzyme Linked Immunosorbent Assay (ELISA). The cells were collected for protein analysis.

For pregnenolone measurements, the enzymes converting pregnenolone to progesterone and 17OH-pregnenolone need to be inhibited. Trilostane was used as inhibitor of 3β-Hsd and abiraterone acetate as an inhibitor of Cyp17a1. During the experiment, KK-1 cells were treated thereafter with 5 µmol trilostane (Sigma, Steinheim, Germany, Cat. no: SML0141) plus 17 nmol abiraterone acetate (Cayman Chemical, USA, Cat. no: 15148) for 30 min. Thereafter, the medium was removed and the cells were incubated with serum-free KK-1 cell culture medium containing 1.5 IE hCG plus trilostane and abiraterone acetate for 8 h.

Since KK-1 cells almost lack the enzyme Cyp17a1, in order to detect estrone and estradiol, Δ4-androstenedione was added as a precursor and FSH was used as stimulus. Before treatment, the serum-containing KK-1 cell culture medium was removed from growing cells, followed by washing with serum free medium. Thereafter the growing KK-1 cells were treated with 10µmol ∆4-Androstene-3,17-dione (Sigma, Steinheim, Germany, Cat. no: 46033) for 15 min. Thereafter, this medium was removed and the cells were treated together with 10 µmol ∆4-Androstene-3,17-dione plus 50ng/ml FSH (Sigma, Steinheim, Germany, Cat. no: F8174) in serum-free KK-1 cell culture medium for 24 h. At last the medium was collected for steroid measurement and proteins were measured prior to further application.

For determining whether the reduction of hormone production was StAR mediated or not, KK-1 cells were treated with 22(R)-hydroxy cholesterol (Santa Cruz, Cat. no: sc-205106) at 40 µmol for 8 h with/without hCG treatment.

3.2.3.2.2 Enzyme Linked Immunosorbent Assay (ELISA) for different steroids measurements

The cultured media was frozen at −20°C until assayed. Steroid concentrations were measured by using ELISA kits (DRG, Marburg, Germany) following the manufacturer's protocol (*http://www.drg-diagnostics.de/44-1-DRG+ELISAs.html*). In this study, five different ELISA kits were used for the following steroids: progesterone (Cat. no: EIA1561), pregnenolone (Cat. no: EIA4170), estrone (Cat. no: EIA4174), estradiol (Cat. no: EIA2693) and testosterone (Cat. no: EIA1559). The absorbance (OD) value of each sample was determined at 450±10 nm with a microtiter plate reader (LB941 Tris, Berthold Technologies, Germany). Before progesterone and pregnenolone measures, the collected media need to be diluted to 1:80 first. The final concentration of each sample was calculated corresponding to the standard curves. The values were calculated with an online ELISA analysis software (© Copyright 2012 Elisakit.com Pty Ltd). All steroids concentrations were normalized to appropriate protein concentrations.

3.2.4 Molecular biological experiments

3.2.4.1 Polymerase chain reaction (PCR)

3.2.4.1.1 RNA isolation from KK-1 cells and first strand cDNA synthesis by reverse transcription

After removing the culture medium, at least 1 ml of RNAzol® RT (Sigma-Aldrich, Germany, Cat. no: R4533) was added to KK-1 cells per 10 cm^2 of culture plate surface area. The resulting cell lysate was passed several times through a 1000 µl pipette tip to form a homogenous lysate. The lysate mixture was moved to a new Eppendorf tube where after 0.4 ml of RNase-free water was added per mL of RNAzol® RT used for homogenization. The sample was covered tightly and vigorously shook for 15 s. The sample was allowed to stand for 15 min at RT. Thereafter, the resulting mixture was centrifuged at 12,000 g for 15 min at 4°C. Subsequently, the supernatant was transferred to a new tube and 1x volume of 100%

isopropanol was added, mixed gently and the sample was allowed to stand for 10 min at RT. Thereafter, the mixture was centrifuged at 12,000 g for 10 minutes at 4°C and the RNA precipitated to a white pellet onto the bottom of the tube. The supernatant was carefully removed and the RNA pellets were washed twice with 0.4-0.6 ml 75% ethanol to remove contaminants. Thereafter, the RNA pellets were solubilized in 0.1% DEPC water (Sigma-Aldrich, Germany, Cat. no: D5758) at a concentration of 1-2 µg/µl. The quantity and integrity of the isolated RNA was analyzed with the NanoDrop™ 8000 Spectro-photometer and RNA 6000 Nano LabChips (Caliper Life Sciences GmbH, Mainz, Germany).

High quality isolated total RNA from KK-1 cells was reversely transcribed to cDNA using the High Capacity cDNA Reverse Transcription Kit (Applied Biosystems, Germany) according to the manufacturer's protocol. 1 µg total RNA was diluted in nuclease-free water to a volume of 10 µl and was added into 10 µl reverse transcriptase mix. The composition of 10µl reverse transcriptase mix is listed in Table 9. The mixture was then incubated in a Trio-Thermoblock at following conditions: 25°C for 10 min, 37°C for 2 h and 85°C for 5 min.

Table 9. The composition of 10 µl reverse transcriptase mix.

25xdNTP (100mM)	0,8 µl
10xRT buffer	2,0 µl
10xRT random primers	2,0 µl
MultiScribe™ reverse transcriptase	1,0 µl
Rnase inhibitor	1,0 µl
Nuclease-free H_2O	3,2 µl

3.2.4.1.2 Semi-quantitative polymerase chain reaction and agarose gel electrophoresis.

The PCR reaction mix (Eppendorf, Hamburg, Germany) is listed in Table 10. The PCR reaction was performed with a Bio-Rad iCycler C1000 (Bio-Rad Laboratories, München, Germany) using the following parameters: denaturation at 95°C for 2 min, followed by 35-45 cycles of: 1) denaturation at 95°C for 30 s, 2) annealing at 50-65°C for 1 min and 3) extension at 72°C for 1 min. A final extension step at 72°C for 7 min was added to complete the cDNA extension.

Table 10. The PCR reaction mix.

cDNA template	1,0 µl
10xRT buffer	2,5 µl
10Mm dNTPs	0,2 µl
Forward Primer	1,0 µl
Reverse Primer	1,0 µl
Tag DAN polymerase	0,2 µl
Sterile H_2O	19,1 µl
Totol volume	25 µl

The amplification of specific target genes was analyzed by agarose gel electrophoresis analysis of the RT-PCR products. A 2% agarose gel, containing 0.5 µg/ml ethidium bromide was prepared and electrophoresis was performed in 1 x TAE buffer. For RT-PCR reaction, 10 µl of the product was mixed with SYBR® Gold (Bio-Rad, Germany). In parallel, a DNA Ladder GeneRuler (100 bp) or 1000 bp ladder (Fermentas) was also added on the gel as a size marker. The gel was run at constant voltage of 90 V for 60 min at RT to separate the DNA bands. Following the electrophoresis, the gel was photographed under UV light by using the Gel-Doc 2000 documentation system (Bio-Rad Laboratories, München, Germany). The sizes of the RT-PCR products were estimated by comparing them to the bands of the DNA standers. The relative alterations of gene expression were analyzed by comparing thickness and intensity of the target gene to the 28S rRNA values which from the same samples processed in parallel on the same agarose gel. All sequences of specific primer sets of the genes analyzed with annealing temperature and size of amplified PCR products are listed in Table 11.

Table 11. Primers for Semi-quantitative polymerase chain reaction.

Gene Names	Forward primer(5'-3')	Reverse primer(5'-3')	Tm (°C)	Product (bp)
Abcd1	GAGGGAGGTTGGGAGGCAGT	GGTGGGAGCTGGGGATAAGG	65	465
Abcd2	TGCAAAATTCTGGGGAAGA	TGACATCAGTCCTCCTGGTG	58	405
Abcd3	CTGGGCGTGAAATGACTAGATTGG	AGCTGCACATTGTCCAAGTACTCC	64	523
Acox1	CTGAACAAGACAGAGGTCCACGAA	TGTAAGGGCCACACACTCACATCT	60	565
Acox2	CTCTTGCACGTATGAGGGTGAGAA	CTGAGTATTGGCTGGGGACTTCTG	58	688
Acox3	GCCAAAGCTGATGGTGAGCTCTAT	AGGGGTGGCATCTATGTCTTTCAG	55	813
Thiolase	TCAGGTGAGTGATGGAGCAG	CACACAGTAGACGGCCTGAC	60	241
Cat	ATGGTCTGGGACTTCTGGAGTCTTC	GTTTCCTCTCCTCCTCATTCAACAC	64	833
Cyp11a1	GCTGGAAGGTGTAGCTCAGG	TTCTTGAAGGGCAGCTTGTT	58	432
Gnpat	CCGTCTCCTTGAGACCTCTG	AGGTGTGGGAATCTGAGTGG	60	198
Gsr	CACTTGCGTGAATGTTGGATG	CCACAGTAGGGATGTTGTCATAG	58	944
Hsd17b4 (Mfp2)	GAGCAGGATGGATTGGAAAA	TGACTGGTACGGTTTGGTGA	60	223
Ehhadh (Mfp1)	ATGGCCAGATTTCAGGAATG	TGCCACTTTTGTTGATTTGC	56	211
Lh-r	ATGGATCCCTCTCACCTATCTCCCTGT	AGTCTAGATCTTTCTTCGGCAAATTCCTG	58	702
Sod1	AGCGGTGAACCAGTTGTGTTGT	CCACACAGGGAATGTTTACTGC	65	405
Sod2	AAGTAGGTAGGGCCTGTCCGATG	CTAAGGGACCCAGACCCAACAAG	58	624
Star	GTTCCTCGCTACGTTCAAGC	TTCCTTCTTCCAGCCTTCCT	58	292
3ß-Hsd	TCAATGTGAAAGGTACCC	ATCATAGCTTTGGTGAGG	55	499
28S rRna	CCTTCGATGTCGGCTCTTCCTAT	GGCGTTCAGTCATAATCCCACAG	65	254

Tm = Annealing temperature; bp = base pairs.

3.2.4.1.3 Quantitative real time-polymerase chain reaction

Quantitative real time-polymerase chain reaction (qRT-PCR) was performed with the IQ5® I cycler (Bio-Rad, Müchen, Germany). A SYBR Green PCR Master Mix (Applied Biosystems) was used according to the standard protocol provided by the manufacturer. Thermal cycling was carried out at 95°C for 3 min followed by 45 cycles with 1) denaturation at 95°C for 30 sec, 2) annealing at 60 °C for 45 s and 3) extension at 72°C for 1 min. The resulting cDNA levels were normalized to the ones of the stable references gene Gapdh. All sequences of specific primer sets of the genes analyzed are listed in Table 12.

Table 12. Primers for Quantitative real time-polymerase chain reaction

Gene Name	Sense 5'-3'	Antisense 5'-3'
Abcd1	ACAGTGCCATCCGCTACCTA	ATGAGCTACTAGACGGCTTCG
Abcd2	ATACACATGCTAAATGCAGCAGC	GCCAATGATGGGATAGAGGGT
Abcd3	TCAGAATGGGACGCTCATTGA	TGGCAGCGATGAAGTTGAATAA
Acox1	CCGCCACCTTCAATCCAGAG	CAAGTTCTCGATTTCTCGACGG
Acox2	ACGGTCCTGAACGCATTTATG	TTGGCCCCATTTAGCAATCTG
Acox3	TTCTAGTGCTGATTAACTGCCTG	AGAAACGAAAACTGTGGTTCCAA
Agps	TGTCCTCCGTGTCTGTTCCT	CATGGTACAACCTGCCCTTC
Akap1	GAAGGAGGAGCTGTCAGACTTA	CGTCAGAACCTCCTGAGTGAT
Catalase	TGGCACACTTTGACAGAGAGC	CCTTTGCCTTGGAGTATCTGG
Cyp11a1	GGCTAAACCTGTACCACTTCT	CCCAGCTTCTCCCTGTAAAT
Ehhadh (Mfp1)	AATACAGCGATACCAGAAGCCA	CCAGCTCTAGTCCTCCTCCA
Gapdh	AACTTTGGCATTGTGGAAGG	GGAGACAACCTGGTCCTCAG
Gnpat	GTGTTACGATGCGCTGTCTT	GCAGGCCCGTTCACATAATA
Hsd3b1	CTCAGTTCTTAGGCTTCAGCAATTAC	CCAAAGGCAGGATATGATTTAGGA
Hsd17b4 (Mfp2)	TTAGGAGGGGACTTCAAGGGA	TCGCCTGCTTCAACTGAATCG
Pex13	TGGATATGGAGCCTACGGAAA	CGGTTAAAGCCCAAACCATTG
Star	ATCATTGTGCCGACTTCC CTAC	ACCAGGTTAGCCTCAGTA TTAGA
Scp2	TGGGTGGTGGATGTGAAGAA	TGAAAGAAGGCCGACTGAGG
Sod1	AAAATGAGGTCCTGCACTGG	AACCATCCACTTCGAGCAGA
Sod2	GGGAGCACGCTTACTACCTTC	GAGCCTGGCACTCAATGTG
Thiolase	TCTCCAGGACGTGAGGCTAAA	CGCTCAGAAATTGGGCGATG

3.2.4.2 Transfection of KK-1 cells with siRNA

3.2.4.2.1 *Pex13* knock down in KK-1 cells by RNAi

Pex13 siRNA with the (sense: GCUAUAGCCCUUAUAGUUATT; antisense: UAACUAUAAGGGCUAUAGCTT, Cat. no: GEHC1-000790 (SO-24886576), Dharmacon, Germany) was used in this study to knockdown the *Pex13* gene in KK-1 cells, scrambled siRNA (Qiagen, Germany, Cat. no: 1027280, the sequence of it is proprietary to the company) was used as the negative control for the siRNA reaction in parallel. To knock down the *Pex13* gene expression KK-1 cells were transfected with ScreenFect®A transfection reagent purchased from InCella (Eggenstein-Leopoldshafen, Germany. Cat. no: S-3001) according to the manufacturer's protocol. $1{,}25 \times 10^5$ KK-1 cells were seeded onto each 6-well plate and grown for 24 h before transfection. For the transfection, 4,5 µl of ScreenFect®A was first diluted to a final volume of 120 µl in dilution buffer and mixed thoroughly. Thereafter 4,5 µl of 10 µmol

siRNA was diluted to a final volume in 120 µl supplied dilution buffer. Subsequently, the diluted ScreenFect®A and *Pex13* siRNA mixture were combined and immediately mixed by using several pipette strokes. Complex formation was allowed to proceed at RT for 20 min. In the meantime, the cell culture medium was exchanged to 1250 µl fresh standard DMEM/F12 medium containing 10% FBS without antibiotics in a 6-well plate. After 20 min, the final pre-incubated solution with the *Pex13* siRNA mixture complex was added to one well drop wise. The final working concentration for the *Pex13* siRNA was 30 nmol. Transfected KK-1 cells were incubated for 48 h at 37 °C in the cell culture incubator before any further application.

3.2.4.2.2 Akap1 protein overexpression in KK-1 cells

3.2.4.2.2.1 Transformation of E.coli DH5α with an AKAP1-overexpression plasmid

One µl PCMV sport plasmid with the full open reading frame of Akap1 was added to 50 µl E. coli DH5α and mixed by gently tapping the tube and thereafter incubated 15 min on ice. Following the incubation, cells in the tube were heat-shocked at 42°C for 90 s with subsequent immediate cooling on ice for 2 min. Thereafter, 500 µl of SOC medium were added to the tube and incubated at 37°C for 30 min at 300 rpm on a rotary shaker. The grown transfected E.coli cells were spread on LB-Ampicillin plates prepared in advance and the plates were incubated upside-down at 37°C overnight. The next morning, to 3 ml of LB medium, 100 µl of Neomycin (50 mg/ml) were added and mixed. The incubated plates with bacteria colonies were taken out of the incubator and a single colony was picked up with a pipet tip and then added into the Neomycin containing medium. The bacteria were grown in the LB/Neomycin medium overnight at 37°C in the Aquatron shaking bacterial incubator. All solutions and materials which were used for the plasmid transformation are listed in table 13.

Table 13. Media for bacterial growth and transfection.

LB medium	0.17 M sodium chloride, 1% Trypton, 0.5% Yeast extract, pH 7.0
LB-Agar	LB medium, 1g/50 ml Agar, 100 µg/ml Ampicillin or 50 µg/ml Neomycin
SOC	Tryptone 2% (w/v), yeast extract 0.5% (w/v), NaCl 10 mM, KCl 2.5 mM, pH 7.0, the solution was autoclaved, then 20mM of glucose was added

3.2.4.2.2.2 Midi prep plasmid preparation

On the third morning, the cultured medium was centrifuged at 6,000 rpm for 10 min at 4°C according to 'High-copy plasmid purification protocol' from EF-Midi plasmid isolation kit (NucleoBond® Xtra Midi EF, Macherey-Nagel, Cat. no: REF740420.50). After removal of the supernatant, the bacterial pellet was resuspended in 8 ml of Res-EF buffer, followed by the addition of 8 ml of lysis buffer. The mixture was gently inverted for around 5 times and incubated at RT for 5 min. In parallel, the NucleoBond® Xtra column together with the inserted filter was equilibrated with 15 ml EQU-EF Buffer. Thereafter, 8 ml of the neutralization buffer NEU-EF was added to the lysate. The tubes were gently inverted until the blue sample became colorless and incubated on ice for 5 min. Thereafter, the solution was loaded onto the column. The column and the filter which contained the sample were washed with 5 ml of buffer FIL-EF. After removing the filter, the column was washed with 15 ml of Wash-EF buffer followed by a two times wash with 35 ml ENDO-EF buffer. The DNA was eluted by adding 5ml of ELU-EF buffer. The eluted plasmid was precipitated with 3.5 ml isopropanol and then centrifuged at 8,500 rpm for 1h at 4°C. The pellet was washed 2 times with 2 ml of 70% Ethanol-EF. At the end, the plasmid was dissolved in an appropriate volume of TE-EF buffer.

3.2.4.2.2.3 Overexpression of Myc-tagged Akap1

To overexpress the Akap1 gene in KK-1 cells, Akap1 was cloned in a myc-tag vector. Two types of recombinant Akap1-plasmids were used for the protein overexpression analysis, leading to a myc tag at the amino terminus (Akap1-3b plasmid) or a myc-tag at the carboxyl terminus (Akap1-5b plasmid) of the fusion protein. Myc-tagged GFP was used as a control in this experiment. Both myc-tagged Akap1 plasmid and the myc-tagged GFP were constructed by Wenwen Wang, a former doctoral student of

Prof. Baumgart-Vogt [179]. Similar to the protocol for *Pex13* siRNA transfection, 1,25x10^5 cells in one well were seeded onto each 6-well plate 24 hours before transfection. First 6 µl of ScreenFect®A were diluted to a final volume of 120 µl in dilution buffer and mixed thoroughly. Then 1000 ng plasmid DNA was diluted in a final volume of 120 µl supplied dilution buffer. Subsequently, the diluted ScreenFect®A and the plasmid solution were combined and immediately mixed by using several pipette strokes. Complex formation was induced at RT for 20 min. In the meantime, the cell culture medium was exchanged to 1250 µl fresh standard DMEM/F12 medium containing 10% FBS without antibiotics in a 6-well plate. After 20 min, the final incubated solution with the plasmid mixture complex was added drop wise to one well. Transfected KK-1 cell cultures were incubated for 24 h at 37 °C in the cell culture incubator before any further application.

3.2.4.2.3 *Pex13* siRNA and Akap1 plasmid double transfection

KK-1 cells were first transfected with *Pex13* siRNA followed after 24 h by plasmid transfection with the distinct myc-tagged Akap1 and GFP plasmid. The exact transfection procedures are described above. After the second transfection with the Akap1 plasmids, the KK-1 cells were incubated for another 24 h at 37 °C in the cell culture incubator before any further application.

3.3 Statistical Analysis

All results presented in this thesis were collected from at least 3 independent experiments. The Graph pad 6.0 software was used for statistical analysis and bar chart drawings. Each column of bar charts represents the mean value for each experimental group. Standard errors (SE) of all groups are represented by error bars on each column. For paired data, the student t-test was chosen and for multi-paired data the ANOVA test was used to examine the statistical difference between experimental groups. $p \leq 0.05$ * , $p \leq 0.01$**, $p \leq 0.001$*** and **** $p \leq 0.0001$ were considered as statistically significant.

4 Results

The results of this thesis are partitioned into two different parts. The first one described the distribution of peroxisomes in different cell types of the mouse ovary and the regulation of peroxisomes during folliculogensis. The second part focusses on peroxisomal functions on steroid metabolisms.

4.1 Part 1: Investigation of peroxisomal functions during mouse ovarian folliculogenesis

4.1.1 Regulation of peroxisomal enzymes during follicular maturation

Figure 8 shows the H&E staining of mouse ovarian follicles during their development process. The different stages in order of occurrence are named: primordial follicle, primary follicle, pre-antral follicle (secondary follicle), antral follicle (tertiary follicle), and pre-ovulatory follicle. In the ovary, oocytes are covered on their surface with epithelial cells, named granulosa cells, building up follicles that are growing and expanding their numbers. A typical pre-antral follicle is composed of a central oocyte surrounded by multiple layers of granulosa cells and bulding up theca cells in the outer layer. During antral follicular phase, the oocyte will be released from the ovary into the fallopian tube for fertilization under LH stimulation. The remainder of the follicle will develop into a corpus luteum.

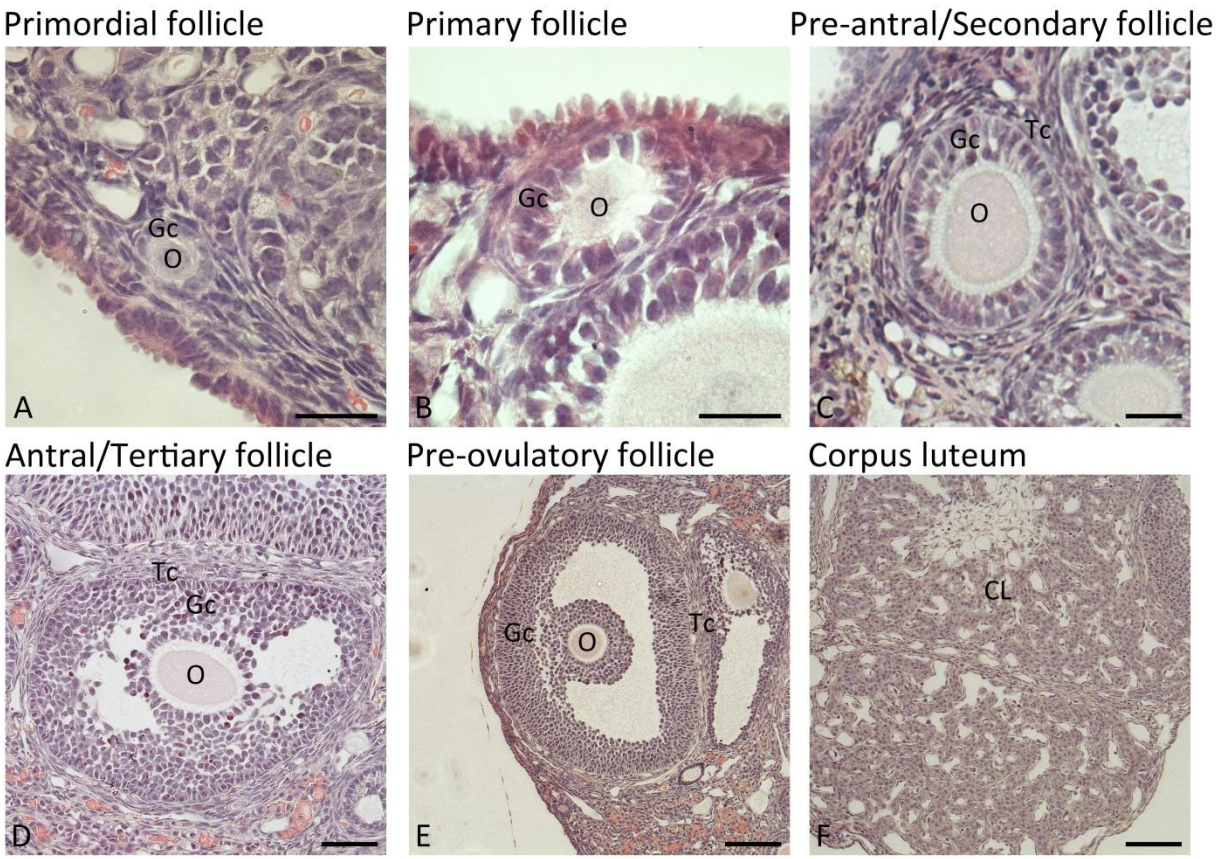

Figure 8. HE staining for adult mouse ovary. The different stages of follicle development are presented in this picture. “O” represents oocyte, ”Gc” represents granulosa cells, “Tc” represents theca cells and “CL” represents corpus lutuem. Scale bar = 20 µm for A, B and C; Scale bar = 40 µm for D, Scale bar = 80 µm for E and F.

In the past, people believed that peroxisomes are scarce in oocytes because in these cells their typical marker enzyme, catalase, is only very low abundant as shown in Figure 9 A-C. At higher magnification and with higher exposure time we could however, prove the presence of catalase within the oocyte (Figure 9B, inset). In which besides some intensively stained organelles at the surface, many weakly stained peroxisomes are visible (Figure 9B, inset). In comparison to oocyte, calatase is highly abundant in granulosa cells as well as interstitial cells in the ovary. Because of the low expression of catalase in the peroxisomal matrix in oocytes we decided to use the peroxisomal marker PEX14p to identify peroxisomes in mouse oocytes (Figure 9D-F), a peroxisomal biogenesis protein in the membrane of all peroxisomes. The IF results showed that PEX14p is highly abundant and that peroxisomes are indeed very numerous in oocytes of antral follicles. After careful observation, we also found that PEX14p was more strongly labelled in the peroxisomes of oocytes than

the neighboring granulocytes, as opposed to the observation of catalase. Moreover, peroxisomes were more numerous in oocytes of antral follicles compared with the ones in oocytes of primary follicles, suggesting the proliferation of these organelles during folliculogenesis and oocyte maturation. We also investigated the distribution of another important peroxisomal matrix protein, namely GNPAT (glyceronephosphate acyltransferase) in distinct follicular stages. Interestingly, GNPAT , which is involved in plasmalogen synthesis, lipids responsible for trapping ROS, was strongly induced within the oocyte during folliculogenesis (Figure 9 G-I). We further observed that PEX14p, catalase as well as GNPAT were all particularly abundant in the inner layer of the granulosa cells directly facing the oocyte in late primary and early pre-antral follicles (Figure 9 A,B,D,E,H arrow labled), but not in antral follicles (Figure 9 C,F,I).

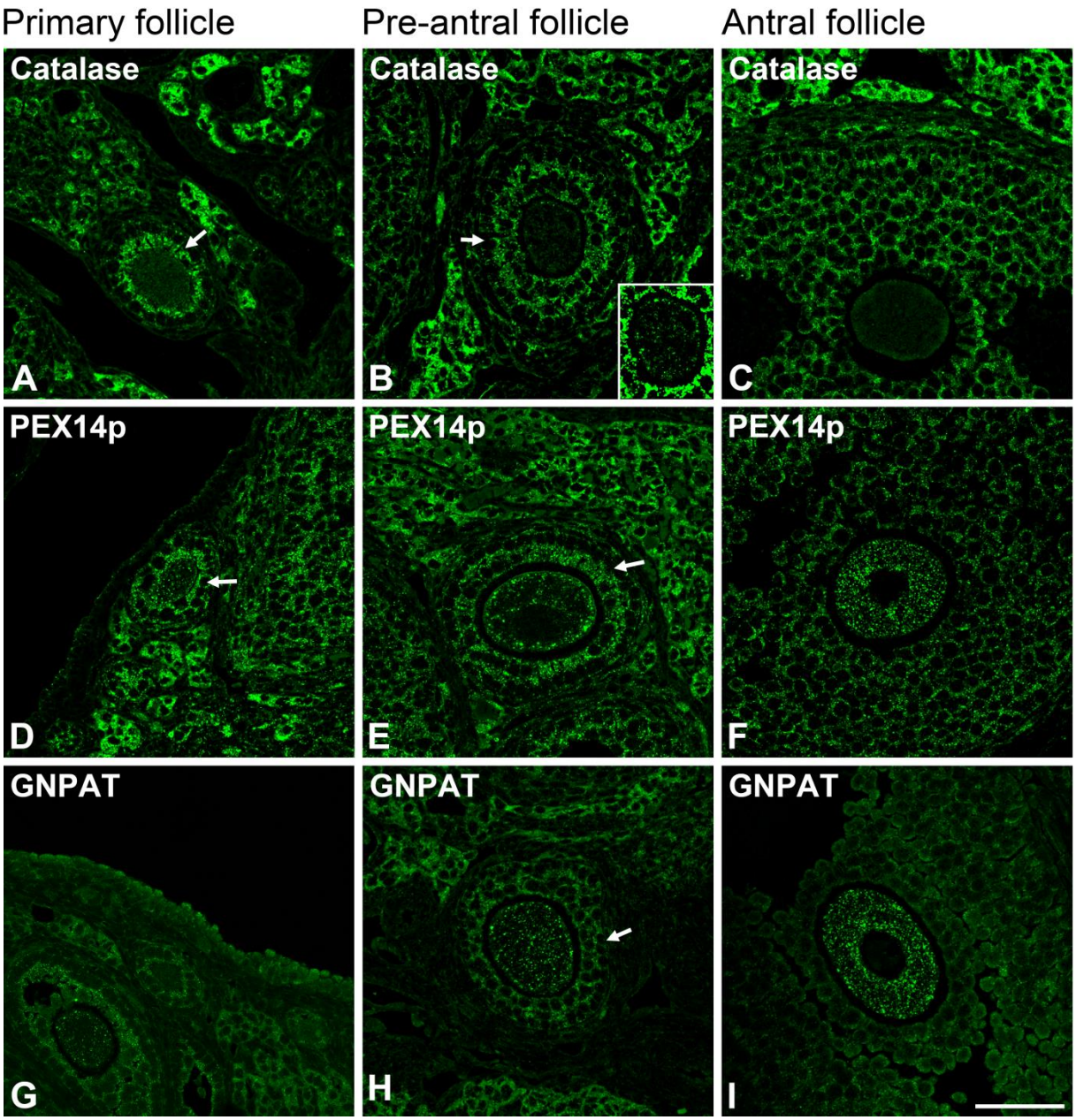

Figure 9. PEX14p and GNPAT expression in oocytes were up-regulated during follicular development while catalase was barely stained in the oocyte. (A-C) Catalase. (D-F) PEX14p: Peroxin 14. (G-I) GNPAT: glyceronephosphate acyltransferase. Scale bar = 40 µm for all images.

During follicular maturation, only few follicles mature into pre-ovulatory follicles under the stimulation of FSH while the rest of them degenerate. As shown in Figure 10 (arrow), in the degenerating oocytes the antibody against peroxisomal membrane protein PEX14p and the matrix enzyme GNPAT labelled *"cluster"* structures in the oocyte.

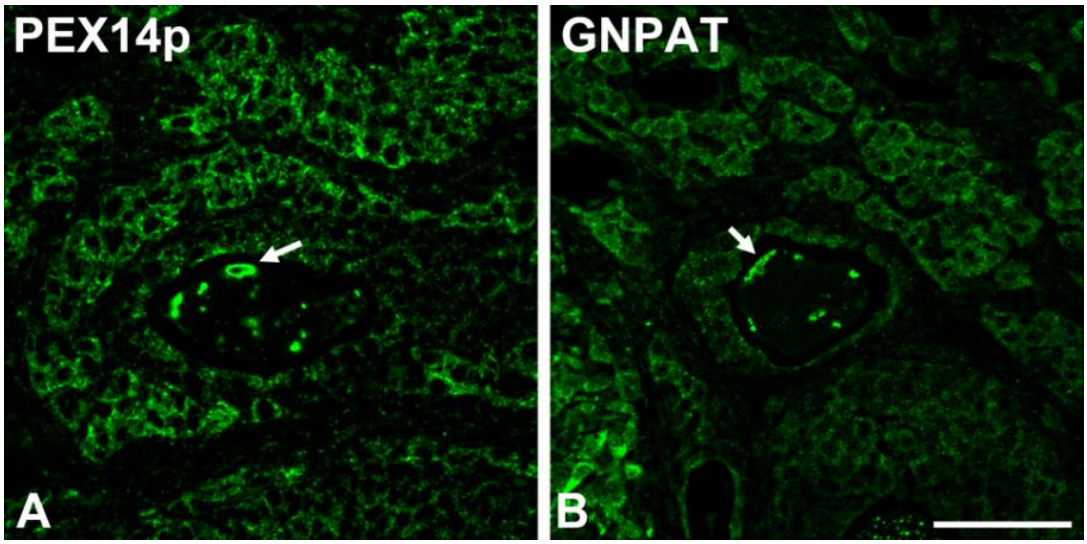

Figure 10. IF staining of PEX14p and GNPAT in degenerating oocytes. (A) PEX14p: Peroxin 14. (B) GNPAT: glyceronephosphate acyltransferase. Scale bar = 40 µm for both images.

After the mature ovum is released from the follicle by the ovulation process for fertilization, in the second half of the ovarian cycle a corpus luteum (CL) is formed [180]. Induced by the luteinization hormone, granulosa cells differentiate into granulosa lutein cells and theca interna cells develop into theca lutein cells, both constituting the parenchyma of the corpus luteum. In granulosa lutein cells, a high number of peroxisomes with strong PEX14p protein abundance were detected (Figure 11 A and B). However, already in the PEX14p staining, heterogeneity in the peroxisome content of individual granulosa lutein cells were noted, with many of them showing a very high number of the organelles, while others exhibiting less peroxisomes. Similarly, also PEX5p was higher abundant in large granulosa lutein cells, apparently also being attached to the peroxisomal surface, suggesting a high matrix protein import into theses organelles (Figure 11 C and D). Indeed, also catalase was heterogeneously present in distinct granulosa lutein cells, with larger cells showing high amount of this protein in numerous peroxisomes (Figure 11 E and F). In addition, also the lipid transporter ABCD3 showed a complete heterogeneous staining pattern of granulosa lutein cells (Figure 11 G and H). By comparing the staining intensities between neighboring interstitial cells with an organelle stained granulosa cells, it was seen that except for the PEX5p abundance, interstitial cells were more intensively labelled with peroxisomal markers.

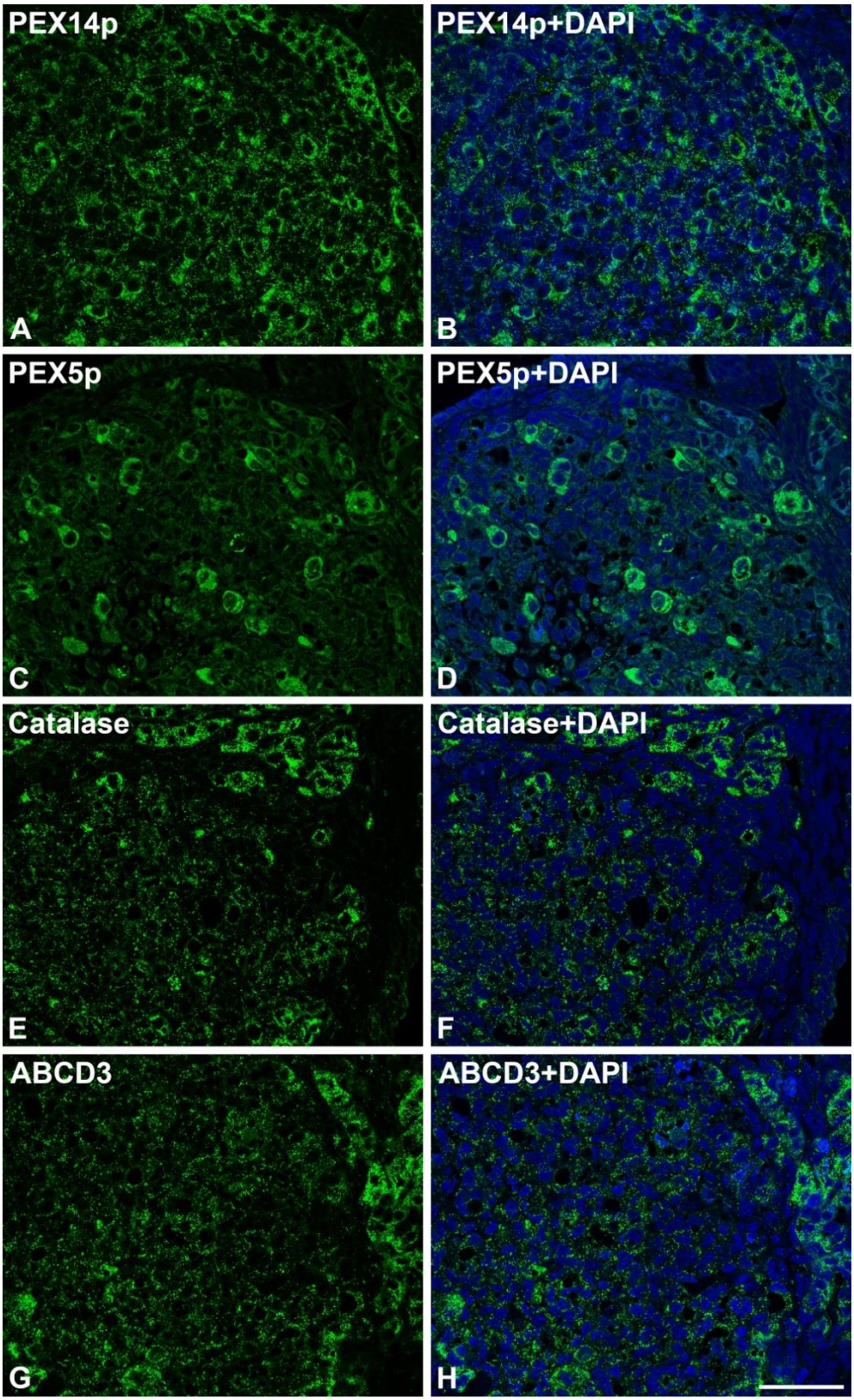

Figure 11. IF staining of peroxisomal enzymes in corpus luteum of mouse ovary. (A) (B) PEX14p: Peroxin 14. (C) (D) PEX5p: Peroxin 5. (E) (F) Catalase. (G) (H) ABCD3: ATP-binding cassette transporter 3. Nuclei were counterstained with TOTO-3 iodide (blue). Scale bar = 40 μm for all figures.

4.1.2 SOD2 and glutathione reductase regulation during follicular maturation

Since it is known that peroxisomes cooperate with mitochondria for fatty acid degradation and oxidative stress management, we were interested to examine also the distribution of mitochondria during follicular development by using antibody against specific marker enzyme SOD2 involved in ROS metabolism. In addition, glutathione reductase, which is located in the cytoplasm and is involved in ROS degradation, was also investigated using immunofluorescence staining. As shown in Figure 12, SOD2 was highly abundant in interstitial cells as well as in granulosa cells. In comparison to what we observed for catalase, PEX14 and GNPAT, the SOD2 content in the oocyte remained stable during folliculogenesis (Figure 12 A and B), Interestingly, glutathione reductase (GR) was very abundant in the oocyte of primordial and primary follicles, while it was reduced in pre-antral follicles (Figure 12 C and D). In contrast to the oocyte, GR was much less abundant in granulosa cells and interstitial cells in the ovary (Figure 12C and D).

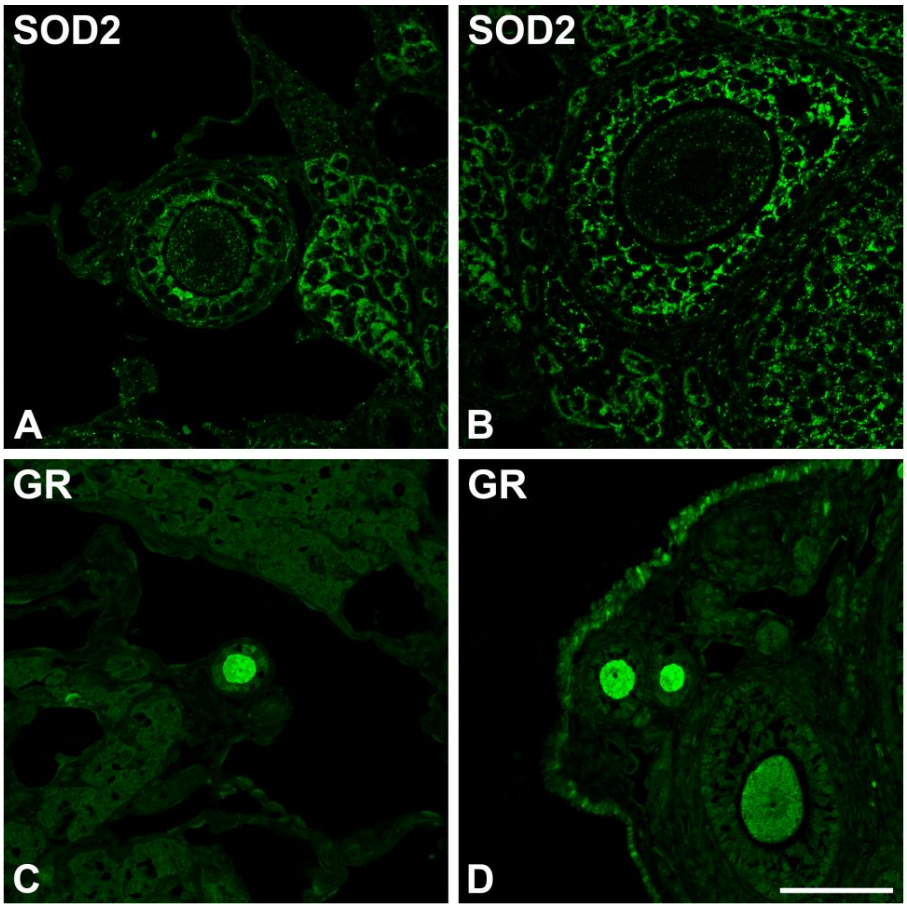

Figure 12. IF staining of mitochondrial SOD2 and cytoplasmic glutathione reductase in mouse ovary. (A) (B) IF staining for SOD2: superoxide dismutase 2. (C) (D) IF staining for GR: glutathione reductase. Scale bar = 40 µm for all figures.

4.2 Part 2 Investigation of peroxisomal functions on steroidogenesis in mouse granulosa tumor cell lines— KK-1 cells

To analyze peroxisomal function in steroid synthesis, we used the murine ovarian granulosa tumor cell line KK-1, which has been developed using a transgenic mouse model [176]. This cell line displayed a dose-dependent increase in cAMP production in response to hCG as well as FSH. The cells express the LH and FSH receptors at early passages and contain most of the granulosa cell´s steroidogenic enzymes [181].

We first characterized peroxisome expression in the KK-1 cell line and then used LH analogue human chorionic gonadotropin (hCG), a hormone that is also clinically used to trigger ovarian steroidogenesis.

4.2.1 Peroxisome abundance in KK-1 granulosa cells

The IF results showed that peroxisomal proteins PEX14p and catalase are highly abundant in KK-1 cells. Moreover, peroxisomes were very numerous (Figure 13), similarly to what we observed for mouse ovary granulosa cells in situ, suggesting that the KK-1 cells are a suitable model to investigate the role of peroxisomes in steroidogenesis in this cell type**.**

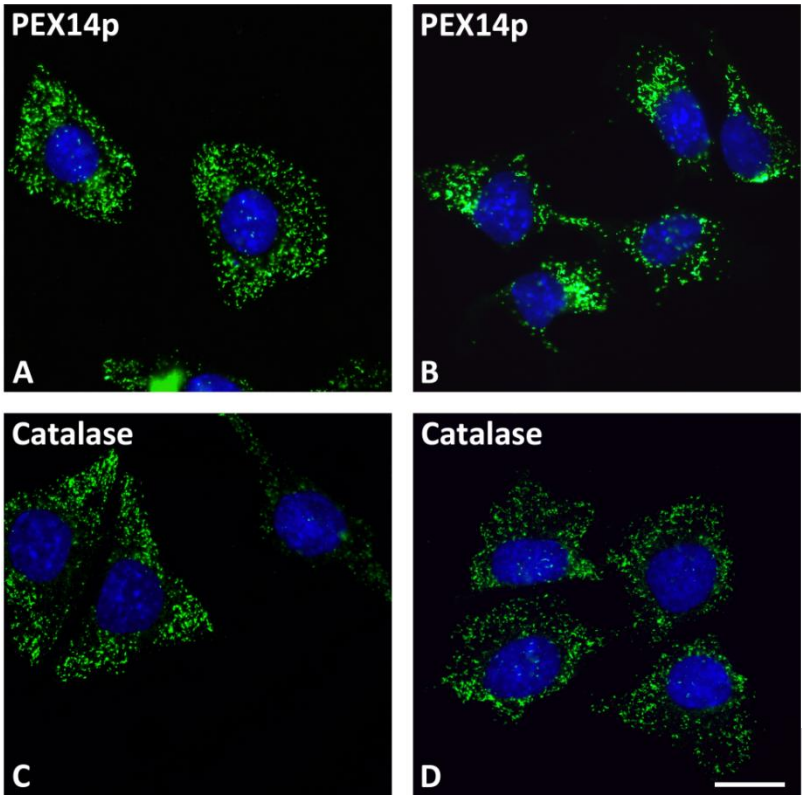

Figure 13. IF staining for the peroxisomal markers Peroxin 14 (PEX14p) and catalase in KK-1 granulosa cells. (A) (B) PEX14p: Peroxin 14. (C) (D) Catalase. Scale bars = 15 µm.

4.2.2 KK-1 granulosa cells respond to hCG and FSH treatment and produce higher amount of steroids

To stimulate steroidogenesis, the KK-1 cells were treated with hCG for 8h. After that, we measured the expression of steroidogenic genes (*Lh-r, Star, Cyp11a1* and *3β-Hsd* were measured) at the mRNA level using semi-quantitative PCR. The results showed that all genes involved in steroidogenesis were up-regulated after hCG treatment and the *Star* mRNA exhibited the highest upregulation (Figure 14A). In accordance with the mRNA levels, Western blots showed that the protein levels of StAR and CYP11A1 were both strongly increased after hCG stimulation (Figure 14B). To determine the capability of KK-1 cells to secrete steroid hormones, ELISA measurements following the hCG treatment were carried out. The highest pregnenolone levels were measured after hCG stimulation in combination with the inhibitions of the activities of *3β-Hsd* and *Cyp17a1* using trilostane and abiraterone acetate respectively (Figure 14C). Also, the synthesis of progesterone was strongly stimulated after hCG (1,5 IE) treatment (Figure 14D). To measure estradiol, 10µmol ∆4-Androstene-3,17-dione was added as precursor and then KK-1 cells were treated with different concentrations (10 ng/ml to100 ng/ml) of FSH plus ∆4-Androstene-3,17-dione for 24h. The results indicated that 50 ng/ml FSH was the optimal concentration for stimulating estradiol synthesis (Figure 14E). According to our results, KK-1 cells are responsive to hCG and to FSH treatment as suggested also in the literature, making the cell a qualified model to study peroxisomal functions in steroidogenesis. The determined optimal conditions for the stimulation of steroidogenesis in KK-1 cells were employed for further experiments on the role of peroxisomes on steroidogenesis.

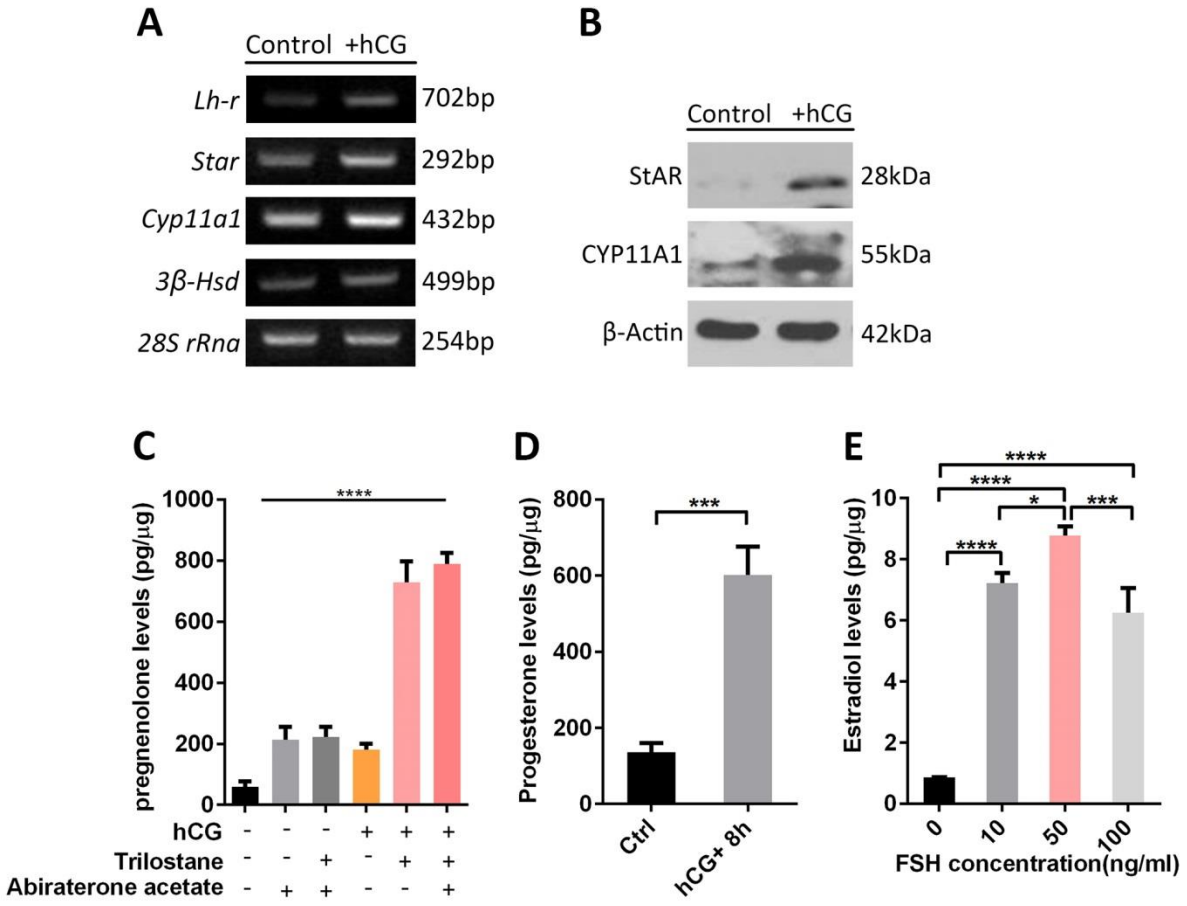

Figure 14. Steroid synthesis is stimulated after treatment with human chorionic gonadotropin (hCG) and follicle-stimulating hormone (FSH). (A) Semi-quantitative PCR results for detecting mRNAs of steroidogenic genes after hCG treatment. *28S-rRna* was used as internal control. *Lhr*: luteinizing hormone receptor; *Star*: steroidogenic acute regulatory protein; *Cyp11a1*: cytochrome P450 side-chain cleavage enzyme; *3β-Hsd*: 3-beta-hydroxysteroid dehydrogenase. (B) Western blot results for detecting steroidogenic enzymes after hCG treatment. β-actin was used as loading control. (C) Pregnenolone determination in the culture medium of KK-1 cells using ELISA. (D) Progesterone determination in the culture medium of KK-1 cells using ELISA. (E) Estradiol determination in the culture medium of KK-1 cells using ELISA. (*$p \leq 0.05$, ** $p \leq 0.01$, *** $p \leq 0.001$, **** $p \leq 0.0001$) (N=3). All data are means ± SD.

4.2.3 Regulation of the peroxisomal compartment involved in fatty acid transport and β-oxidation under hCG treatment

To study peroxisomal regulation in steroid biosynthesis, we investigated the expression of peroxisome-related genes and the abundance of peroxisomal proteins involved in fatty acid transport and β-oxidation. Both semi-quantitive (Figure 15A) and real time PCR results (Figure 15B) revealed that many of the investigated mRNAs are up-regulated after hCG treatment. These mRNAs encode the ABCD3 transporter (possibly involved in steroid transport), the acyl-CoA oxidase 3 (ACOX3), the 17beta

hydroxysteroid dehydrogenase 4 (17bHSD4 / MFP2), the peroxisomal 3-keto-acyl-CoA thiolase, and sterol carrier protein x (SCPx). In accordance with the PCR results, also Western blots confirmed the upregulation of peroxisomal enzymes involved in beta-oxidation after hCG treatment (Figure 15C), suggesting that the peroxisomal compartment is strongly activated by the action of this hormone through gonadotropin receptors.

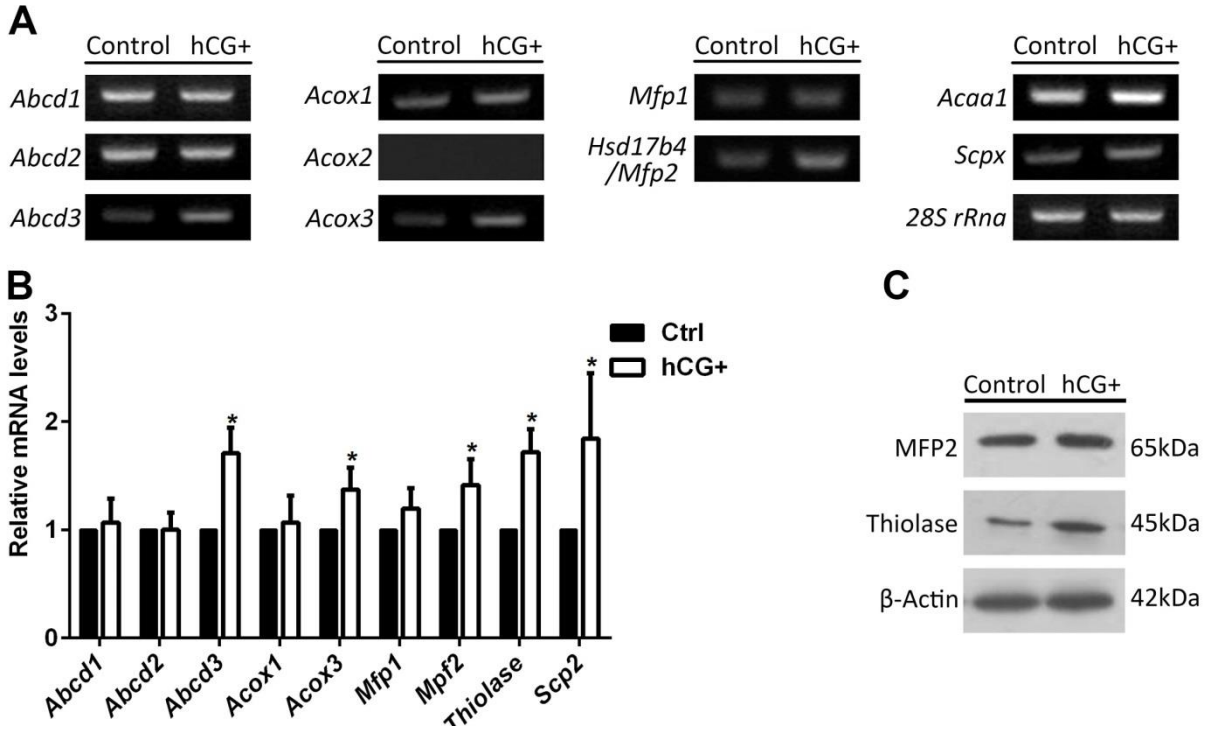

Figure 15. PCR and Western blot results revealed that peroxisomal fatty acid transport and β-oxidation are up-regulated after treatment with hCG. (A) Total RNA derived from hCG-stimulated (hCG+) and not-hCG-stimulated (control) KK-1 cells was analyzed by semi-quantitive PCR to determine the expression levels of genes coding for peroxisomal β-oxidation enzyme. *28S rRna* was used as internal control (B) Total RNA from hCG-stimulated (hCG+) and not-hCG-stimulated (control) KK-1 cells was analyzed by q-RT PCR to determine the expression levels of genes coding for peroxisomal β-oxidation enzymes. *Gapdh* was used as internal control. (C) Comparative Western blot analyses to examine the peroxisomal β-oxidation enzymes 17β-HSD4 (MFP2) and Thiolase in KK-1 cells after hCG treatment. (*$p \leq 0.05$) (N=3). All data are means ± SD.

4.2.4 Regulation of peroxisomal metabolism involved in ROS degradation under hCG treatment

We further examined the genes and proteins linked to the peroxisomal metabolic pathways involved in ROS degradation. The mRNA levels of *catalase* and the mRNA levels of *Gnpat and Apgs*, which two enzymes are involved in the synthesis of ROS-

trapping ether lipids (plasmalogens) were measured. Their mRNA levels were significantly elevated after hCG treatment, which was further confirmed by qRT-PCR (Figure 16 A and B). In accordance with the mRNA levels, the protein abundance of catalase and GNPAT were also increased (Figure 16C).

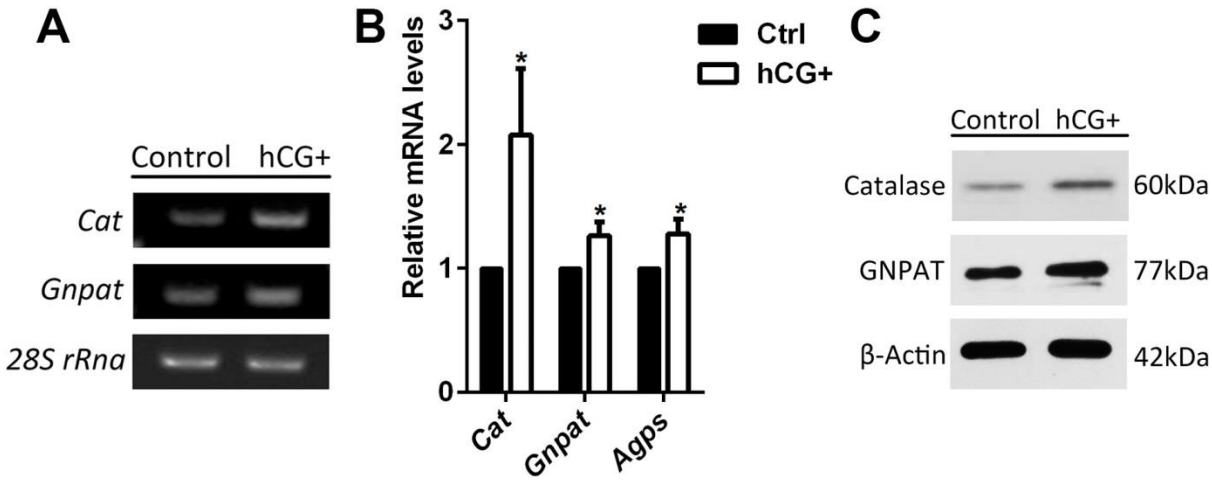

Figure 16. PCR and Western blot results indicated that peroxisomal antioxidative metabolism is activated after hCG stimulation. (A) Total RNA derived from hCG-stimulated (hCG+) and not-hCG-stimulated (control) KK-1 cells was analyzed by semi-quantitive PCR to determine the expression levels of genes coding for peroxisomal anti-oxidative genes by semi-quantitive PCR. *28S rRna* was used as internal control. (B) Total RNA derived from hCG-stimulated (hCG+) and not-hCG-stimulated (control) KK-1 cells was analyzed by qRT-PCR to determine the expression levels of genes coding for peroxisomal anti-oxidative enzymes. *Gapdh* was used as internal control. (C) Western blot analyses to examine the peroxisomal anti-oxidative enzyme catalase and the GNPAT protein contents in KK-1 cells after hCG treatment. (*$p \leq 0.05$) (N=3). All data are means ± SD.

4.2.5 Establishment of a siRNA- mediated *Pex13* knock-down in KK-1 cells to induce peroxisome deficiency

Since we have demonstrated that the peroxisomal metabolism was induced after hCG stimulation, we speculated that peroxisomes may be involved in the synthesis of steroids in granulosa cells. To further investigate the putative involvement of these organelles in steroidogenesis we established a KK-1 cell peroxisome deficiency model. For this purpose, the *Pex13* gene was knocked down in KK-1 cells. PEX13p is a peroxisomal membrane protein of the peroxin family which functions as membrane docking factor and is responsible for matrix protein import into the organelle. As demonstrated by Western blotting (Figure 17A), a strong down

regulation of the PEX13 protein was observed after 48 h of transfection induced by the *Pex13*-siRNA (75% knock-down as shown in Figure 17B).

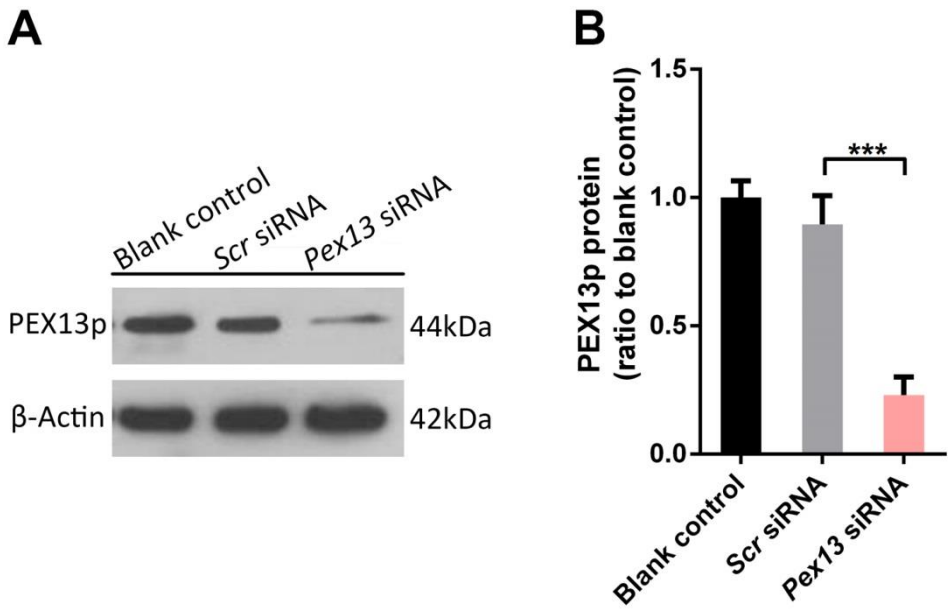

Figure 17. The abundance of the PEX13 protein was significantly diminished in *Pex13*-siRNA transfected KK-1 cells. (A) Protein expression of PEX13p was analyzed by Western blotting. Three experimental groups were analyzed: the blank group was incubated with transfection reagent only; the control group was transfected with scrambled siRNA (*Scr* siRNA); the knock-down group was transfected with *Pex13* siRNA. (B) The PEX13p band intensities of all different groups were analyzed with the Image J software ("gels" program). Three independent experiments were performed. (*** $p \leq 0.001$). All data are means ± SD.

Since peroxisomal matrix protein import is blocked by the depletion of PEX13p, catalase was not correctly imported into the peroxisomal matrix and was mis-targeted to the cytoplasm as shown by IF (Figure 18). This demonstrates that a real deficiency of the peroxisomal matrix protein import was induced in KK-1 cells. This deficiency in matrix protein import is typically observed in fibroblasts of Zellweger syndrome patients with the most severe peroxisomal disorders.

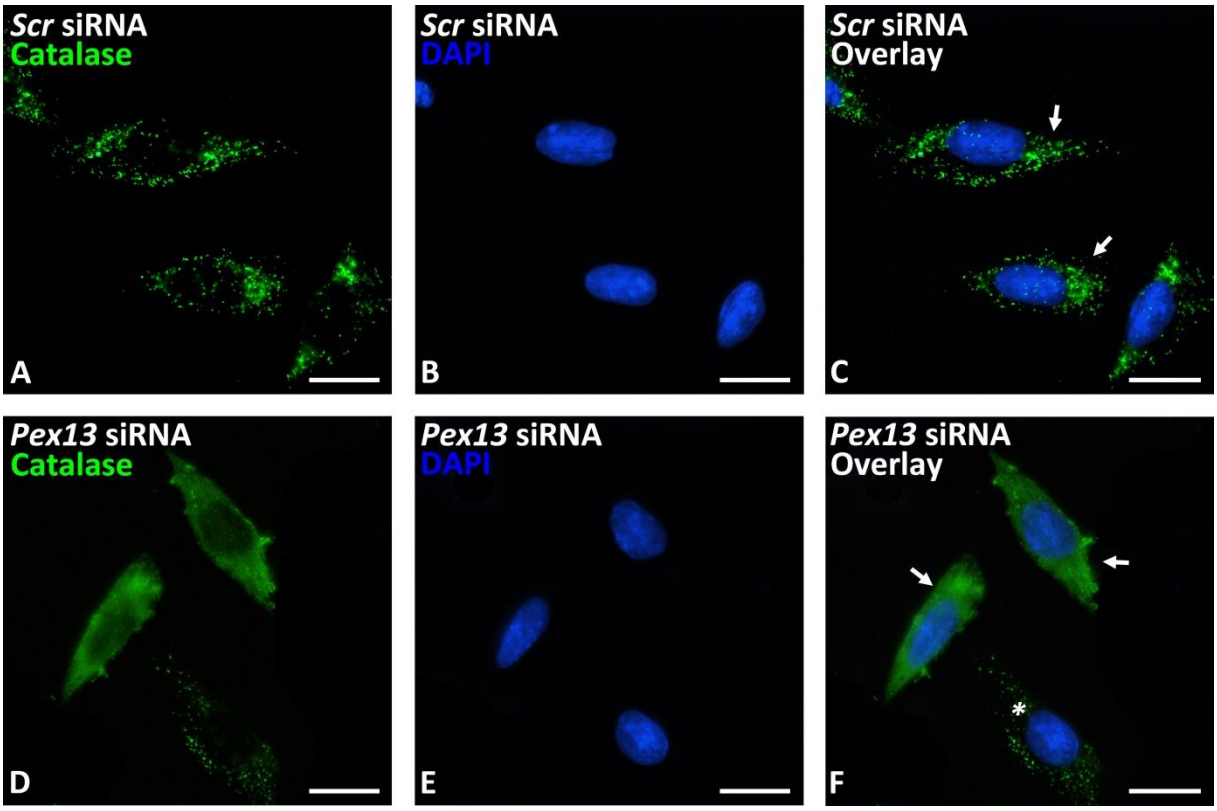

Figure 18. Peroxisomal catalase is mistagerted to the cytoplasm due to the matrix protein import defect induced by the *Pex13* KD in KK-1 cells. Immunofluorescence staining of catalase was performed to examine the consequence of *Pex13* KD on the peroxisomal compartment. (A) - (C) Catalase in control cells is localized inside of peroxisomes. (D) - (F) Catalase was mis-localized to the cytoplasm (arrow) as comparison with the punctuate pattern in a non-transfected cell shows (asterisk). Nuclei were counterstained with DAPI (blue). Scale bars represent: 20 µm.

4.2.6 Impact of *Pex13* knock-down on steroid synthesis under hCG treatment

Using the optimal conditions which have determined before, the effect of the *Pex13* KD on the synthesis of pregnenolone and progesterone was analyzed. ELISA measurement revealed that the secretion of pregnenolone and progesterone was 49% and 47% down-regulated when peroxisomes were dysfunctional (Figure 19 A and B). No significant effect was noted on estrone synthesis under ∆4-androstendione supplementation conditions. ∆4-androstendione is a direct precursor of estrone, suggesting that the aromatase activity was not influenced by the *Pex13* KD (*p*= 0,4451) (Figure 19C). In contrast to the values for estrone, FSH induced estradiol levels were 45% downregulated after *Pex13* KD, indicating an alteration in the activity of a 17beta hydroxysteroid dehydrogenase (Figure 19D). Whether this is due to the dysfunction of peroxisomal 17bHSD4 has to be analyzed in the future.

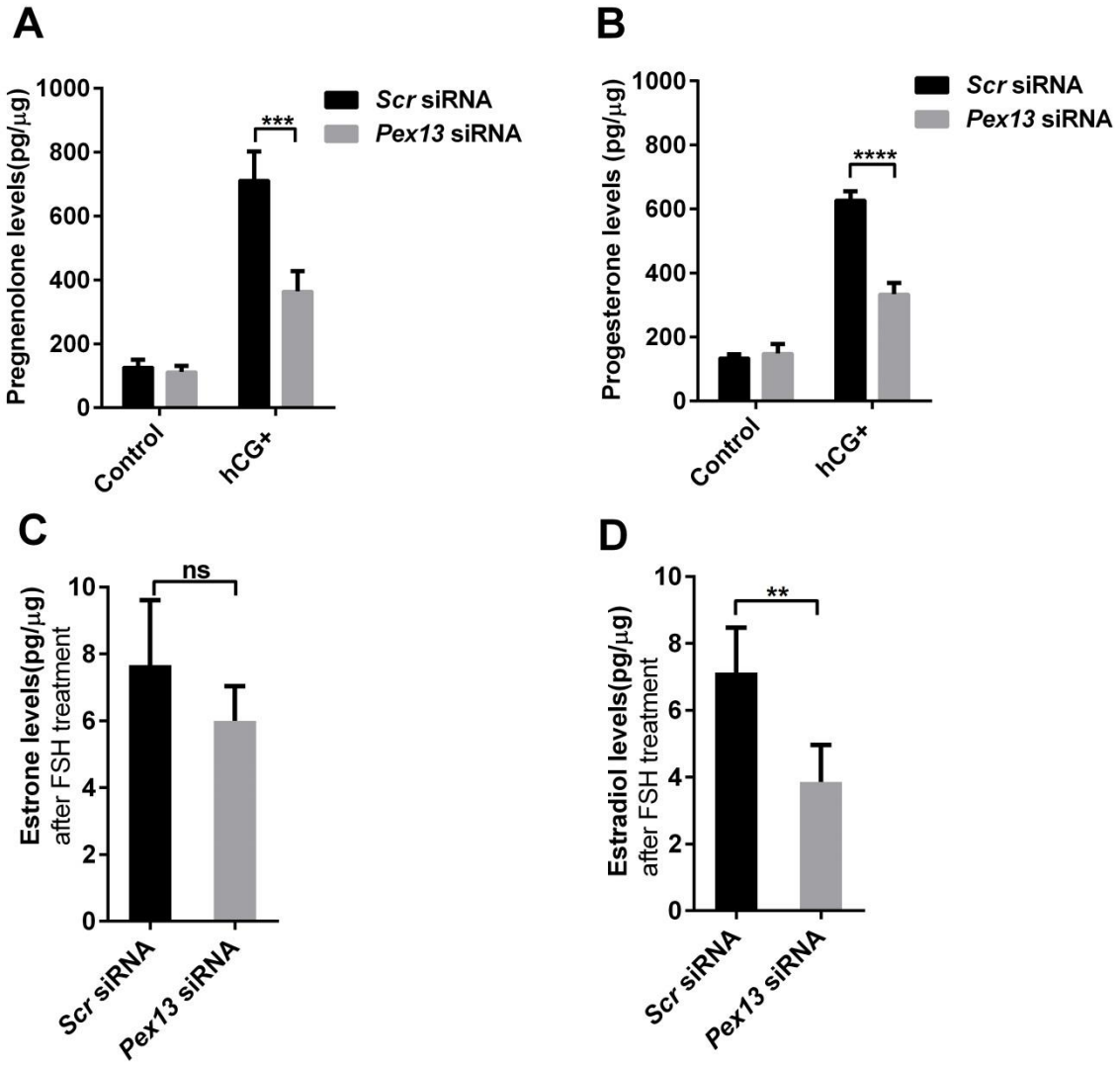

Figure 19. ELISA was performed to analyze the hormone secretion of KK-1 cells after *Pex13* KD. Progesterone and pregnenolone were measured in the presence or absence of hCG (hCG+ and Control) whereas estrone and estradiol were measured after FSH treatment. (A) Pregnenolone ELISA. (B) Progesterone ELISA. (C) Estrone ELISA. (D) Estradiol ELISA. Three independent experiments were performed. (*$p \leq 0.05$, ** $p \leq 0.01$, *** $p \leq 0.001$, **** $p \leq 0.0001$, "ns" means no significant difference). All data are means $\pm$ SD.

As progesterone, pregnenolone and estradiol were all decreased, we further investigated the effect of the *Pex13* KD on the abundance of steroidogenic enzymes by Western blotting to figure out which component of the steroidogenic pathway was affected (Figure 20A). The results show that after the *Pex13* KD the abundance of StAR, a protein that is induced by hCG, was much lower (by 57%, *** $p \leqslant 0.001$) in comparison to the control group (Figure 20D). The reduction of the StAR abundance was only induced in *Pex13* KD cells that were stimulated with hCG. Moreover, PKAc-

α, which phosphorylates and activates StAR also exhibited a slight down-regulation (*p*= 0,0713) (Figure 20C). In contrast, the abundance of CYP11A1 (Cyp450scc), which converts cholesterol to pregnenolone showed no alterations (Figure 20E). In contrast to the protein values, the *Star* mRNA expression levels showed no alteration after *Pex13* KD, suggesting a post-translational mechanism of StAR (Figure 20F). These results strongly suggest that the hCG induced StAR dysfunction in mitochondria is responsible for the lower progesterone, pregnenolone and estrone values.

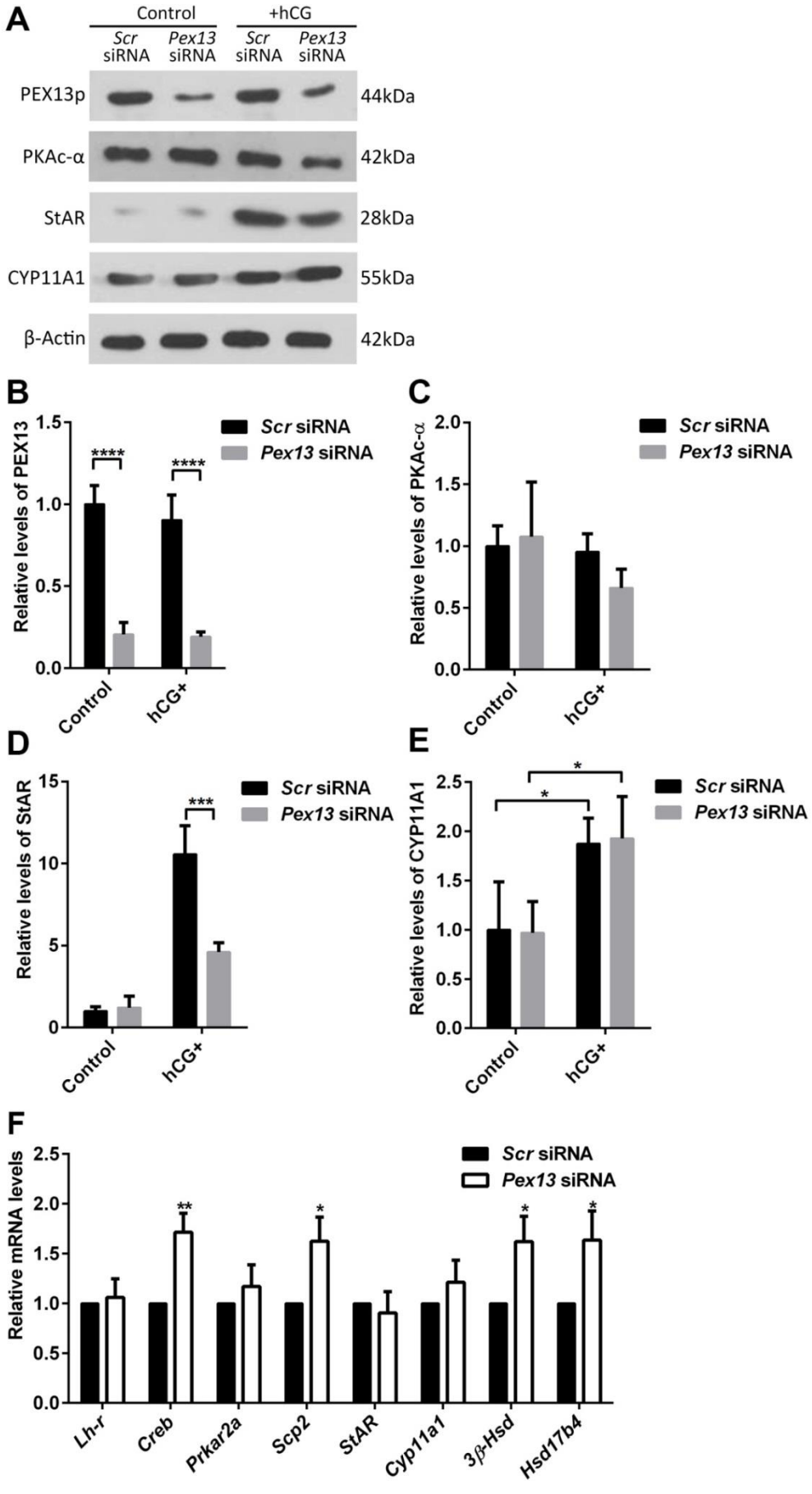
A
Control
+hCG
Scr siRNA
Pex13 siRNA
Scr siRNA
Pex13 siRNA
PEX13p
44kDa
PKAc-α
42kDa
StAR
28kDa
CYP11A1
55kDa
β-Actin
42kDa
B
Relative levels of PEX13
Scr siRNA
Pex13 siRNA
****
****
Control
hCG+
C
Relative levels of PKAc-α
Scr siRNA
Pex13 siRNA
Control
hCG+
D
Relative levels of StAR
Scr siRNA
Pex13 siRNA
***
Control
hCG+
E
Relative levels of CYP11A1
Scr siRNA
Pex13 siRNA
*
*
Control
hCG+
F
Relative mRNA levels
Scr siRNA
Pex13 siRNA
**
*
*
*
Lh-r
Creb
Prkar2a
Scp2
StAR
Cyp11a1
3β-Hsd
Hsd17b4

Figure 20. Steroidogenic enzyme regulation after *Pex13* KD. (A) Western blot analysis to examine the steroidogenic protein abundance. The *Pex13* siRNA transfected group and the *Scr* siRNA group were both analyzed without and with hCG treatment (control and hCG+ groups). (B-E) Band intensities were analyzed by ImageJ software. Protein abundance was normalized to β-actin. Quantification of protein abundances for: (B) PEX13p: Peroxin 13. (C) PKAc-α: catalytic subunit of protein kinase A (D) StAR: steroidogenic acute regulatory protein. (E) CYP11A1: cytochrome P450 side chain cleavage enzyme. (F) qRT-PCR results to reveal steroidogenic gene expression after *Pex13* KD. Three independent experiments were performed. (*$p \leq 0.05$, ** $p \leq 0.01$, *** $p \leq 0.001$, **** $p \leq 0.0001$). All data are means ± SD.

StAR mediated cholesterol transport from outer mitochondrial to inner mitochondrial membrane is the rate-limiting step for steroid synthesis. After that, cholesterol is converted to pregnenolone inside the mitochondria under the stimulation of CYP11A1, which is the initial step for steroid biogenesis. Based on our results, the reduction in StAR following hCG stimulation is particularly likely the cause of hormone suppression under *Pex13* KD conditions. To further confirm our hypothesis, after *Pex13* siRNA transfection the cells were treated with 22R-cholesterol instead of using hCG for the stimulation of steroidogenesis. This induced a pathway that is StAR independent since 22R-cholesterol can pass the mitochondrial membrane without StAR mediation. Using these StAR-independent conditions, no changes in progesterone levels were observed (Figure 21A). The same results were obtained when we treated KK-1 cells with a combination of hCG and 22R-cholesterol (Figure 21B). Our results strongly suggest that the StAR mediated cholesterol transport inhibition is the main reason for the reduction of the synthesis of progesterone, pregnenolone and estrone after *Pex13* KD in KK-1 cells.

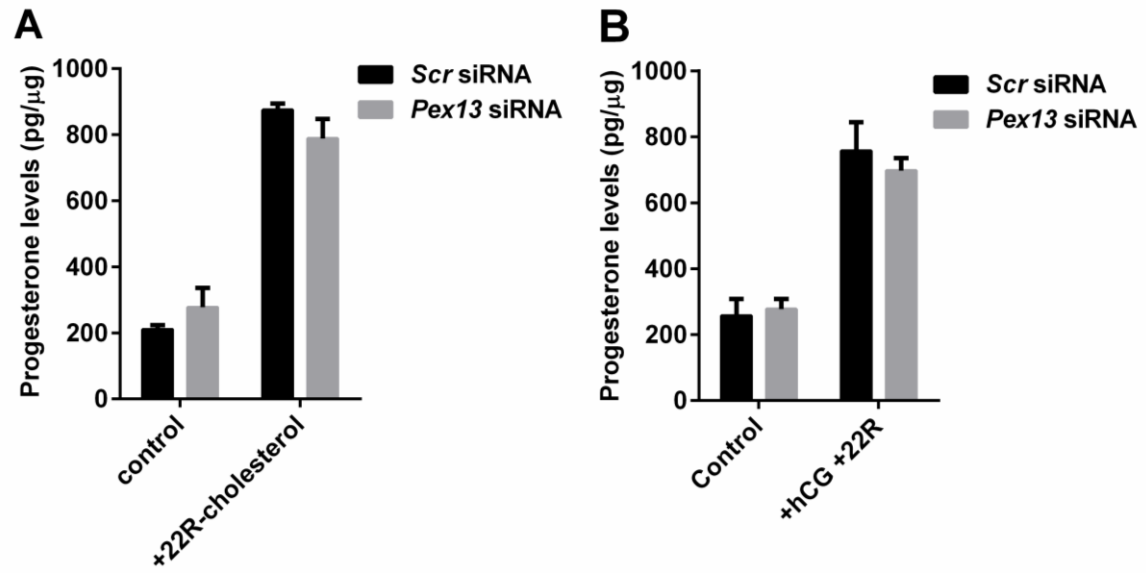

Figure 21. *Pex13* KD has no effect on progesterone synthesis after 22R-cholesterol treatment. ELISAs were performed to detect progesterone secretion of KK-1 cells after *Pex13* KD. (A) Progesterone levels without and with 22R-cholesterol treatment (control and +22R-cholesterol). (B) Progesterone levels without and with 22R-cholesterol and +hCG treatment (control and +hCG +22R). Three independent experiments were performed. All data are means ± SD.

4.2.7 AKAP1 overexpression in KK-1 cells

To further prove that mitochondrial bound StAR is responsible for the alterations in steroidogenesis after *Pex13* KD, we overexpressed the A-kinase anchoring protein 1 (AKAP1 = AKAP121), which normally recruits PKA onto the surface of the mitochondria to phosphorylate and activate StAR, thereby increasing its translocation from the cytoplasm into mitochondria. We expected that the overexpression of AKAP1 could counteract the reduced StAR expression that was detected after *Pex13* KD, through the activation of PKA. For this purpose, two different overexpression vectors were used, which were generated previously in our groups by the doctoral student Wenwen Wang [179]: pCMV-3B adds an N-terminal myc-tag to AKAP1 while pCMV-5B adds a C-terminal myc-tag to AKAP1 [182]. Immunofluorescence was performed with either of t

he two plasmids by Wenwen Wang, the data showing that C-terminally tagged AKAP1 (AKAP1-5B) co-localized with the mitochondrial marker SOD2 whereas the N-terminally tagged AKAP1 (AKAP1-3B) demonstrated a cytoplasmic localization pattern [179]. The co-localization of AKAP1-5B with SOD2 was further confirmed by our IF (Figure 21 A-C). To compare the localization of peroxisomes with the one of AKAP1, the AKAP-5B plasmid was transfected with KK-1 cells and IF staining against the myc-tag and PEX14p was performed, revealing that AKAP1-myc did not bind to the peroxisomal surface (Figure 22 D-F). Since it is known that the addition of the C-terminal tag interfered with the subcellular localization of AKAP1, AKAP1-5B plasmid was used for further investigation. Thereafter western blot analysis was performed and proved that the AKAP1 bearing the myc-tag was successfully expressed (Figure 23A). As indicated by the qRT-PCR results, the *Akap1* (endogenous + recombinant) was 120 times up-regulated compared with GFP control plasmid transfected group (Figure 23B).

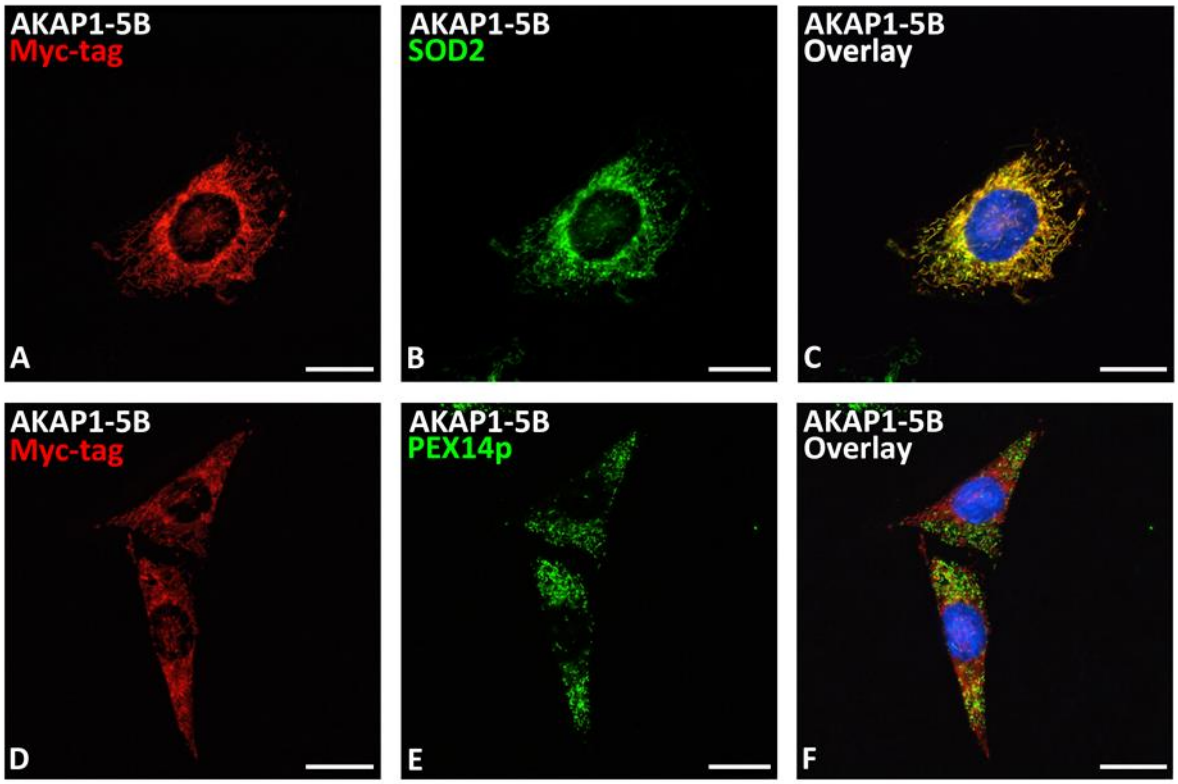

Figure 22. Double immunofluorescence staining for AKAP1-myc with SOD2 and PEX14p. (A) - (C) AKAP1-myc co-localized with mitochondrial SOD2. (D) - (F) AKAP1-myc is not localized on peroxisomes. Scale bar = 20 µm.

To examine how the overexpression of AKAP1 impacts on steroid synthesis, AKAP1-5B-transfected KK-1 cells were treated with hCG. Western blot and qRT-PCR analyses revealed that the steroidogenic enzyme CYP11A1 was induced in both mRNA and protein levels while StAR was up-regulated only at the protein levels after AKAP1 overexpression (Figure 23 A and B). Not surprisingly, as indicated by ELISA, both pregnenolone and progesterone secretion were increased after Akap1 overexpression (Figure 23 C and D).

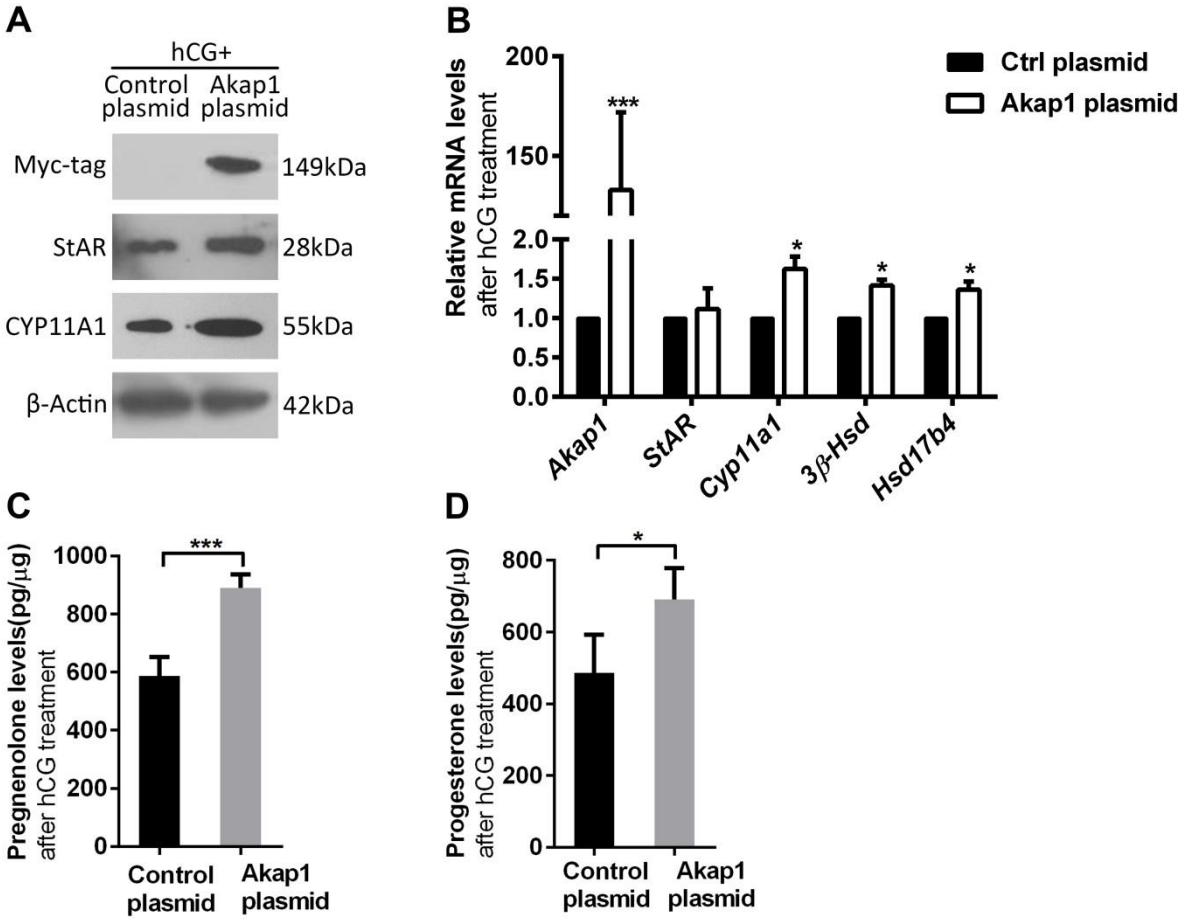

Figure 23. Steroid biosynthesis was induced by Akap1-myc overexpression. KK-1 cells were transfected with GFP control plasmid and Akap1 plasmid respectively and treated with hCG. (A) Western blots were carried out to determine the effects of Akap1-myc on StAR and CYP11A1 protein abundances. β-Actin was used as loading control. (B) mRNA levels of genes encoding for proteins involved in steroidogenesis were analyzed by qRT-PCR. (C) Pregnenolone analysis using ELISA after Akap1-myc transfection and hCG treatment. (D) Progesterone analysis using ELISA after Akap1-myc transfection and hCG treatment.

4.2.8 The mitochondrial steroidogenesis defect was rescued by AKAP1-myc overexpression in peroxisome deficient KK-1 cells

To explore whether Akap1-myc overexpression could rescue the StAR deficiency and hormone reduction induced by the *Pex13* KD, we double transfected KK-1 cells first with *Pex13* siRNA to induce the *Pex13* KD, and after 24 h with the AKAP1-5B plasmid. Indeed, progesterone levels were increased by the overexpression of Akap1-myc in both Scr and *Pex13* KD groups. As shown in Figure 24, progesterone synthesis was 39% augmented in the *Scr* siRNA group while in the *Pex13* siRNA transfected group the degree of increase number was 32% (Figure 24). Likewise (Figure 25), Western blot demonstrated that AKAP1-myc overexpression induced

StAR expression levels by 36% in the *Scr* siRNA group and by 34% in the *Pex13* siRNA group (Figure 25D). The protein expression of CYP11A1 was also up-regulated after AKAP1 overexpression in both *Scr* and *Pex13* siRNA transfected groups showing increase of 39% and 34% respectively (Figure 25E).

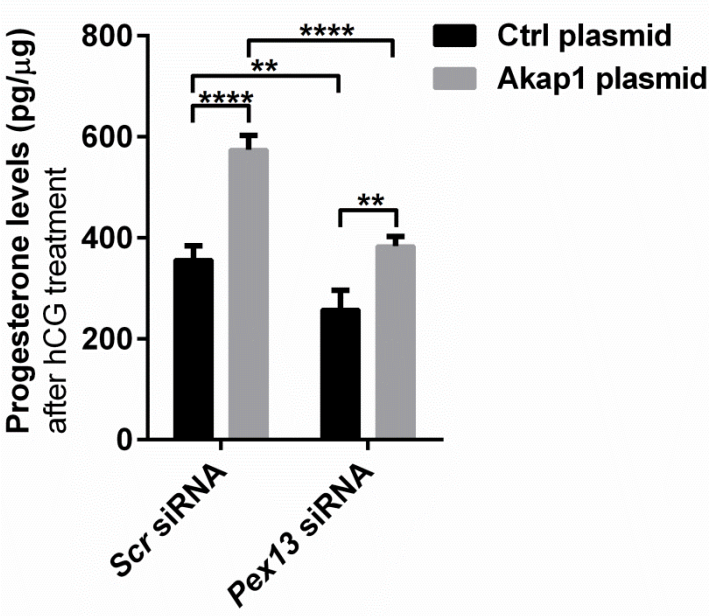

Figure 24. Progesterone synthesis was increased by Akap1 overexpression. Progesterone measurement after *Pex13* siRNA and Akap1-5B double transfection and hCG treatment. Three independent experiments were performed. (*$p \leq 0.05$, ** $p \leq 0.01$, *** $p \leq 0.001$, **** $p \leq 0.0001$). All data are means ± SD.

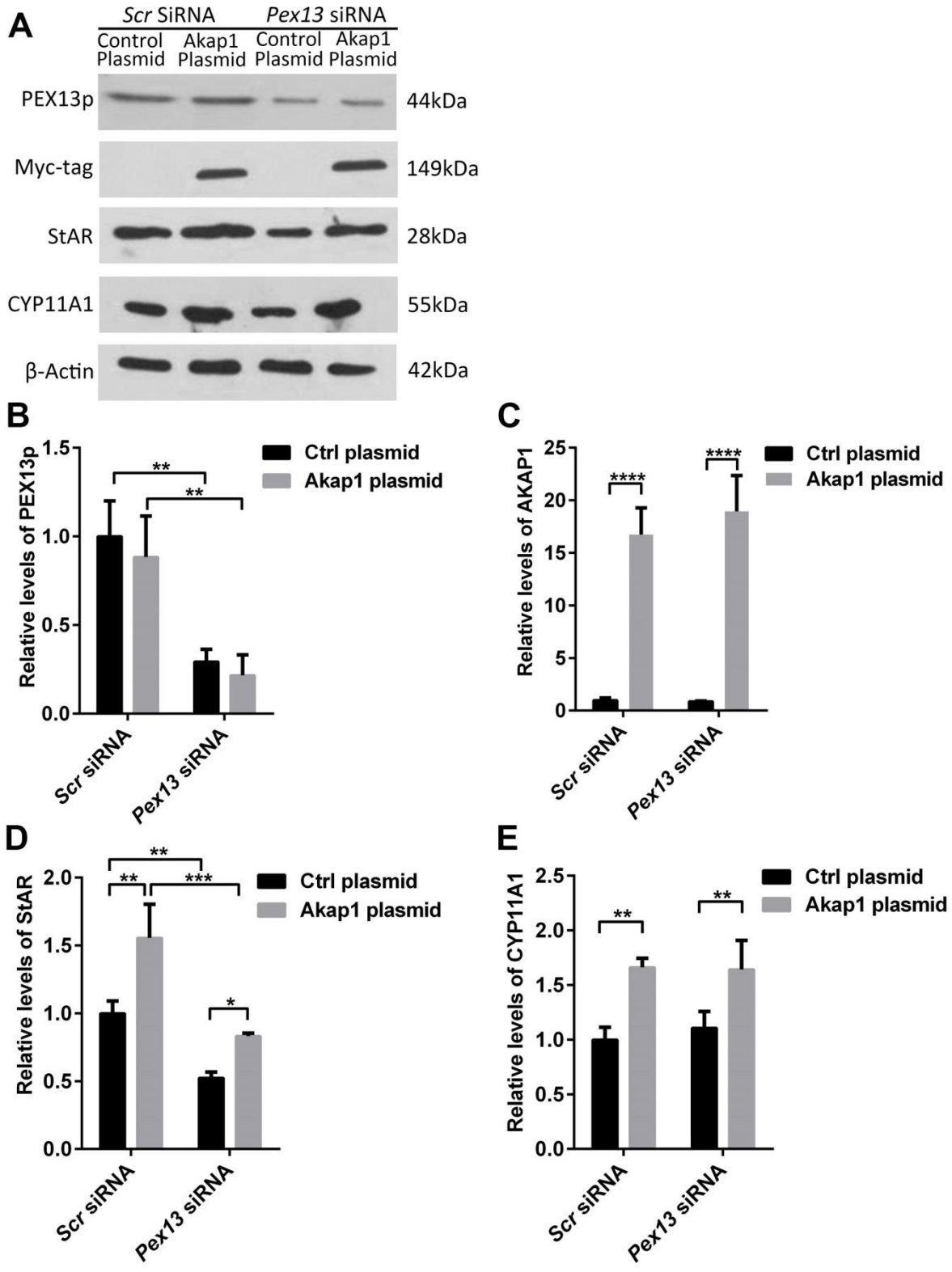

Figure 25. AKAP1-myc overexpression can compensate the reduction of steroidogenic enzymes when PEX13p is deficient. KK-1 cells were transfected with *Scr* siRNA or *Pex13* siRNA respectively. After 24 h each group was further transfected with either the control plasmid or the AKAP1-5B plasmid. Following the double transfection, all groups were treated with hCG for 8h. (A) Western blotting was performed to determine the abundance of proteins involved in steroidogenesis after *Pex13* siRNA and Akap1-5B double transfection. (B-E) Band intensities were analyzed using the ImageJ software. Protein abundance was

normalized to β-actin abundance. (B) PEX13p: Peroxin 13. (C) AKAP1: A kinase anchoring protein 1. (D) StAR: steroidogenic acute regulatory protein. (E) CYP11A1: cytochrome P450 side chain cleavage enzyme. Three independent experiments were performed. (*$p \leq 0.05$, ** $p \leq 0.01$, *** $p \leq 0.001$, **** $p \leq 0.0001$). All data are means ± SD.

4.2.9 Peroxisomal enzyme regulation after Akap1-5B overexpression in KK-1 cells

Since Akap1 was able to compensate the reduced steroidogenesis observed under peroxisome deficient conditions, we investigated how peroxisomal genes are altered after Akap1 overexpression in KK-1 cells. For that purpose, we analyzed mRNA expression and protein abundance of the peroxisomal enzymes catalase and PEX13p after Akap1 plasmid transfection by qRT-PCR and Western blotting. Catalase was up-regulated at both mRNA and protein levels while Pex13p was unaffected (Figure 26).

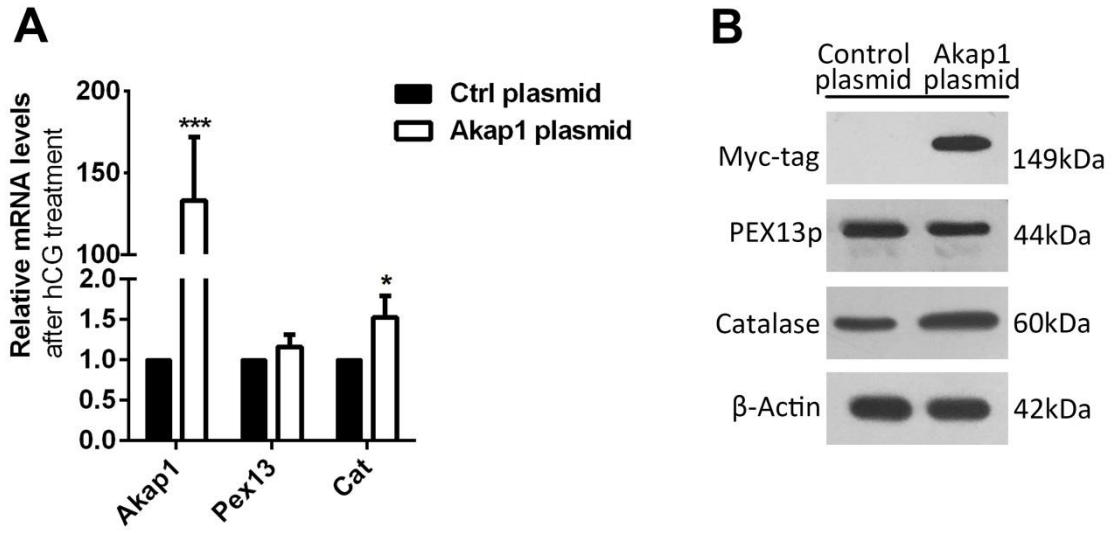

Figure 26. Catalase was induced after Akap1-5B overexpression. (A) mRNA levels of *Pex13* and *catalase* were analyzed by qRT-PCR. (B) Western blotting was carried out to determine the effects of Akap1 overexpression on peroxisomal proteins PEX13p and catalase.

4.2.10 ROS production was increased in KK-1 cells with *Pex13* knock-down

As shown by the Western blot in Figure 27, catalase, a major peroxisomal anti-oxidative enzyme was upregulated in KK-1 cells after the PEX13 KD. Similarly, the mitochondrial SOD2 and the cytosolic glutathione reductase (GR) and SOD1 were induced.

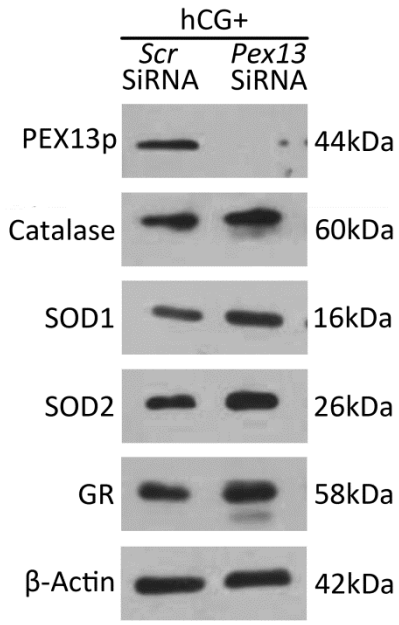

Figure 27. Increased antioxidant enzymes in KK-1 cells with *Pex13* gene KD. Comparison of the protein abundance of antioxidant enzymes in *Scr* siRNA and *Pex13* siRNA transfected KK1-cells treated with hCG after transfection. PEX13p: Peroxin 13; SOD1: superoxide dismutase 1; SOD2: superoxide dismutase 2; GR: glutathione reductase.

Since antioxidant enzymes were up-regulated after the PEX13 KD we have further examined the ovarall cellular ROS production using dihydroethidium (DHE) staining in KK-1 cells with *Pex13* siRNA KD. The fluorensence intensity was quantified in 100 cells using the Image J software. In comparison with the value of *Scr* siRNA transfected cells, *Pex13* siRNA KD led to a 25% ($p \leq 0.01$) increase in ROS production suggesting that oxidative stress is induced when peroxisomes are deficient (Figure 28C). The increase was clearly visible in the fluorescence pictures of DHE stained cells as shown in Figure 28 A and B.

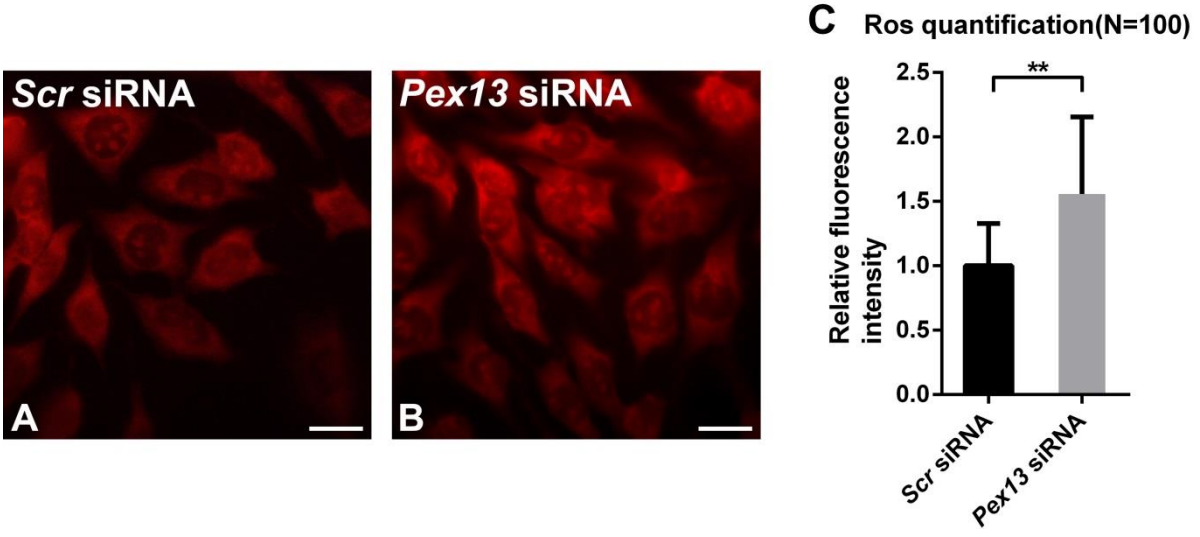

Figure 28. Quantification of ROS production after DHE staining of KK-1 cells with a PEX13 KD. The cells were transfected with *Scr* siRNA and *Pex13* siRNA. Following the

transfection, the cells were stained with DHE for 30min. (A) DHE staining of the *Scr* siRNA group. (B) DHE staining of the *Pex13* siRNA group. (C) Quantification of ROS production. Scale bar = 20 µm. (** $p \leq 0.01$). All data are means ± SD.

Elevated ROS are known to be involved in a variety of pathophysiological conditions and oxidative stress can also inhibit ovarian and testicular steroidogenesis [183]. According to our results, reduced steroidogenesis and increased oxidative stress were both induced after *Pex13* KD. To check whether the decreased StAR protein and hormone synthesis resulted at least part from the increased ROS production caused by the peroxisomal dysfunction, we treated KK-1 cells with H_2O_2 to determine the effects of excessive ROS on the regulation of steroidogenic pathways. H_2O_2 is one of the major forms of ROS generated after $O2^{\cdot-}$ dismutation by SODs, and can be neutralized by catalase [184].

In a first set of experiments, we treated KK-1 cells with different H_2O_2 concentrations (0 µmol, 100 µmol and 250 µmol) and DHE staining was performed to determine the alterations of ROS production related to increasing H_2O_2 concentration. The relative fluorescence intensity was examined by analysis of 100 cells using image J software. The results displayed in Figure 29 A-D demonstrated that the level of ROS production was directly proportional to the H_2O_2 concentration. ROS production was induced by 20% with 100 µmol H_2O_2 and further increased by 40% under 250 µmol H_2O_2 concentration. The effect of H_2O_2 treatment on the viability of KK-1 cells was evaluated by the MTT assay and Trypan blue test. In a second set of experiments an additional group of 350 µmol H_2O_2 was added to the experimental set up to test the cell viability. The cell viability was stable until H_2O_2 concentration reached 350 µmol (Figure 29 E and F). We therefore used this H_2O_2 concentration for the next experiments to ensure that the results obtained after the H_2O_2 treatment reflected the effects of the oxidative stress and not the ones derived from apoptosis.

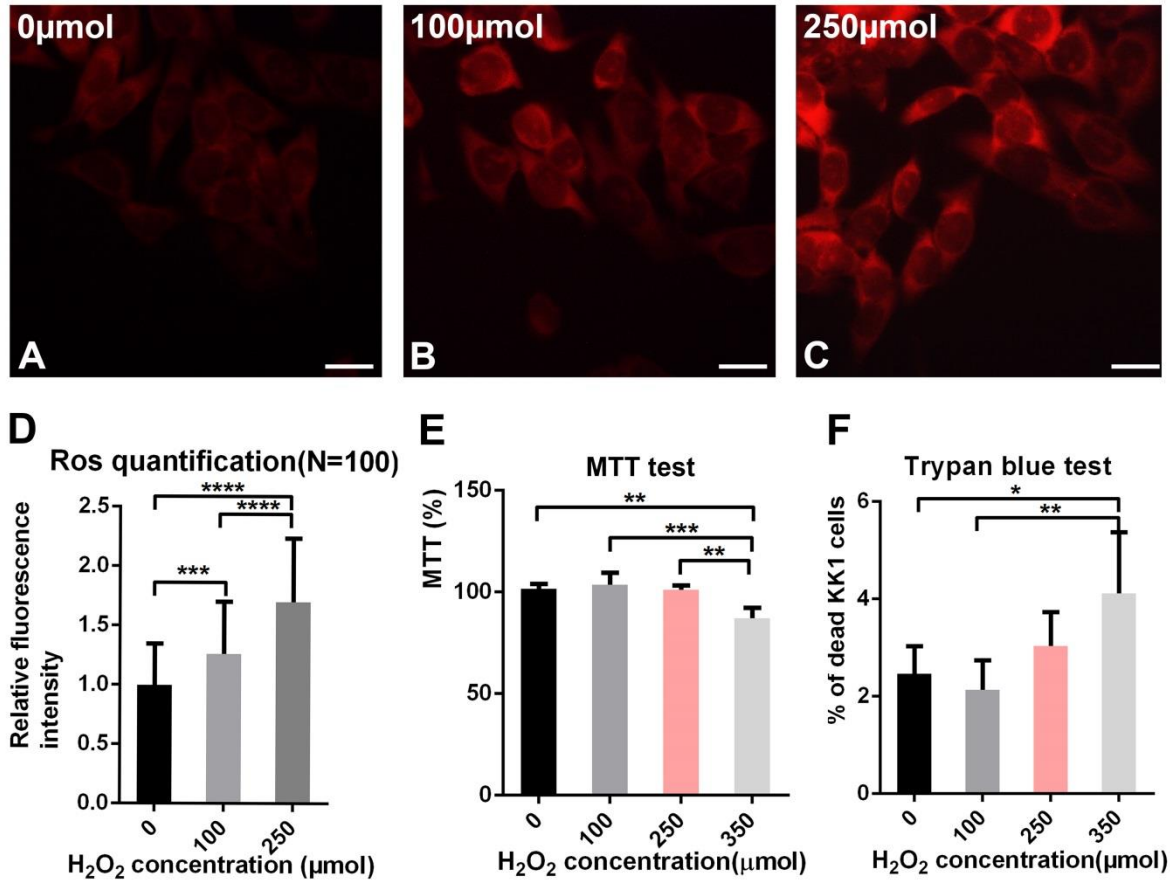

Figure 29. ROS production and cell viability in KK-1 cells after H_2O_2 treatment. (A) DHE staining of KK-1 cells without H_2O_2 treatment. (B) DHE staining of KK-1 cells after 100 µmol H_2O_2 treatment. (C) DHE staining of KK-1 cells after 250 µmol H_2O_2 treatment. (D) Quantification of ROS production among three groups. (E) MTT assay. KK-1 cells were treated with different concentrations of H_2O_2 for 3h and then incubated with 0.5 mg/ml MTT, results were read at 570 nm using a spectrophotometer. (F) Trypan blue test. Number of viable and non-viable (blue stained cells) KK-1 cells were counted to compare the cell viability in dependence of the H_2O_2 concentrations. (*$p \leq 0.05$, ** $p \leq 0.01$, *** $p \leq 0.001$, **** $p \leq 0.0001$, "ns" means no significant difference). Scale bar = 20 µm. One-way ANOVA and Tukey's multiple comparisons test were used as statistical methods (Graph pad 6.0 software). All data are means ± SD.

4.2.11 Effects of H_2O_2 on steroid biogenesis and steroidogenic enzymes

To determine the effects of oxidative stress on steroidogenesis, KK1- cells were treated with different amounts of H_2O_2 and the secretion of progesterone was measured by ELISA. Treatment of hCG-stimulated KK-1 cells with 100 µmol, 250 µmol and 350 µmol H_2O_2 caused a dose-dependent decrease in the progesterone secretion by 19%, 51% and 70% respectively (Figure 30).

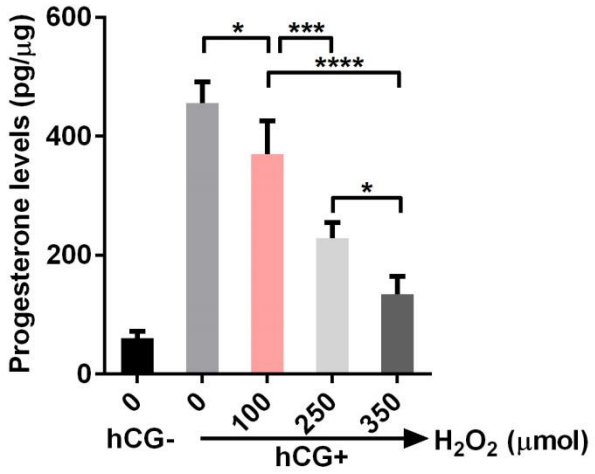

Figure 30. Effect of H_2O_2 on hCG-stimulated progesterone production in KK-1 cells. KK-1 cells were grown in culture to 75% confluency and preincubated in DMEM/F12 for 1 h and treated in DMEM/F12 containing 1,5 IE hCG plus increasing concentrations of H_2O_2 for 3 h. Media were collected and subjected to progesterone ELISA and the final results were normalized to protein concentrations of each group. (*$p \leq 0.05$, ** $p \leq 0.01$, *** $p \leq 0.001$, **** $p \leq 0.0001$). All data are means ± SD.

To examine which components of the steroidogenic pathway were influenced by the ROS treatment, proteins involved in steroidogenesis were analyzed by Western blotting after the treatment with H_2O_2 (Figure 31). Exposure of KK-1 cells to H_2O_2 induced a significant reduction in hCG-stimulated StAR protein induction: treatment with 100 µmol and 250 µmol H_2O_2 reduced StAR protein by 39% and 90% respectively (Figure 31B). In contrast to the protein levels of StAR, the mRNA levels of *Star* showed no alterations. This suggests that StAR protein but not mRNA was decreased under oxidative stress, indicating that ROS might act at a post-transcriptional stage (Figure 31D). In contrast to StAR, treatment of KK-1 cells with hCG plus increasing concentrations of H_2O_2 for 3h had no effect on CYP11A1 protein levels (Figure 31C).

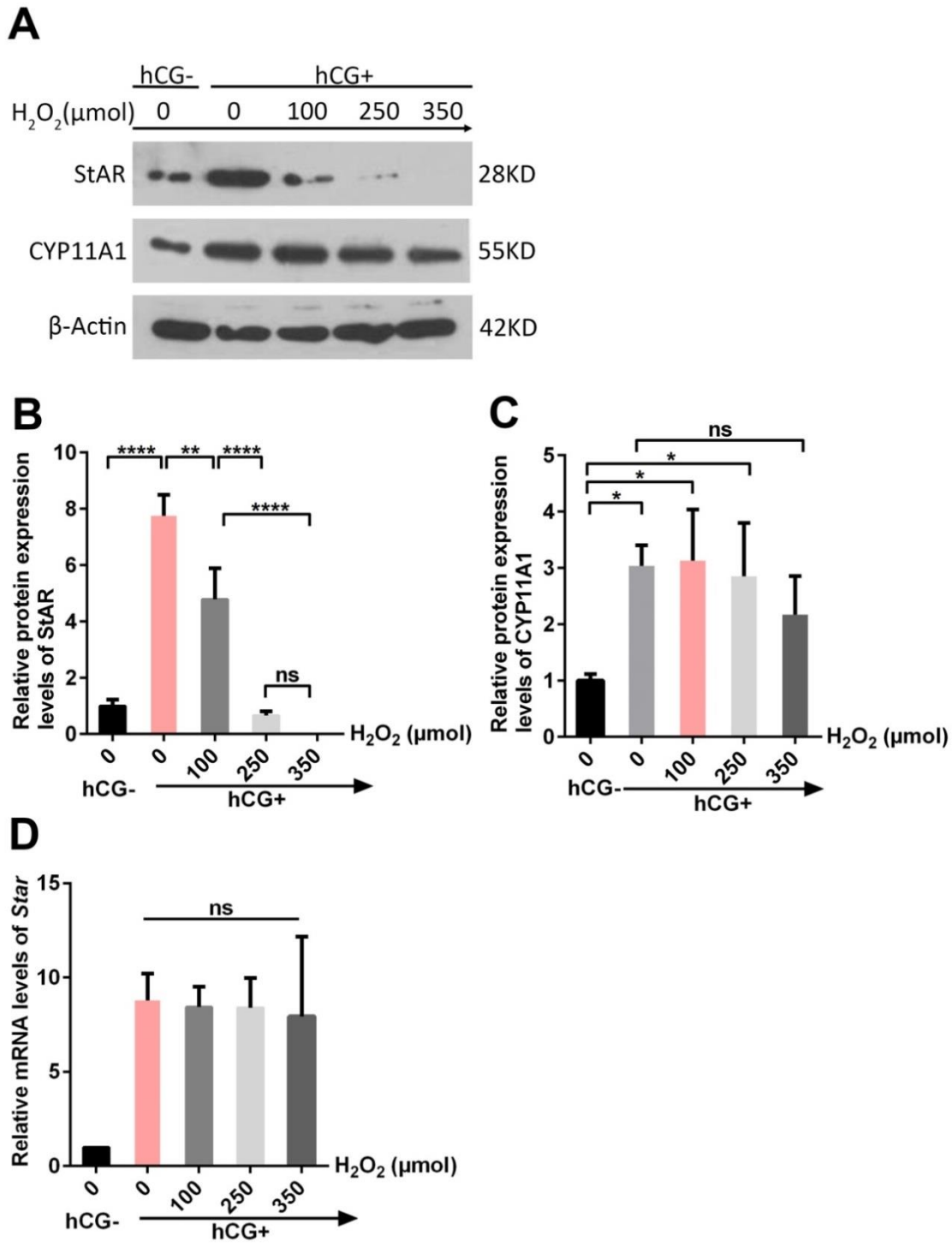

Figure 31. Effect of H_2O_2 on StAR and CYP11A1. KK-1 cells were treated with hCG plus increasing concentrations of H_2O_2 for 3 h. After treatment, cells were either subjected to Western blotting or qRT-PCR. (A) Western blot of StAR and CYP11A1 proteins. (B) and (C) Quantification of StAR and CYP11A1 levels by analyzing band intensities with the ImageJ software. Protein abundance was normalized using β-actin. (D) Relative mRNA levels of the *Star* gene. Three independent experiments were performed. (*$p \leq 0.05$, ** $p \leq 0.01$, *** $p \leq 0.001$, **** $p \leq 0.0001$, "ns" means no significant difference). One-way ANOVA and Tukey's multiple comparisons test were used as statistical methods (Graph pad 6.0 software). All data are means ± SD.

4.2.12 Effects of H_2O_2 on peroxisomal and mitochondrial compartments

To determine the impact of H_2O_2 on peroxisomes and mitochondrial components of ovarian granulosa cells, KK-1 cells were treated with H_2O_2 and cells were subjected to Western blotting using antibodies against PEX14p, Catalase and SOD2. According to the results, the peroxisomal protein PEX14p and Catalase were up-regulated in a dose-dependent manner after H_2O_2 treatment. In contrast, mitochondrial SOD2 levels were reduced in a dose dependent manner (Figure 32).

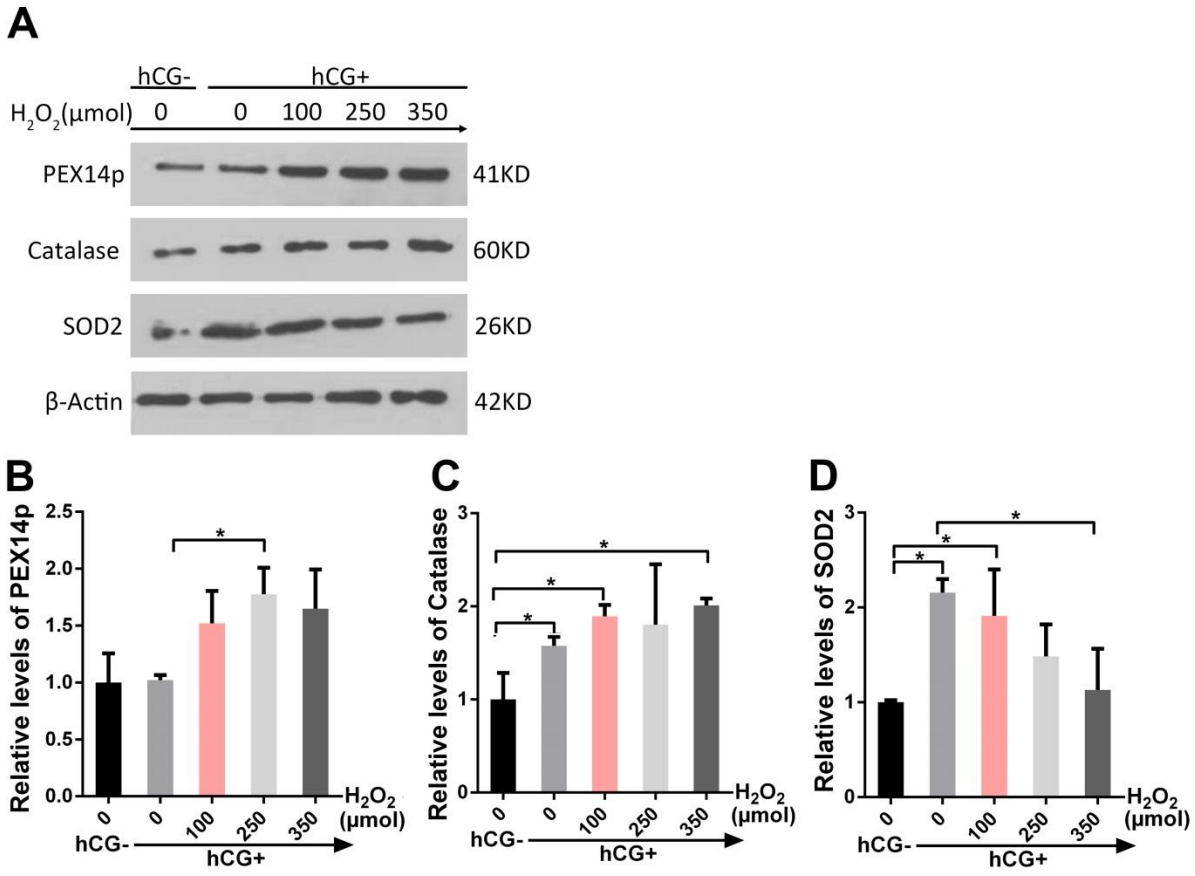

Figure 32. The abundances of the peroxisomal proteins PEX14p and Catalase were increased under oxidative stress while mitochondrial enzyme SOD2 was reduced in hCG stimulated cells. KK-1 cells were treated without and with hCG for 3h, the hCG+ group were treated together with increasing concentrations of H_2O_2 for 3h. After H_2O_2 and hCG treatment, cells were lysed and subjected to Western blotting. (A) Western blot analysis of peroxisomal PEX14p, catalase and mitochondrial SOD2. (B) - (D) Quantification of PEX14p, catalase and SOD2 abundance by analyzing band intensities using the ImageJ software. Protein abundance was normalized to β-actin levels. Three independent experiments were performed. (*$p \leq 0.05$, ** $p \leq 0.01$, *** $p \leq 0.001$, **** $p \leq 0.0001$). One-way ANOVA and Tukey's multiple comparisons test were used as statistical methods (Graph pad 6.0 software). All data are means ± SD.

4.2.13 The reduced mitochondrial steroidogenesis observed in KK-1 cells after *Pex13* knock-down was rescued by the addition of the antioxidant α-tocopherol

Several cellular antioxidants exist to maintain the redox balance by scavenging excessive ROS. Molecular α-tocopherol (Vitamin E) is considered one of the most important antioxidants [185]. Our results strongly indicate that in KK-1 cells oxidative stress caused by the peroxisomal deficiency lead to an inhibition of StAR with concomitant decrease of hormone synthesis. To confirm this hypothesis, peroxisome deficient KK-1 cells were treated with α-tocopherol. To establish the best concentration to induce a protection against ROS we have tested several concentrations of α-tocopherol treatment on peroxisome deficient (*Pex13* KD) KK1-cells as shown by DHE staining (Figure 33). Quantification of ROS staining as shown in Figure 33E exhibited that ROS production after the *Pex13* KD was attenuated by 23% with 5 µmol tocopherol and further reduced to almost the normal levels obtained using *Pex13* siRNA with 10 µmol tocopherol.

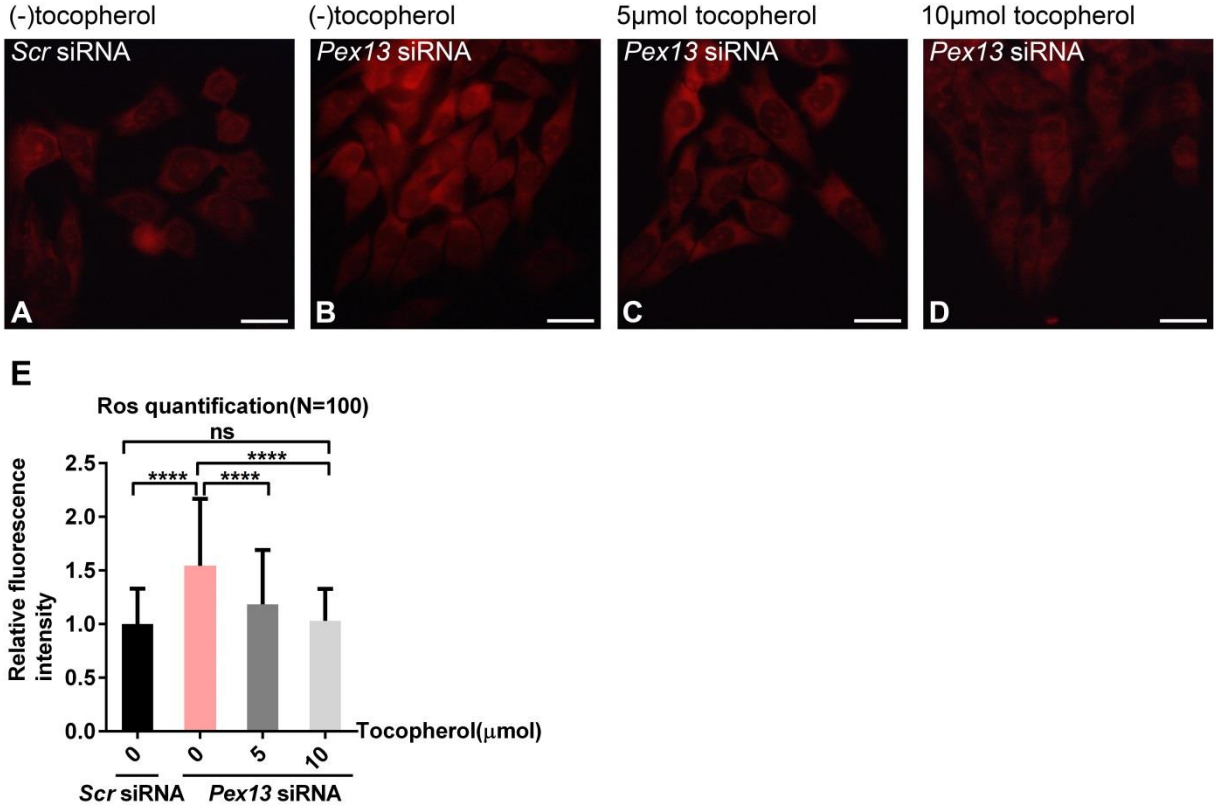

Figure 33. Measurement of ROS production by relative fluorescence intensity quantification of DHE - stained peroxisome-deficient KK-1 cells using different α-tocopherol concentrations. KK-1 cells were transfected with *Scr* siRNA and *Pex13* siRNA and the *Pex13* siRNA transfected cells were simultaneously treated with α-tocopherol (0 µmol, 5 µmol and 10 µmol). Cells were stained with DHE 48h after transfection. For each

group, 100 cells were analyzed by measuring the fluorescence intensity using the image J software. (A) DHE staining of the *Scr* siRNA group. (B) - (D) DHE staining of the *Pex13* siRNA group. (E) Quantification of ROS production. Scale bar = 20 µm. Three independent experiments were performed. (*** $p \leq 0.001$, **** $p \leq 0.0001$). One-way ANOVA and Tukey's multiple comparisons test were used as statistical methods (Graph pad 6.0 software). All data are means ± SD.

According to these results, we selected 10 µmol as the working concentration for the α-tocopherol experiments. Four groups were set up as follows: *Scr* siRNA and *Pex13* siRNA transfected KK-1 cells both either treated with or not with 10 µmol α-tocopherol for 48 h, after which all four groups were treated with hCG for 8 h. Finally, the KK-1 cells were subjected to Western blotting and the culture medium was collected for progesterone ELISA. As shown in Figure 34A, progesterone secretion was inhibited after *Pex13* KD compared with the *Scr* siRNA groups. Very interestingly, the level of progesterone after the α-tocopherol treatment was slightly higher in the *Pex13* siRNA transfected group but could not be rescued to normal progesterone levels as compared to the Scr group. Additionally, Western blot results showed that the StAR protein abundance was also partially recovered (44%) after the α-tocopherol treatment (Figure 34 B).

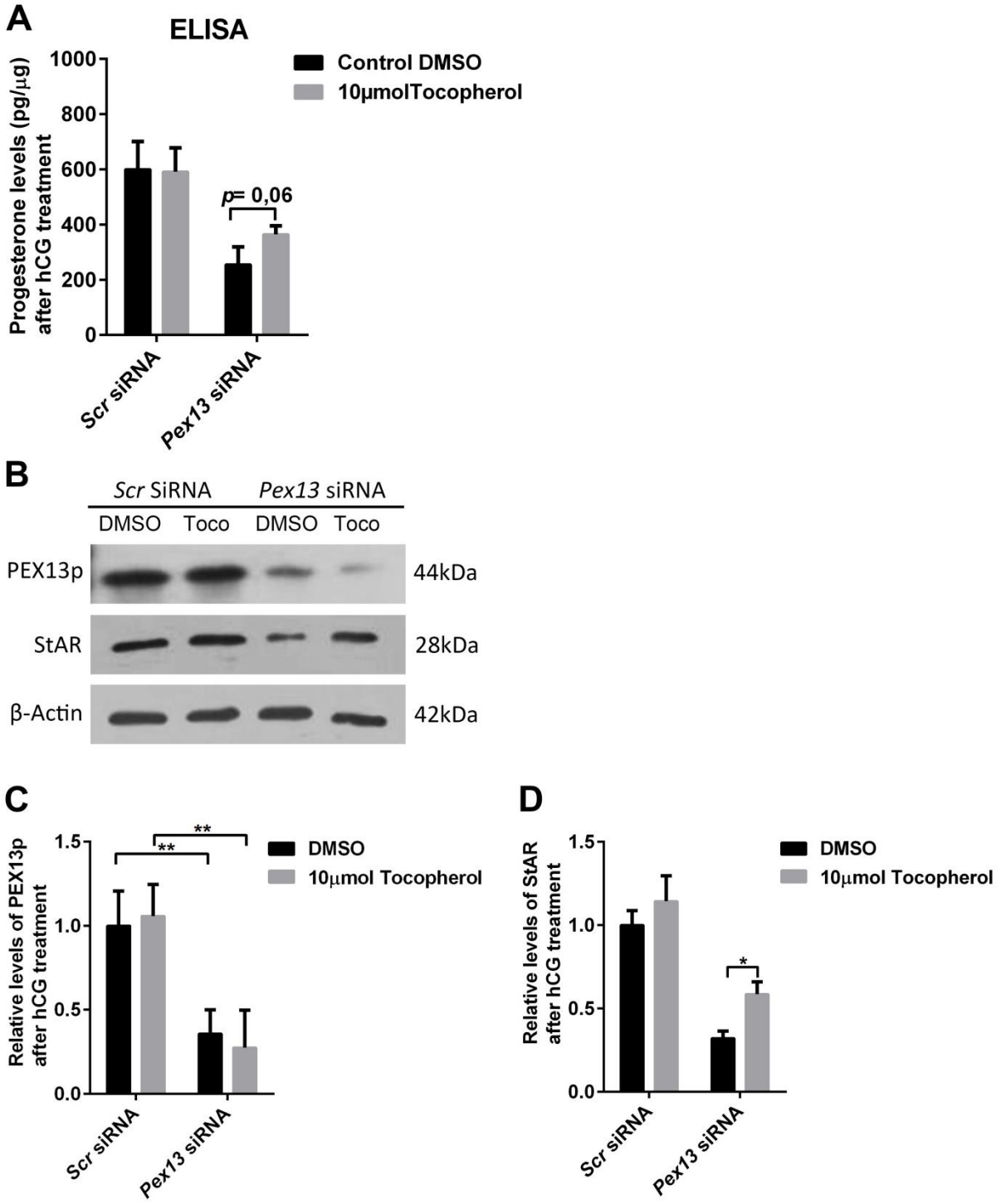

Figure 34. Effect of α-tocopherol on steroidogenesis after *Pex13* KD. (A) Progesterone ELISA. (B) Western blot of PEX13p and StAR. (C) (D) Quantification of PEX13p and StAR levels by analyzing band intensities using the ImageJ software. Protein abundance was normalized using β-actin. Three independent experiments were performed. (*$p \leq 0.05$, ** $p \leq 0.01$, *** $p \leq 0.001$, **** $p \leq 0.0001$). Two-way ANOVA and Sidak's multiple comparisons test were used as statistical methods (Graph pad 6.0 software). All data are means ± SD.

5 Discussion

Patients with Zellweger syndrome, the most severe peroxisomal biogenesis disorder leading to a general peroxisomal deficiency exhibit pathological alterations in the reproductive systems. To date, however, only very limited evidences exist in the literature from peroxisomal gene knock-out mice with peroxisomal gene deficiencies, indicating that peroxisome is involved in folliculogenesis and steroid metabolism in the ovary. In the experimental work of this thesis it was proved that the peroxisomal distribution pattern and regulation in distinct ovarian cell types during follicular development is altered and that peroxisomes are highly enriched in granulosa lutein cells. Also the role of peroxisomes during steroidogenesis and the potential mechanism behind the pathological alterations of steroid synthesis induced by peroxisomal deficiency have been elucidated.

5.1 Part 1 Peroxisomal functions on mouse ovarian folliculogenesis

5.1.1 The history of peroxisomes in the mouse ovary

Peroxisomes were first studied in the ovary of mice in 1972 by Böck and colleagues by detecting the activity of the peroxisomal marker enzyme catalase using electron microscopic cytochemistry with the 3, 3'-diaminobenzidine (DAB) method [159]. According to this report, peroxisomes in the ovary differ in size and morphology to the "classical" peroxisomes detected in hepatocytes of the liver, they are much smaller and less numerous than the peroxisomes in hepatocytes of the liver [159, 160]. According to their results, peroxisomes are heterogeneously distributed in different cell types in the mouse ovary [159]. In early times, catalase and peroxisomes are reported absent in the oocytes of different species [186, 187]. But later, it was reported that catalase was present in oocytes in a lower amount compared to other cell types in the follicles [188]. In 2000, Figueroa *et al.* showed by using immunocytochemistry that catalase-stained peroxisomes were only localized to the periphery of the oocyte in rats. A similar peroxisomal distribution pattern was obtained by the same group using an antiserum against total peroxisomal proteins [189].

5.1.2 Peroxisomes detected with PEX14p as optimal marker protein in mouse ovarian follicular maturation

During the follicular maturation process from primordial follicles to pre-ovulatory follicles which then released oocytes during ovulation for fertilization, the morphological appearance and protein composition changes for adapting to the follicular maturation process. As an important organelle involved in ROS trapping and lipid metabolism, peroxisomes were strong candidates involved in this process. However, in the literature existed there is no comprehensive study of peroxisomal distribution and regulation during folliculogenesis. In my thesis, PEX14p was chosen to analyze peroxisomal distribution in mouse ovary since it was proved from our group that PEX14p is a perfect marker to detect peroxisomes in morphological studies in many different cell types and organs [190]. According to my results, PEX14p-positive peroxisomes are present in all the cell types of the mouse ovary and they are also numerous in oocytes and distributed all over the oocyte cytoplasm (Figure 9 D, E and F). The highest abundance of PEX14p was detected in the hormone producing interstitial cells, followed by granulosa cells, and exhibited a low abundance in theca cells. These results are different from previous study which reported that peroxisomes are more abundant in granulosa cells than interstitial cells by detecting catalase activity with the DAB procedure via electronmicroscopic analysis [159]. High amount of peroxisomes in interstitial cells suggest that peroxisomes are required for the initial steps for steroidogenesis in these cell types. Interestingly, PEX14p labelled peroxisomes were increased in numbers in oocytes during their maturation process exhibiting their strongest proliferation from secondary to tertiary follicles, which was proved by Distler in 2015 in our group by morphometric analysis of peroxisomal density in oocytes using a PEX14p antibody [191]. Peroxisomal proliferation in oocytes during folliculogenesis indicates that especially in the mature oocyte of a tertiary follicle peroxisomal metabolism is probably necessary for keeping the redox balance and protecting the oocytes against lipotoxicity.

5.1.3 Antioxidative enzymes catalase, SOD2 and glutathione reductase (GR) in mouse ovarian follicular maturation

The normal progression of the follicular development is crucial to sustain proper ovarian functions and female fertility. During the regulation of these ovarian

processes also reactive oxygen species (ROS) play a significant role, e.g. during the preparation of follicle in the preovulatory phase. ROS are generated as by-products of normal ovarian physiological metabolism, and cellular defense mechanisms in form of antioxidative enzymes (e.g. SOD, catalase or other peroxidases) and molecular antioxidants (e.g. glutathione or Vitamin C and E) maintain the balance between ROS production and clearance. However, a disturbed balance between ROS production and antioxidant defense mechanisms can cause pathological changes in follicular growth, ovarian cycle, oocyte maturation, steroidogenesis, ovulation, fertilization, and implantation that ultimately affect fertility [192, 193].

Therefore, catalase, a peroxisomal enzyme with high potency to degrade H_2O_2 at lower concentration should play a role during the follicular maturation process and steroidogenesis in the ovary. The experiments of this thesis revealed that catalase could be visualized very clearly in oocytes at higher magnification by using very long exposure times and higher antibody concentrations (Figure 9B). Especially in the periphery of oocytes large peroxisomes or peroxisomal clusters are present, which might explain the results attained by using immunocytochemical analysis of catalase, depicting catalase positive particles only in the periphery of oocytes [189]. Similar to PEX14p, catalase was highest abundant in interstitial cells, but it was also highly detectable in other ovarian cell types, such as granulosa cells and theca cells. Interestingly, in primary and secondary follicles, catalase was specifically abundant in the layer of granulosa cells facing the oocyte. In this respect, it is of interest that gap junctions start to form in primary follicles [194, 195] and nutrients and molecules from granulosa cell are transferred to oocytes through gap junctions for supporting oocyte maturation and differentiation [196]. From the literature it is known that in hematopoietic stem cells, ROS are transported through gap junctions to bone marrow for protection against the oxidative stress [197]. Therefore, according to our results the probabilities exists that H_2O_2 generated from oocytes are transferred to granulosa cells where it can be further degraded by catalase through gap junctions. Moreover, ROS produced on the surface of oocytes could also be degraded easily by the peroxisomes laying at the periphery in the oocyte cytoplasm. Vice versa, it is possible that peroxisomes in these inner layers of the granulosa cells underneath of the apical surface trap ROS before entering into oocytes through gap junctions. This is very likely, since granulosa cells produce steroids and provide nutrients for neighboring

oocytes. Moreover, the catalase activity in granulosa cells was shown to be higher in large follicles compared to small follicles in different animals (pigs, goats and rats) [162, 165, 198]. Gonadotropins like FSH regulate follicular maturation, differentiation and steroidogenesis [199]. Interestingly, catalase activity has been reported to be up-regulated after gonadotropin stimulation in different mammals [165, 200, 201]. According to all these reports, catalase was suggested to participate in the follicular maturation process. The increased catalase activities in large tertiary follicles certainly contribute to the maintenance of the ROS balance and protect the oocyte from excessive ROS production before ovulation or even during the ovulation process. Additionally, the abundance of catalase in the ovary has been shown to correlate to the content of cytochrome P450scc that converts cholesterol to pregnenolone during steroidogenesis [202]. Indeed, the conversion from cholesterol to pregnenolone was reported to produce a very large amount of ROS released from mitochondria during the steroidogenic pathway, requiring the presence of antioxidative enzymes [203, 204]. In this thesis, it was shown that the amount of catalase was increased under oxidative stress conditions in KK-1 cells. Accordingly, catalase might function as a protective factor to reduce excessive ROS to maintain the redox balance to maintain the normal production of steroids.

In addition to catalase, we have examined the regulation of two other anti-oxidative enzymes (SOD2 and GR) in the mouse ovary. The mitochondrial marker SOD2 removes harmful superoxide radicals that are produced during mitochondrial respiration. Superoxide is dismutated to H_2O_2 by SOD2 in the mitochondrial matrix which is then degraded further by the mitochondrial isoform of the glutathione peroxidases (GPX) to H_2O and O_2 [205, 206]. GR catalyzes the reduction of GSSH (oxidized glutathione) to GSH (reduced glutathione) in the cytosol to maintain constant GSH-levels within cells [207]. Immunofluorescence analysis of mouse ovary in this thesis showed that similar to catalase SOD2 is most highly abundant in ovarian interstitial cells and granulosa cells (Figure 12 A and B). However, in comparison with catalase, the activity of SOD2 was reported to be constant during follicular maturation [208]. But in the follicular fluid, SOD2 activity was reported to be lower in large follicles [209, 210]. Interestingly, high SOD activity was proven to have negative effects on fertility in humans [211] and the inhibition of ROS lead to impaired ovulation process [212, 213]. The reason is that a certain amount of ROS is important

for the regulation of ovulation and embryonic development [214]. Decreased SOD activity in large follicular fluid is necessary to ensure that ROS levels reach a threshold value that is required for ovulation and it is therefore not surprising that also the abundance of GR in the oocytes was reduced in the large antral follicles compared to the primary and primordial follicles (Figure 12D). However, excessive ROS are detrimental for correct follicular development, so compared with SOD2 and GR, catalase is augmented in large follicles in order to keep the balance of ROS production.

Conclusively, the intracellular levels of ROS are tightly controlled by different antioxidants in distinct types of follicles during follicular maturation to guarantee normal ovarian functions and female fertility.

5.1.4 Lipid metabolism in mouse ovarian follicular maturation

GNPAT catalyzes the first step of plasmalogen synthesis [66]. Similar to PEX14p, our results revealed that the amount of GNPAT was also induced in oocytes during follicular growth (Figure 9 G, H and I). Plasmalogens are critical cell membrane constituents of oocytes that function in ROS trapping as well as in the regulation of membrane dynamics, which might especially be important during fertilization [215-217]. The up-regulation of GNPAT during oocyte maturation in tertiary follicles strongly suggests that oocyte membranes are protected against ROS by these lipid species. Apart from that, it has been proven that the phospholipid composition of oocyte varies during oocyte maturation dependent on the size of the follicles and their maturity [215, 216, 218]. Phospholipids are not only an important source of energy for the oocyte development but are also signaling molecules for the oocyte´s competence acquisition [219]. Indeed, degenerating oocytes have been described in a GNPAT-knockout mouse, suggesting that plasmalogen phospholipids play an important role for protection of oocytes during follicular maturation [100].

Like GNPAT, also MFP2, a peroxisomal fatty acid β-oxidation enzyme [60], and ABCD3 [62], a lipid transporter involved in the transport of peroxisomal β-oxidation substrates, displayed higher abundance in tertiary follicles according to Distler's results from our group [191]. In the oocyte nutritional lipids are stored as lipid droplets and they undergo changes in number, composition, size and aggregation during

follicular maturation process [220-222]. How the metabolism of lipids is regulated and influences the oocyte development is still not fully clarified to date [223]. Experimental evidences have shown that in the mouse, mature and competent oocytes display a different lipid spectrum to immature ones [224]. Moreover, in cows the amount of lipids is elevated in mature oocyte [220]. The increased abundance of peroxisomal proteins involved in lipid metabolism in tertiary follicles [191] and the close proximity of peroxisomes to lipid droplets and mitochondria in granulosa and luteal cells [118, 159] suggest an involvement of the peroxisomal lipid metabolism in the oocyte during the follicular development process. Functional relationships of lipid droplets and mitochondria have been previously postulated due to their close proximity [221]. In the oocyte fatty acids stored within lipid droplets are transferred to mitochondria for energy generation through β-oxidation and it has been proven that β-oxidation is increased during oocyte maturation and in the preovulatory phase [225]. Most of the information concerning β-oxidation in the literature is derived from mitochondrial β-oxidation while the function of peroxisomal β-oxidation in the ovary remains to be clarified. Despite the fact that peroxisomal β-oxidation is not directly involved in cellular ATP-provision, it shortens long-chain and very-long-chain fatty acids for further metabolisation within the mitochondria [33]. Further, peroxisomal β-oxidation degrades a broad spectrum of bioactive proinflammatory and toxic lipid intermediates that cannot be processed by the mitochondrial β-oxidation, such as n-3 fatty acids, polyunsaturated fatty acids, retinoic acid and bile acid intermediates [33]. It also has been proposed from our group that peroxisomes might be responsible for the regulation of the homeostasis of fatty acid species that are ligands of peroxisome proliferator activated receptors [33]. In this respect it is of interest that the long chain fatty acids linoleic, oleic, stearic and palmitic acid that are detrimental for the oocyte´s development [226-228].

In addition, female mice with a deletion in the enzyme that catalyses the first step of the peroxisomal β-oxidation (ACOX1) developed sterility within 6-12 weeks after birth [104]. Missense mutation in MFP2 in women leads to ovarian dysgenesis [229] and its disruption in male mice caused the accumulation of lipids in sertoli cells, testis atrophy and infertility [102, 230, 231].

5.1.5 Peroxisomes in the corpus luteum (CL)

Corpus luteum is a very important endocrine structure in female ovaries, since they can produce a large amount of progesterone, moderate amount of estrogen and inhibin A. Moreover, corpus luteum contributes to maintaining the early period of pregnancy. When the ovum is not fertilized, the corpus luteum degenerates into a fibrous scar tissue, called corpus albicans. In contrast to granulosa cells in the developing follicles, peroxisomes are very heterogeneously distributed in luteinized granulosa cells (Figure 11). As we know, granulosa cells are the specific cell type for estrogen synthesis because aromatase is only localized in this cell type [132]. Interestingly, also aromatase is very heterogeneously located in the Macaque corpus luteum, the strongly stained cells were interspersed among other weakly stained cells [232]. Accordingly, the heterogeneous peroxisomal distribution pattern may indicate very active steroidogenesis in those cells. In addition, a large amount of ROS is generated during steroid synthesis, so it's not surprising that the peroxisomal antioxidative enzyme catalase is intensively labelled in these cells to protect against oxidative stress.

5.2 Part 2 Peroxisomal functions on steroidogenesis in mouse granulosa tumor cell lines—KK-1 cells

5.2.1 Peroxisomal involvement in steroidogenesis

Very often peroxisomal biogenesis disorders are accompanied by gonadal dysfunction. The most severe disease caused by a peroxisomal deficiency is called Zellweger syndrome (ZS), which is accompanied either by cryptorchism in males or clitoromegaly in females [98]. Additionally, patients with peroxisomal single enzyme deficiencies, such as X-linked adrenoleukodystrophy (X-ALD) or adrenomyeloneuropathy (AMN, a milder phenotype of XALD) exhibit an adreno-testiculo-leukomyelo-neuropathic complex of symptoms that affect fertility [98, 99]. These symptoms indicate that peroxisomal disorders can cause pathological changes in genital organs, and disrupt the balance of androgen and estrogen synthesis.

5.2.2 The link between peroxisomal β-oxidation and steroid synthesis

A first hint that peroxisomes and steroid biosynthesis might be linked is indicated by the peroxisomal localization of some of the enzymes that might be involved in this process. Cholesterol is a component of cellular membranes and the obligatory precursor for steroid synthesis. Cholesterol can be synthesized *de novo* from acetate in gonads in a process that involves around 30 enzymes. Peroxisomes contain all enzymes involved in the synthesis of cholesterol precursors prior to squalene [233]. Apart from that, HMG-CoA reductase, a key rate-limiting enzyme for cholesterol synthesis, is an enzymatic component of the peroxisomes [68, 234]. Moreover, experiments suggest that acetyl-CoA derived from peroxisomal β-oxidation might be channeled to cholesterol synthesis inside the peroxisomes and that the pre-squalene segment of cholesterol biosynthesis is localized to peroxisomes [71, 168].

In this thesis, we have shown that the abundance of peroxisomal SCPx and MFP2 were increased upon hCG stimulation in the granulosa cell-line KK-1. SCPx is a peroxisomal 58-kDa β-oxidation protein with 3-ketoacyl-CoA thiolase activity in the N-terminal domain and with SCP2 (a lipid carrier or transfer protein) function in the C-terminal domain [45]. A substantial amount of SCP2 is located in peroxisomes of Leydig cells, liver and adrenal gonads [235-237]. SCP2 exists in a separate form as cytoplasmic cholesterol transport protein. Cytoplasmic SCP2 is involved in the movement of cholesterol to the outer membrane of mitochondria after which it is imported into mitochondria by StAR for further steroidogenesis [238-242]. SCP2 can enhance the pregnenolone synthesis in isolated mitochondria [243] and is highly expressed in steroidogenic compartments of the rat ovary [244]. However, in these papers, whether SCP was mainly present or induced in the cytoplasm or in the peroxisomal compartment has not been analyzed. In addition, hormones, which stimulate steroid synthesis, can induce SCP2 up-regulation at both mRNA and protein levels [244, 245]. Furthermore, the β-oxidation enzyme MFP2, which participates in hydration and dehydrogenation processes during peroxisomal β-oxidation was also called 17-β-hydroxysteroid dehydrogenase 4 (HSD17B4) [44, 45]. This enzyme was reported to be involved in converting estradiol to estrone [172]. Further, we show here that also other peroxisomal β-oxidation enzymes, including ABCD3, ACOX3, *and* 3-ketoacyl-CoA thiolase, that were not reported to be directly

involved in steroidogenesis, were up-regulated after hCG treatment in the KK-1 cells (Figure 15).

The peroxisomal subcellular localization of enzymes involved in steroidogenesis and the hCG dependent regulation of many peroxisomal enzymes and transporters, which were demonstrated in this thesis, indicate that peroxisomes are directly linked to the metabolism of steroid hormones. Until now, only very few evidence proving that peroxisome is indeed involved in steroidogenesis in the ovary is available in the literature. However, the relationship of peroxisomes to endocrine regulation has been documented in the adrenals and testis of male animals. For example after inhibiting the conversion from cholesterol to pregnenolone and in addition also 11β-hydroxylation with drugs, the number of peroxisomes increased in male rat adrenal cortex [246]. Also after lowering the levels of cholesterol, the major precursor for steroid synthesis, in serum using nafenopin, or by blocking HMG-CoA reductase with mevilonin peroxisomes proliferation was observed in male rat adrenal gonads [247, 248]. Furthermore, during inactive stages of spermatogenesis, the absolute volume of peroxisomes as well as the testicular testosterone concentrations were decreased [249]. In 1988 Mendis-Handagama and colleagues demonstrated that the testosterone secretion in Leydig cells was directly proportional to peroxisome proliferation in rat, hamster, and guinea pig [250]. These data strongly suggested that peroxisomes are metabolically linked to steroidogenesis in males and, as our data show, also in females.

5.2.3 ROS production and anti-oxidants regulation during steroid synthesis

A large amount of ROS are produced during the steroidogenic process especially in the mitochondrial cytochrome P450scc reaction that converts cholesterol to pregnenolone [251], an effect that is counteracted by anti-oxidants and increased catalase activity after gonadotropin stimulation [165, 200, 201, 252]. We found that after hCG stimulation of the KK-1 cells ROS were elevated and anti-oxidative enzymes such as catalase, SOD, GR as well as GNPAT were up-regulated (Figure 16). We have also shown that an exposure to oxidative stress decreased the progesterone synthesis and induced the translation of catalase. During the steroidogenic process not only H_2O_2 but also oxygen free radicals like superoxide radicals are produced [203, 204, 253, 254]. SODs are scavenging these radicals and

dismutate them to H_2O_2 for further detoxification by glutathione peroxidase or catalase. Sugino, N. *et al.* have found that SOD1 expression was largely enhanced after hCG stimulation in the corpus luteum in mid-luteal phase [255]. Since SOD1 is localized in the cytoplasm as well as in peroxisomes [256], it remains unclear that to which extent peroxisomal SOD1 contribute to the increase of this enzyme after hCG stimulation. Moreover, we found that in the granulosa cell line KK-1 also mitochondrial SOD2 was elevated after hCG stimulation. Formerly, this enzyme has also been suggested to be associated with peroxisomes [257]. However, our group has shown that SOD2 is only present in mitochondria but not in peroxisomes [258].

To conclude, our results suggest that anti-oxidants such as catalase and SODs protect the granulosa cells against excessive superoxide and H_2O_2 production to maintain the redox balance during the steroid biosynthesis under highly oxidative process of steroid biosynthesis. Given the relationship of catalase to this process we speculated that functional peroxisomes are required to guarantee the intactness of steroidogenesis in granulosa cells, which we then investigated using a KK-1 peroxisomal deficiency model.

5.2.4 *Pex13* knock-down *in vitro* and its influence on steroidogenesis

Girls suffering from Zellweger syndrome often exhibit clitoromegaly, suggesting a problem in the development of the genital organs [98]. How this malformation arises is still unclear. Several peroxisome-deficient mouse models have been employed to study the effect of peroxisome deficiency in males *in vivo*: i) The Pex7 knockout mice, which were infertile and displayed disorganized seminiferous epithelium [259]; ii) The Acox1 knockout mice, which were also infertile and manifested hypospermatogenesis and decreased Leydig cell numbers [104]; and iii) The Mfp2 knockout that displayed gradual degeneration of the seminiferous epithelium but retained Leydig cell function [102]. Next to the general knockout mouse models also Sertoli cell-specific peroxisome knockout mice were established using the Cre-loxP technique i) The Sertoli cell-specific knockout of the Pex5 gene resulted in the arrest of spermatogenesis and lipid accumulation [102] and ii) The Sertoli cell-specific knockout of Pex13 resulted in testicular disorders with the proliferation of Leydig cells and elevated VLCFA in Sertoli cells [103]. All these findings are in agreement with testicular disorders often found in ZS and/or X-ALD/AMN patients. Alterations in the

ovary were only analyzed in the ACOX1 knockout mice, which had smaller ovaries [104] and in the GNPAT general knockout mice, which displayed a numerical reduction of secondary and tertiary follicles as well as of corpora lutea [100].

In the previous chapter, we discussed that hCG stimulation increased the amount of several peroxisomal proteins. To investigate the functional effects of peroxisomal dysfunction on ovarian granulosa cells and their possible effect on female fertility, we established an *in vitro* model by knocking down the *Pex13* in the granulosa tumor cell line KK-1. Compared to the animal models, the *in vitro* KD model offers the possibility to apply different treatments to cells, in order to analyze biological processes in a relatively efficient way. We have found that the *Pex13* deletion results in a disruption of the peroxisomal matrix protein import resulting in a general failure of the peroxisomal metabolism [36]. Indeed, our experiments showed that in granulosa cells the antioxidant enzyme catalase was mis-targeted to the cytoplasm after the knockdown of PEX13, suggesting a malfunction of the import of proteins into the peroxisomal matrix. Catalase mis-targeting has been previously observed in patients with peroxisomal deficiency and in corresponding mouse models [260, 261]. We also showed that hCG-induced pregnenolone and progesterone secretion was strongly reduced when peroxisomes were dysfunctional in granulosa cells. Similarly, the estradiol levels after FSH treatment were also reduced (Figure 19). This indicates that the steroid hormone synthesis in the granulosa cell line KK-1 is affected when peroxisomes are disrupted. As the consequence of peroxisomal deficiency, frequently mitochondrial pathological alterations are observed [262]. In this respect, it is of interest that StAR mediated cholesterol transport from the outer to the inner mitochondrial membrane is the rate-limiting step for steroidogenesis. After the *Pex13* knockdown we found that the abundance of the StAR protein was strongly reduced (Figure 20). The abundance of CYP11A1, the enzyme that initially converts cholesterol to pregnenolone, remained unchanged. This suggested that the inhibition of StAR caused by the peroxisomal dysfunction (either the peroxisomal metabolic failure or the mistargeting of peroxisomal proteins to the cytoplasm), might account for the decreased hormone production. Compared with the StAR protein levels, the mRNA of *Star* showed no alterations after *Pex13* KD, indicating that the decreased protein abundance of StAR was probably regulated post-translationally, e.g. through proteasomal degradation. Unlike cholesterol, 22R-cholesterol is able to pass the

mitochondrial membrane freely without StAR mediation. When KK-1 cells were treated with 22R-cholesterol, no changes of the progesterone levels were observed. This supported our hypothesis that mitochondrial enzymatic reactions involved late steps of steroidogenesis were unaffected by the peroxisome deficiency, but that the StAR-mediated cholesterol transport into mitochondria was inhibited after the *Pex13* knockdown.

StAR mediated inhibition of hormone secretion after *Pex13* knockdown was further confirmed by the overexpression of Akap1 in the *Pex13* knockdown background in KK-1 cells. AKAPs are scaffolding proteins that are attached to the mitochondrial surface [263]. The AKAP family consists of more than 50 proteins that all share the ability of binding the R subunits of PKA [264] through an amphipathic helix structure [265]. AKAPs are able to target the PKA holoenzyme to different subcellular compartments to activate different cellular signaling pathways [266]. Recently, with electron microscopy and three-dimensional reconstruction techniques, researchers have found that AKAP–PKA complex enabled PKA to adopt its optimal conformation for subsequent substrate phosphorylation [267]. AKAP1, as the most prevalent somatic isoform encoded by the Akap1 gene, is of particular interest since it is known to promote cAMP signaling to mitochondria as well as to target mRNAs to the mitochondria through its RNA-binding domain [151-157]. AKAP1 was able to recruit both PKA and StAR to the mitochondria to promote effective phosphorylation of StAR [158, 268]. StAR is translated as a 37KDa precursor in the cytoplasm, and is then transferred to mitochondria and activated by PKA phosphorylation (Stocco, DM 2001). After cleavage of the N-terminal mitochondrial import sequence, the 30KDa mature form of StAR is produced that mediates the mitochondrial import of cholesterol [269]. In our experimental setup, the overexpression of Akap1-myc induced the up-regulation of StAR protein in *Pex13*-deficient KK-1 cells. Accordingly, the StAR protein abundance and the progesterone levels, which were reduced with the peroxisome deficiency, were partially reconstituted after the Akap1 overexpression (Figure 24, 25). To our knowledge, Dyson and colleagues are the only ones who have shown in the literature that StAR expression and steroidogenesis are linked to the abundance of AKAP1 [158]. Here we suggest a relationship between peroxisomal metabolism, AKAP1 abundance, phosphorylation state of the StAR protein and steroidogenesis. It would be interesting for us to investigate the phosphorylation

status of StAR in response to the peroxisomal deficiency and AKAP1 overexpression. However, unfortunately, there is no commercially antibody against phosphorylated StAR protein available at the moment.

5.2.5 Underlying mechanisms for StAR inhibition under *Pex13* knock-down conditions

Reactive oxygen species (ROS) are formed as by-products of aerobic metabolism. Superoxide radicals (O_2^-), hydrogen peroxide (H_2O_2) and hydroxyl radical ($^{\cdot}OH$) are commonly defined ROS species. Like in other organs also, within the ovary a basal amount of ROS is important for cell signaling and in addition also for ovulation [270-272]. However, excessive ROS production can induce toxic effects on ovarian cells and reduce fertility [192, 193]. Catalase, SODs and glutathione peroxidase (GPX) are described as the three most common antioxidative enzymes that play roles in scavenging ROS [273]. We have found that catalase, SOD1, SOD2 and GR abundance were increased after the knockdown of *Pex13* in KK-1 cells, indicating that due to peroxisomal deficiency, increased oxidative stress leads to the activation of the antioxidative response, which was proven also in macrophages. We further confirmed this by DHE staining, which is a direct indicator for ROS production. Moreover, a similar reaction was shown in the testis in sertoli cells specific *Pex13* KO mice in which catalase, SOD2 and GPX1 abundance were increased [103]. Other studies have demonstrated the great impact of a deregulated redox balance in follicular development, ovulation, fertilization, implantation and embryogenesis [274]. When this balance is disturbed in reproductive organs due to a decreased scavenging capability or increased ROS generation, negative cellular effects or even pathological symptoms can be induced, for example the polycystic ovarian syndrome (PCOS), endometriosis, age-related fertility decline, and defects in early embryogenesis [275-278].

Researchers have demonstrated that ROS exert negative effects on steroidogenesis. H_2O_2 was shown to inhibit steroid synthesis by blocking cholesterol transportation into mitochondria in both luteal cells [279] and Leydig cells [183]. In rat granulosa lutein cells, H_2O_2 decreased the basal and evoked progesterone production by inhibiting adenylyl cyclase activity [280, 281]. Moreover, Diemer *et al.* reported the reduction of progesterone and StAR protein after H_2O_2 treatment in mouse Leydig

cells due to the dissipation of mitochondria membrane potential [185]. Another group has demonstrated a decreased testosterone secretion due to inhibition of P450scc activity and StAR protein expression after H_2O_2 treatment in cultured Leydig cells [282]. According to these reports and to the results we presented here, StAR and progesterone inhibition were, at least partially, exerted by the increased ROS generation after peroxisome deficiency. To confirm this hypothesis, we treated KK-1 cells with H_2O_2. We found in consistence with our expectation that a H_2O_2 dose-dependent reduction of StAR and progesterone secretion with no changes of P450scc, indicating that mitochondrial steroidogenic enzymes were unaffected, similar to the *Pex13* KD results. Analysis of the StAR mRNAs after H_2O_2 treatment showed that the StAR protein abundance regulation is controlled post-translationally, similar to what we observed in case of knockdown of PEX13. The StAR protein is particularly susceptible to ROS exposure and therefore the StAR-mediated translocation of cholesterol responds critically to a disrupted redox balance [185]. Also, an intact mitochondrial membrane potential is critical for StAR mediated cholesterol translocation [283-285]. Excessive ROS can cause mitochondrial membrane potential dissipation leading to StAR protein inhibition [185]. Indeed, peroxisome deficiency can also cause mitochondrial dysfunction, e.g., the *Pex5* knock-out mice exhibited very severe mitochondrial abnormalities in various different organs, including steroid producing adrenal cortex [262]. In Sertoli cell- specific *Pex13* knockout mice, complex III of the mitochondrial respiratory chain was strongly reduced and a mislocalisation of mitochondrial SOD2 to the cytosol was observed, indicating mitochondrial fragility [103]. The underlying mechanisms for mitochondrial dysfunction due to peroxisome deficiency is most probably the accumulation of ROS together with the accumulation of toxic fatty acids that are usually degraded by intact peroxisomes and are unable to be metabolized by mitochondria.

5.2.6 Protective role of tocopherol on steroidogenic enzymes and steroid biosynthesis

To further confirm that the disturbance of steroid synthesis after the knock-down of *Pex13* may be due to increased ROS accumulation, we have investigated whether tocopherol treatment would reestablish hormone secretion. Tocopherol (Vitamin E) is one of the major non-enzymatic antioxidants in mammalian cells, which mainly

derives from diet [286]. Vitamine E is located within the cellular membrane and protects the cells against DNA damage and toxic effects by directly scanvenging free radicals and/or down-regulating mitochondrial superoxide generation [287, 288]. Tocopherol is shown to have a positive impact on fertility [289]. Chen *et al.* in 2005 have investigated testosterone secretion from isolated Leydig cells cultured with or without vitamin E, and showed that the testosterone production was enhanced [290]. In rat testis, cadmium was reported to induce ROS damage and to exert negative effects on StAR and steroid synthesis and that these effects were counteracted by Vitamin E supplementation [291]. In addition, in rat Leydig and Sertoli cells, administration of vitamin E was reported to ameliorate ROS induced testicular toxicity from polychlorinated biphenyls (PCBs), which are ubiquitous environmental contaminants. [292, 293]. Therefore, Vitamin E significantly contributes to protect steroidogenic cells and tissues against ROS. Our results show that in KK-1 granulosa lutein cells, the decrease of StAR protein abundance and of progesterone secretion observed due to the peroxisomal dysfunction, was also partially counteracted after tocopherol treatment (Figure 34). Our study is the first one to demonstrate the protective role of vitamin E on StAR protein and progesterone synthesis under oxidative stress induced by peroxisomal deficiency in luteinized granulosa cells.

6 Summary

Human disorders with peroxisomal deficiency show a range of pathologies in the reproductive system leading to human infertility. In recent years, the relationship between peroxisomes and male infertility has been examined in different groups. However, until now nobody has focused on the pathological consequences happening in the ovary in case of peroxisomal deficiency. Peroxisomes are cell organelles involved in fatty acid β-oxidation, plasmalogen synthesis and cholesterol synthesis on which steroidogenesis depends. Besides this, peroxisomes are able to maintain the equilibrium between production and scavenging of ROS, which are involved in the regulation of follicular development. The aim of this thesis was therefore to study the role of peroxisomes in granulosa cells, follicular development and steroid synthesis in the ovary.

Paraformaldehyde-fixed paraffin-embedded (FFPE) sections of adult mouse ovaries were stained to analyze peroxisome distribution and regulation during follicular development. A highly differentiated mouse granulosa tumor cell line (KK-1 cells) was established as cell culture model to study peroxisomal function in granulosa cells. Peroxisome related gene expression and protein abundance were compared before and after hCG treatment in KK-1 cells. Moreover, the *Pex13* gene, encodes a peroxisomal biogenesis protein, was knocked down in KK-1 cells by *Pex13* RNAi. Moreover, the effects of the peroxisomal deficiency on mitochondrial cholesterol transport (StAR protein) as well as steroidogenesis were analyzed. As trial to stimulate StAR cholesterol transportation, the cloned A kinase anchoring protein Akap1 was overexpressed in KK-1 cells. Thereafter, H_2O_2 treatment and α-Tocopherol treatment were used to figure out the influence of ROS and antioxidants on steroidogenesis respectively.

The results of this thesis provide clear evidence that peroxisomal proteins are highly abundant in the mouse ovary and exhibit a distinct heterogeneous location pattern during folliculogenesis. Generally, the abundance of peroxisomal proteins is increasing in oocytes during follicular development, suggesting that peroxisomes are protecting mature oocytes against ROS and lipotoxicity. The *in vitro* studies showed with KK-1 cells that hCG induced the upregulation of peroxisomal proteins and their corresponding mRNAs, suggesting a strong regulatory effect of gonadotropic

hormones on the peroxisomal compartment in granulosa cells. Under peroxisome deficiency conditions, induced by the *Pex13* KD, the steroidogenic pathway in granulosa cells was disturbed and the peroxisome deficiency-exerted reduction of the steroid hormone secretion is at least partially mediated via StAR inhibition. The underlying mechanisms for this may at least partly result from increased oxidative stress after the Pex13 KD. In this thesis it was indeed shown that ROS were increased after the Pex13 KD and it is well known that excessive ROS leads to the inhibition of steroidogenesis. This hypothesis is further confirmed by the protective effect of tocopherol on StAR protein and progesterone synthesis under oxidative stress induced by the peroxisomal deficiency. Moreover, the results of this thesis provide also evidence that an increase of AKAP1 can also partly compensate the peroxisomal deficiency- induced mitochondrial alteration. In addition, it was shown in the literature that the lipid structure and the lipid composition of cell membrane are related to the activity of adenylyl cyclase (AC) and G protein-coupled receptor signaling, but the direct relationship between peroxisomal deficiency with adenylyl cyclase needs to be clarified in the future. According to my results and related international literatures, the possible mechanism of peroxisome-deficiency exerted defects on mitochondrial steroidogenesis is summarized in Figure 34.

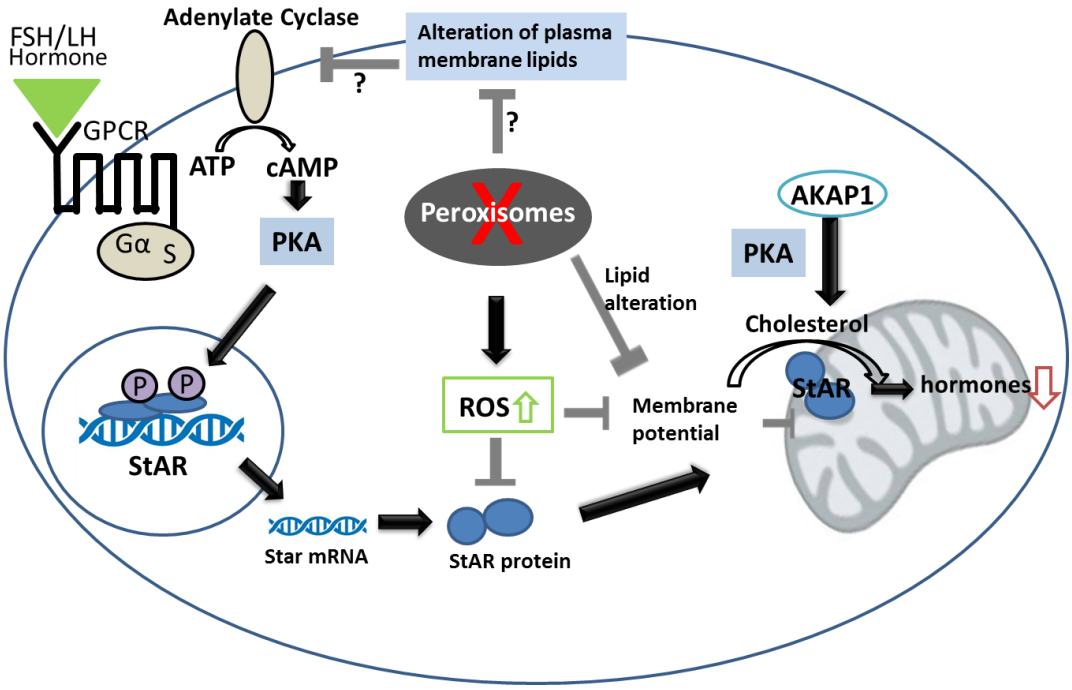

Figure 34. Schematic illustration of the mechanism of peroxisome regulation on steroidogenesis.

7 Zusammenfassung

Menschliche Erkrankungen, die auf peroxisomale Dysfunktion zurückzuführen sind, verursachen pathologische Veränderungen in den Geschlechtsorganen, die zu Infertilität führen können. In den letzten Jahren wurde der Zusammenhang zwischen männlicher Infertilität und peroxisomalen Defekten bereits in der Fachliteratur diskutiert, jedoch wurde im Gegensatz hierzu der Einfluss peroxisomaler Erkrankungen auf die weiblichen Geschlechtsorgane kaum untersucht.

Peroxisomen sind Zellorganellen, die in der β-Oxidation von Fettsäuren, Plasmalogenbiosynthese, und in die für die Steroidogenese wichtige Cholesterin-Biosynthese involviert sind. Peroxisomen spielen auch eine wichtige Rolle für die Aufrechterhaltung des Redox Gleichgewichtes. Da Studien gezeigt haben, dass eine Zuname oxidativen Stresses negative Auswirkungen auf die Follikulogenese haben kann, war unsere Hypothese, dass Peroxisomen eine protektive Rolle für die Zellen im Ovar haben könnten. Ziel dieser Arbeit war daher, die Funktion von Peroxisomen in den Granulosa Zellen des Ovars und während der Steroid-Biosynthese zu analysieren.

Die stark differenzierte Granulosa Tumor Zelllinie (KK-1 Zellen) wurde als Zellkultur Modell für die Untersuchungen der peroxisomalen Funktion etabliert. Die Expression von Genen, die für peroxisomale Proteine kodieren wurde vor und nach Behandlung der KK-1 Zellen mit humanen Choriongonatropin gemessen. Als Modell für die peroxisomale Dysfunktion, wurde *Pex13*, ein Gen, welches für ein peroxisomales Biogenese Protein kodiert, über RNA Interferenz runterreguliert und die darauf folgenden Auswirkungen auf Steroidogenese und mitochondrialen Cholesterin Transport analysiert. Weiterhin wurde der Effekt von oxidativen Stress, Antioxidantien und überaktivierung des mitochondrialen Cholesterin Imports auf die Steroidogenese in KK-1 Zellen untersucht. Peroxisomale Veränderungen die während der Follikulogenese stattfinnden wurden anhand von Immunofluoreszenzen an Paraffin eingebetteten Ovarien untersucht.

Die Ergebnisse dieser Arbeit zeigen, dass peroxisomale Proteine hoch abundant in Maus Ovarien sind und dass sie eine heterogene Verteilung in den unterschiedlichen Zellen des Ovars aufweisen. Während der Follikulogenese kommt es zu einer deutlichen, Stadium-spezifische Regulation der peroxisomalen Protein Mengen: Es

zeigt sich, dass speziell in Oocyten, die Menge an peroxisomalen Proteine während der Follikulogenese zunimmt. Dies deutet darauf hin, dass Peroxisomen eine Schutzfunktion während der Reifung der Eizelle im Hinblick auf oxidative Stress und Lipid-Toxizität haben könnten.

Die *in vitro* Studie an KK-1 Zellen zeigt, dass hCG eine Erhöhung der peroxisomalen Protein Menge bewirkt. Unsere Ergebnisse zeigen auch, dass wenn eine peroxisomale Dysfunktion besteht die Stereoidogenese negativ beeinflusst wird indem die Sekretion von Steroid Hormone und der mitochondriale Cholesterin Transport herabgesetzt wurde. Eine mögliche Ursache dieser Beobachtungen ist auf erhöhten oxidativen Stress zurückzuführen. Auch konnten wir zeigen, dass die durch die RNA Interferenz induzierte peroxisomale Dysfunktion zu einer nennenswerten Zuname oxidativen Stresses führte, welche durch die Zugabe von Antioxidantien kompensiert werden konnte. Auch konnten wir zeigen, dass eine Zuname des mitochondrialen Cholesterin-Transports durch Stimulation von StAR über Überexpression von AKAP1 den negativen Effekt des peroxisomalen Defizits teilweise kompensieren konnte.

Zusammenfassend, wurden die Ergebnisse dieser Arbeit mit Hinzuname bereits publizierten Informationen für die Anfertigung der in Figur 34 gezeigten Schemas verwendet.

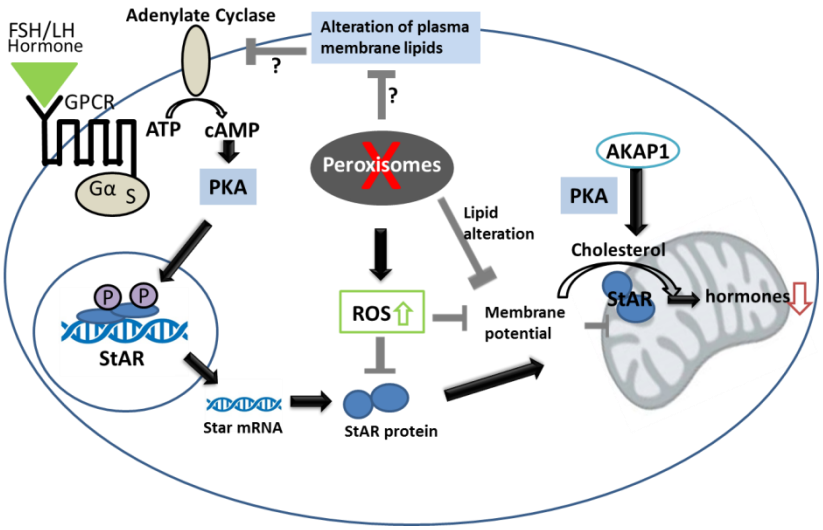

Figur 34. Schematische Abbildung der peroxisomalen Regulierung der Steroidogenesis

8 References

1. Treuting P, Dintzis S. Comparative Anatomy and Histology-a mouse and human atlas, London, Waltham, San Diego: Elsevier, Academic Press. 2012.
2. Rhodin J. Correlation of ultrastructural organization and function in normal and experimentally changed proximal tubule cells of the mouse kidney. Karolinska Institutet, Stockholm; 1954. Doctor thesis.
3. De Duve C, Baudhuin P. Peroxisomes (microbodies and related particles). Physiol Rev 1966; 46:323-357.
4. Angermuller S, Bruder G, Volkl A, Wesch H, Fahimi HD. Localization of xanthine oxidase in crystalline cores of peroxisomes. A cytochemical and biochemical study. Eur J Cell Biol 1987; 45:137-144.
5. Usuda N, Reddy MK, Hashimoto T, Rao MS, Reddy JK. Tissue specificity and species differences in the distribution of urate oxidase in peroxisomes. Lab Invest 1988; 58:100-111.
6. Volkl A, Baumgart E, Fahimi HD. Localization of urate oxidase in the crystalline cores of rat liver peroxisomes by immunocytochemistry and immunoblotting. J Histochem Cytochem 1988; 36:329-336.
7. Goldfischer S, Moore CL, Johnson AB, Spiro AJ, Valsamis MP, Wisniewski HK, Ritch RH, Norton WT, Rapin I, Gartner LM. Peroxisomal and mitochondrial defects in the cerebro-hepato-renal syndrome. Science 1973; 182:62-64.
8. Fujiki Y. Peroxisome biogenesis and peroxisome biogenesis disorders. FEBS Lett 2000; 476:42-46.
9. Gould SJ, Valle D. Peroxisome biogenesis disorders: genetics and cell biology. Trends Genet 2000; 16:340-345.
10. Wanders RJ, Schutgens RB, Barth PG. Peroxisomal disorders: a review. J Neuropathol Exp Neurol 1995; 54:726-739.
11. Distel B, Erdmann R, Gould SJ, Blobel G, Crane DI, Cregg JM, Dodt G, Fujiki Y, Goodman JM, Just WW, Kiel JA, Kunau WH, et al. A unified nomenclature for peroxisome biogenesis factors. J Cell Biol 1996; 135:1-3.
12. Smith JJ, Aitchison JD. Regulation of peroxisome dynamics. Curr Opin Cell Biol 2009; 21:119-126.
13. Baumgart E, Volkl A, Hashimoto T, Fahimi HD. Biogenesis of peroxisomes: immunocytochemical investigation of peroxisomal membrane proteins in proliferating rat liver peroxisomes and in catalase-negative membrane loops. J Cell Biol 1989; 108:2221-2231.
14. Lazarow PB, Fujiki Y. Biogenesis of peroxisomes. Annu Rev Cell Biol 1985; 1:489-530.
15. Imanaka T, Small GM, Lazarow PB. Translocation of acyl-CoA oxidase into peroxisomes requires ATP hydrolysis but not a membrane potential. J Cell Biol 1987; 105:2915-2922.
16. Pause B, Diestelkotter P, Heid H, Just WW. Cytosolic factors mediate protein insertion into the peroxisomal membrane. FEBS Lett 1997; 414:95-98.
17. Suzuki Y, Orii T, Takiguchi M, Mori M, Hijikata M, Hashimoto T. Biosynthesis of membrane polypeptides of rat liver peroxisomes. J Biochem 1987; 101:491-496.
18. Suzuki Y, Shimozawa N, Orii T, Aikawa J, Tada K, Kuwabara T, Hashimoto T. Biosynthesis of peroxisomal membrane polypeptides in infants with Zellweger syndrome. J Inherit Metab Dis 1987; 10:297-300.
19. Eckert JH, Erdmann R. Peroxisome biogenesis. Rev Physiol Biochem Pharmacol 2003; 147:75-121.
20. Hettema EH, Erdmann R, van der Klei I, Veenhuis M. Evolving models for peroxisome biogenesis. Curr Opin Cell Biol 2014; 29:25-30.

21. Imanaka T, Takano T, Osumi T, Hashimoto T. Sorting of the 70-kDa peroxisomal membrane protein into rat liver peroxisomes in vitro. Ann N Y Acad Sci 1996; 804:663-665.
22. Pause B, Saffrich R, Hunziker A, Ansorge W, Just WW. Targeting of the 22 kDa integral peroxisomal membrane protein. FEBS Lett 2000; 471:23-28.
23. Diestelkotter P, Just WW. In vitro insertion of the 22-kD peroxisomal membrane protein into isolated rat liver peroxisomes. J Cell Biol 1993; 123:1717-1725.
24. van der Zand A, Braakman I, Geuze HJ, Tabak HF. The return of the peroxisome. J Cell Sci 2006; 119:989-994.
25. Gould SJ, Keller GA, Hosken N, Wilkinson J, Subramani S. A conserved tripeptide sorts proteins to peroxisomes. J Cell Biol 1989; 108:1657-1664.
26. Rachubinski RA, Subramani S. How proteins penetrate peroxisomes. Cell 1995; 83:525-528.
27. Rehling P, Marzioch M, Niesen F, Wittke E, Veenhuis M, Kunau WH. The import receptor for the peroxisomal targeting signal 2 (PTS2) in Saccharomyces cerevisiae is encoded by the PAS7 gene. EMBO J 1996; 15:2901-2913.
28. Swinkels BW, Gould SJ, Bodnar AG, Rachubinski RA, Subramani S. A novel, cleavable peroxisomal targeting signal at the amino-terminus of the rat 3-ketoacyl-CoA thiolase. EMBO J 1991; 10:3255-3262.
29. Dammai V, Subramani S. The human peroxisomal targeting signal receptor, Pex5p, is translocated into the peroxisomal matrix and recycled to the cytosol. Cell 2001; 105:187-196.
30. Ghys K, Fransen M, Mannaerts GP, Van Veldhoven PP. Functional studies on human Pex7p: subcellular localization and interaction with proteins containing a peroxisome-targeting signal type 2 and other peroxins. Biochem J 2002; 365:41-50.
31. Girzalsky W, Platta HW, Erdmann R. Protein transport across the peroxisomal membrane. Biol Chem 2009; 390:745-751.
32. Mukai S, Ghaedi K, Fujiki Y. Intracellular localization, function, and dysfunction of the peroxisome-targeting signal type 2 receptor, Pex7p, in mammalian cells. J Biol Chem 2002; 277:9548-9561.
33. Colasante C, Chen J, Ahlemeyer B, Baumgart-Vogt E. Peroxisomes in cardiomyocytes and the peroxisome / peroxisome proliferator-activated receptor-loop. Thromb Haemost 2015; 113:452-463.
34. Albertini M, Rehling P, Erdmann R, Girzalsky W, Kiel JA, Veenhuis M, Kunau WH. Pex14p, a peroxisomal membrane protein binding both receptors of the two PTS-dependent import pathways. Cell 1997; 89:83-92.
35. Stein K, Schell-Steven A, Erdmann R, Rottensteiner H. Interactions of Pex7p and Pex18p/Pex21p with the peroxisomal docking machinery: implications for the first steps in PTS2 protein import. Mol Cell Biol 2002; 22:6056-6069.
36. Gould SJ, Kalish JE, Morrell JC, Bjorkman J, Urquhart AJ, Crane DI. Pex13p is an SH3 protein of the peroxisome membrane and a docking factor for the predominantly cytoplasmic PTs1 receptor. J Cell Biol 1996; 135:85-95.
37. Erdmann R, Blobel G. Giant peroxisomes in oleic acid-induced Saccharomyces cerevisiae lacking the peroxisomal membrane protein Pmp27p. J Cell Biol 1995; 128:509-523.
38. Marshall PA, Krimkevich YI, Lark RH, Dyer JM, Veenhuis M, Goodman JM. Pmp27 promotes peroxisomal proliferation. J Cell Biol 1995; 129:345-355.
39. Passreiter M, Anton M, Lay D, Frank R, Harter C, Wieland FT, Gorgas K, Just WW. Peroxisome biogenesis: involvement of ARF and coatomer. J Cell Biol 1998; 141:373-383.
40. Schrader M, Reuber BE, Morrell JC, Jimenez-Sanchez G, Obie C, Stroh TA, Valle D, Schroer TA, Gould SJ. Expression of PEX11beta mediates peroxisome proliferation in the absence of extracellular stimuli. J Biol Chem 1998; 273:29607-29614.
41. Li X, Baumgart E, Dong GX, Morrell JC, Jimenez-Sanchez G, Valle D, Smith KD, Gould SJ. PEX11alpha is required for peroxisome proliferation in response to 4-

phenylbutyrate but is dispensable for peroxisome proliferator-activated receptor alpha-mediated peroxisome proliferation. Mol Cell Biol 2002; 22:8226-8240.
42. Li X, Gould SJ. PEX11 promotes peroxisome division independently of peroxisome metabolism. J Cell Biol 2002; 156:643-651.
43. Baumgart E. Application of in situ hybridization, cytochemical and immunocytochemical techniques for the investigation of peroxisomes. A review including novel data. Robert Feulgen Prize Lecture 1997. Histochem Cell Biol 1997; 108:185-210.
44. Hashimoto T. Peroxisomal beta-oxidation: enzymology and molecular biology. Ann N Y Acad Sci 1996; 804:86-98.
45. Hashimoto T. Peroxisomal beta-oxidation enzymes. Neurochem Res 1999; 24:551-563.
46. Suzuki H, Kawarabayasi Y, Kondo J, Abe T, Nishikawa K, Kimura S, Hashimoto T, Yamamoto T. Structure and regulation of rat long-chain acyl-CoA synthetase. J Biol Chem 1990; 265:8681-8685.
47. Subramani S. Components involved in peroxisome import, biogenesis, proliferation, turnover, and movement. Physiol Rev 1998; 78:171-188.
48. Mannaerts GP, Van Veldhoven PP, Casteels M. Peroxisomal lipid degradation via beta- and alpha-oxidation in mammals. Cell Biochem Biophys 2000; 32 Spring:73-87.
49. Wanders RJ. Peroxisomes, lipid metabolism, and human disease. Cell Biochem Biophys 2000; 32 Spring:89-106.
50. Lombard-Platet G, Savary S, Sarde CO, Mandel JL, Chimini G. A close relative of the adrenoleukodystrophy (ALD) gene codes for a peroxisomal protein with a specific expression pattern. Proc Natl Acad Sci U S A 1996; 93:1265-1269.
51. Netik A, Forss-Petter S, Holzinger A, Molzer B, Unterrainer G, Berger J. Adrenoleukodystrophy-related protein can compensate functionally for adrenoleukodystrophy protein deficiency (X-ALD): implications for therapy. Hum Mol Genet 1999; 8:907-913.
52. Schaffer JE, Lodish HF. Expression cloning and characterization of a novel adipocyte long chain fatty acid transport protein. Cell 1994; 79:427-436.
53. Reddy JK, Hashimoto T. Peroxisomal beta-oxidation and peroxisome proliferator-activated receptor alpha: an adaptive metabolic system. Annu Rev Nutr 2001; 21:193-230.
54. Lazarow PB, De Duve C. A fatty acyl-CoA oxidizing system in rat liver peroxisomes; enhancement by clofibrate, a hypolipidemic drug. Proc Natl Acad Sci U S A 1976; 73:2043-2046.
55. Vanhooren JC, Marynen P, Mannaerts GP, Van Veldhoven PP. Evidence for the existence of a pristanoyl-CoA oxidase gene in man. Biochem J 1997; 325 (Pt 3):593-599.
56. Baumgart E, Vanhooren JC, Fransen M, Van Leuven F, Fahimi HD, Van Veldhoven PP, Mannaerts GP. Molecular cloning and further characterization of rat peroxisomal trihydroxycoprostanoyl-CoA oxidase. Biochem J 1996; 320 (Pt 1):115-121.
57. Schepers L, Van Veldhoven PP, Casteels M, Eyssen HJ, Mannaerts GP. Presence of three acyl-CoA oxidases in rat liver peroxisomes. An inducible fatty acyl-CoA oxidase, a noninducible fatty acyl-CoA oxidase, and a noninducible trihydroxycoprostanoyl-CoA oxidase. J Biol Chem 1990; 265:5242-5246.
58. Kroetz DL, Yook P, Costet P, Bianchi P, Pineau T. Peroxisome proliferator-activated receptor alpha controls the hepatic CYP4A induction adaptive response to starvation and diabetes. J Biol Chem 1998; 273:31581-31589.
59. Palosaari PM, Vihinen M, Mantsala PI, Alexson SE, Pihlajaniemi T, Hiltunen JK. Amino acid sequence similarities of the mitochondrial short chain delta 3, delta 2-enoyl-CoA isomerase and peroxisomal multifunctional delta 3, delta 2-enoyl-CoA isomerase, 2-enoyl-CoA hydratase, 3-hydroxyacyl-CoA dehydrogenase enzyme in rat liver. The proposed occurrence of isomerization and hydration in the same catalytic domain of the multifunctional enzyme. J Biol Chem 1991; 266:10750-10753.

60. Dieuaide-Noubhani M, Asselberghs S, Mannaerts GP, Van Veldhoven PP. Evidence that multifunctional protein 2, and not multifunctional protein 1, is involved in the peroxisomal beta-oxidation of pristanic acid. Biochem J 1997; 325 (Pt 2):367-373.
61. Bun-ya M, Maebuchi M, Kamiryo T, Kurosawa T, Sato M, Tohma M, Jiang LL, Hashimoto T. Thiolase involved in bile acid formation. J Biochem 1998; 123:347-352.
62. Reddy JK, Mannaerts GP. Peroxisomal lipid metabolism. Annu Rev Nutr 1994; 14:343-370.
63. Desvergne B, Wahli W. Peroxisome proliferator-activated receptors: nuclear control of metabolism. Endocr Rev 1999; 20:649-688.
64. Singh H, Usher S, Poulos A. Dihydroxyacetone phosphate acyltransferase and alkyldihydroxyacetone phosphate synthase activities in rat liver subcellular fractions and human skin fibroblasts. Arch Biochem Biophys 1989; 268:676-686.
65. Wanders RJ. Peroxisomes, lipid metabolism, and peroxisomal disorders. Mol Genet Metab 2004; 83:16-27.
66. Brites P, Waterham HR, Wanders RJ. Functions and biosynthesis of plasmalogens in health and disease. Biochim Biophys Acta 2004; 1636:219-231.
67. Karnati S, Baumgart-Vogt E. Peroxisomes in mouse and human lung: their involvement in pulmonary lipid metabolism. Histochem Cell Biol 2008; 130:719-740.
68. Keller GA, Barton MC, Shapiro DJ, Singer SJ. 3-Hydroxy-3-methylglutaryl-coenzyme A reductase is present in peroxisomes in normal rat liver cells. Proc Natl Acad Sci U S A 1985; 82:770-774.
69. Keller GA, Pazirandeh M, Krisans S. 3-Hydroxy-3-methylglutaryl coenzyme A reductase localization in rat liver peroxisomes and microsomes of control and cholestyramine-treated animals: quantitative biochemical and immunoelectron microscopical analyses. J Cell Biol 1986; 103:875-886.
70. Kovacs WJ, Olivier LM, Krisans SK. Central role of peroxisomes in isoprenoid biosynthesis. Prog Lipid Res 2002; 41:369-391.
71. Kovacs WJ, Tape KN, Shackelford JE, Duan X, Kasumov T, Kelleher JK, Brunengraber H, Krisans SK. Localization of the pre-squalene segment of the isoprenoid biosynthetic pathway in mammalian peroxisomes. Histochem Cell Biol 2007; 127:273-290.
72. Kovacs WJ, Shackelford JE, Tape KN, Richards MJ, Faust PL, Fliesler SJ, Krisans SK. Disturbed cholesterol homeostasis in a peroxisome-deficient PEX2 knockout mouse model. Mol Cell Biol 2004; 24:1-13.
73. Elliott BM, Dodd NJ, Elcombe CR. Increased hydroxyl radical production in liver peroxisomal fractions from rats treated with peroxisome proliferators. Carcinogenesis 1986; 7:795-799.
74. Zwacka RM, Reuter A, Pfaff E, Moll J, Gorgas K, Karasawa M, Weiher H. The glomerulosclerosis gene Mpv17 encodes a peroxisomal protein producing reactive oxygen species. EMBO J 1994; 13:5129-5134.
75. Stolz DB, Zamora R, Vodovotz Y, Loughran PA, Billiar TR, Kim YM, Simmons RL, Watkins SC. Peroxisomal localization of inducible nitric oxide synthase in hepatocytes. Hepatology 2002; 36:81-93.
76. Fransen M, Nordgren M, Wang B, Apanasets O. Role of peroxisomes in ROS/RNS-metabolism: implications for human disease. Biochim Biophys Acta 2012; 1822:1363-1373.
77. Droge W. Oxidative stress and aging. Adv Exp Med Biol 2003; 543:191-200.
78. Saran M. To what end does nature produce superoxide? NADPH oxidase as an autocrine modifier of membrane phospholipids generating paracrine lipid messengers. Free Radic Res 2003; 37:1045-1059.
79. Oshino N, Oshino R, Chance B. The characteristics of the "peroxidatic" reaction of catalase in ethanol oxidation. Biochem J 1973; 131:555-563.
80. Purdue PE, Castro SM, Protopopov V, Lazarow PB. Targeting of human catalase to peroxisomes is dependent upon a novel C-terminal peroxisomal targeting sequence. Ann N Y Acad Sci 1996; 804:775-776.

81. Siraki AG, Pourahmad J, Chan TS, Khan S, O'Brien PJ. Endogenous and endobiotic induced reactive oxygen species formation by isolated hepatocytes. Free Radic Biol Med 2002; 32:2-10.
82. Hashimoto F, Hayashi H. Significance of catalase in peroxisomal fatty acyl-CoA beta-oxidation. Biochim Biophys Acta 1987; 921:142-150.
83. Schriner SE, Linford NJ, Martin GM, Treuting P, Ogburn CE, Emond M, Coskun PE, Ladiges W, Wolf N, Van Remmen H, Wallace DC, Rabinovitch PS. Extension of murine life span by overexpression of catalase targeted to mitochondria. Science 2005; 308:1909-1911.
84. Litwin JA, Beier K, Volkl A, Hofmann WJ, Fahimi HD. Immunocytochemical investigation of catalase and peroxisomal lipid beta-oxidation enzymes in human hepatocellular tumors and liver cirrhosis. Virchows Arch 1999; 435:486-495.
85. Lauer C, Volkl A, Riedl S, Fahimi HD, Beier K. Impairment of peroxisomal biogenesis in human colon carcinoma. Carcinogenesis 1999; 20:985-989.
86. Singh I. Mammalian peroxisomes: metabolism of oxygen and reactive oxygen species. Ann N Y Acad Sci 1996; 804:612-627.
87. Antonenkov VD, Grunau S, Ohlmeier S, Hiltunen JK. Peroxisomes are oxidative organelles. Antioxid Redox Signal 2010; 13:525-537.
88. Barth PG, Gootjes J, Bode H, Vreken P, Majoie CB, Wanders RJ. Late onset white matter disease in peroxisome biogenesis disorder. Neurology 2001; 57:1949-1955.
89. Moser HW. Genotype-phenotype correlations in disorders of peroxisome biogenesis. Mol Genet Metab 1999; 68:316-327.
90. Wanders RJ, Tager JM. Lipid metabolism in peroxisomes in relation to human disease. Mol Aspects Med 1998; 19:69-154.
91. Lazarow PB. Peroxisome structure, function, and biogenesis--human patients and yeast mutants show strikingly similar defects in peroxisome biogenesis. J Neuropathol Exp Neurol 1995; 54:720-725.
92. Moser HW, Powers JM, Smith KD. Adrenoleukodystrophy: molecular genetics, pathology, and Lorenzo's oil. Brain Pathol 1995; 5:259-266.
93. Moser AB, Rasmussen M, Naidu S, Watkins PA, McGuinness M, Hajra AK, Chen G, Raymond G, Liu A, Gordon D, et al. Phenotype of patients with peroxisomal disorders subdivided into sixteen complementation groups. J Pediatr 1995; 127:13-22.
94. Baes M, Gressens P, Baumgart E, Carmeliet P, Casteels M, Fransen M, Evrard P, Fahimi D, Declercq PE, Collen D, van Veldhoven PP, Mannaerts GP. A mouse model for Zellweger syndrome. Nat Genet 1997; 17:49-57.
95. Faust PL, Hatten ME. Targeted deletion of the PEX2 peroxisome assembly gene in mice provides a model for Zellweger syndrome, a human neuronal migration disorder. J Cell Biol 1997; 139:1293-1305.
96. Li X, Baumgart E, Morrell JC, Jimenez-Sanchez G, Valle D, Gould SJ. PEX11 beta deficiency is lethal and impairs neuronal migration but does not abrogate peroxisome function. Mol Cell Biol 2002; 22:4358-4365.
97. Maxwell M, Bjorkman J, Nguyen T, Sharp P, Finnie J, Paterson C, Tonks I, Paton BC, Kay GF, Crane DI. Pex13 inactivation in the mouse disrupts peroxisome biogenesis and leads to a Zellweger syndrome phenotype. Mol Cell Biol 2003; 23:5947-5957.
98. Powers JM. Adreno-leukodystrophy (adreno-testiculo-leukomyelo-neuropathic-complex). Clin Neuropathol 1985; 4:181-199.
99. Powers JM, Schaumburg HH. The testis in adreno-leukodystrophy. Am J Pathol 1981; 102:90-98.
100. Rodemer C, Thai TP, Brugger B, Kaercher T, Werner H, Nave KA, Wieland F, Gorgas K, Just WW. Inactivation of ether lipid biosynthesis causes male infertility, defects in eye development and optic nerve hypoplasia in mice. Hum Mol Genet 2003; 12:1881-1895.
101. Baes M, Van Veldhoven PP. Generalised and conditional inactivation of Pex genes in mice. Biochim Biophys Acta 2006; 1763:1785-1793.

102. Huyghe S, Schmalbruch H, De Gendt K, Verhoeven G, Guillou F, Van Veldhoven PP, Baes M. Peroxisomal multifunctional protein 2 is essential for lipid homeostasis in Sertoli cells and male fertility in mice. Endocrinology 2006; 147:2228-2236.
103. Nenicu A. Influence of peroxisomes on development, maturation and adult functions of the testis. Justus-Liebig-Universität Gießen; 2010.
104. Fan CY, Pan J, Chu R, Lee D, Kluckman KD, Usuda N, Singh I, Yeldandi AV, Rao MS, Maeda N, Reddy JK. Hepatocellular and hepatic peroxisomal alterations in mice with a disrupted peroxisomal fatty acyl-coenzyme A oxidase gene. J Biol Chem 1996; 271:24698-24710.
105. McGee EA, Hsueh AJ. Initial and cyclic recruitment of ovarian follicles. Endocr Rev 2000; 21:200-214.
106. Hirshfield AN. Development of follicles in the mammalian ovary. Int Rev Cytol 1991; 124:43-101.
107. Gomperts M, Garcia-Castro M, Wylie C, Heasman J. Interactions between primordial germ cells play a role in their migration in mouse embryos. Development 1994; 120:135-141.
108. Pepling ME, Spradling AC. Female mouse germ cells form synchronously dividing cysts. Development 1998; 125:3323-3328.
109. Rankin T, Dean J. The molecular genetics of the zona pellucida: mouse mutations and infertility. Mol Hum Reprod 1996; 2:889-894.
110. Bukulmez O, Arici A. Leukocytes in ovarian function. Hum Reprod Update 2000; 6:1-15.
111. Carabatsos MJ, Elvin J, Matzuk MM, Albertini DF. Characterization of oocyte and follicle development in growth differentiation factor-9-deficient mice. Dev Biol 1998; 204:373-384.
112. Orisaka M, Tajima K, Tsang BK, Kotsuji F. Oocyte-granulosa-theca cell interactions during preantral follicular development. J Ovarian Res 2009; 2:9.
113. Zhu N, Jia HX, Liu XK, Zhao XE, Wei Q, Ma BH. [Measuring the estrus cycle and its effect on superovulation in mice]. Dongwuxue Yanjiu 2012; 33:276-282.
114. Soccio RE, Breslow JL. Intracellular cholesterol transport. Arterioscler Thromb Vasc Biol 2004; 24:1150-1160.
115. Mesmin B, Maxfield FR. Intracellular sterol dynamics. Biochim Biophys Acta 2009; 1791:636-645.
116. Chang TY, Chang CC, Ohgami N, Yamauchi Y. Cholesterol sensing, trafficking, and esterification. Annu Rev Cell Dev Biol 2006; 22:129-157.
117. Vahouny GV, Chanderbhan R, Noland BJ, Irwin D, Dennis P, Lambeth JD, Scallen TJ. Sterol carrier protein2. Identification of adrenal sterol carrier protein2 and site of action for mitochondrial cholesterol utilization. J Biol Chem 1983; 258:11731-11737.
118. Mendis-Handagama SM, Aten RF, Watkins PA, Scallen TJ, Berhman HR. Peroxisomes and sterol carrier protein-2 in luteal cell steroidogenesis: a possible role in cholesterol transport from lipid droplets to mitochondria. Tissue Cell 1995; 27:483-490.
119. Miller WL. Steroidogenic acute regulatory protein (StAR), a novel mitochondrial cholesterol transporter. Biochim Biophys Acta 2007; 1771:663-676.
120. Lambeth JD. Cytochrome P-450scc a review of the specificity and properties of the cholesterol binding site. Endocr Res 1986; 12:371-392.
121. Hall PF. Steroidogenic cytochromes P450: do the properties of the homogeneous enzymes reveal important aspects of the regulation of steroid synthesis in vivo? Endocr Res 1984; 10:311-317.
122. Stocco DM, Sodeman TC. The 30-kDa mitochondrial proteins induced by hormone stimulation in MA-10 mouse Leydig tumor cells are processed from larger precursors. J Biol Chem 1991; 266:19731-19738.
123. Clark BJ, Wells J, King SR, Stocco DM. The purification, cloning, and expression of a novel luteinizing hormone-induced mitochondrial protein in MA-10 mouse Leydig

tumor cells. Characterization of the steroidogenic acute regulatory protein (StAR). J Biol Chem 1994; 269:28314-28322.
124. Young JM, McNeilly AS. Theca: the forgotten cell of the ovarian follicle. Reproduction 2010; 140:489-504.
125. Craig ZR, Wang W, Flaws JA. Endocrine-disrupting chemicals in ovarian function: effects on steroidogenesis, metabolism and nuclear receptor signaling. Reproduction 2011; 142:633-646.
126. Payne AH, Hales DB. Overview of steroidogenic enzymes in the pathway from cholesterol to active steroid hormones. Endocr Rev 2004; 25:947-970.
127. Pikuleva IA. Cholesterol-metabolizing cytochromes P450. Drug Metab Dispos 2006; 34:513-520.
128. Miller WL. Steroidogenic enzymes. Endocr Dev 2008; 13:1-18.
129. Hedin L, Rodgers RJ, Simpson ER, Richards JS. Changes in content of cytochrome P450(17)alpha, cytochrome P450scc, and 3-hydroxy-3-methylglutaryl CoA reductase in developing rat ovarian follicles and corpora lutea: correlation with theca cell steroidogenesis. Biol Reprod 1987; 37:211-223.
130. Sasano H, Mason JI, Sasano N. Immunohistochemical analysis of cytochrome P-450 17 alpha-hydroxylase in pig adrenal cortex, testis and ovary. Mol Cell Endocrinol 1989; 62:197-202.
131. Patel SS, Beshay VE, Escobar JC, Carr BR. 17alpha-Hydroxylase (CYP17) expression and subsequent androstenedione production in the human ovary. Reprod Sci 2010; 17:978-986.
132. Stocco C. Aromatase expression in the ovary: hormonal and molecular regulation. Steroids 2008; 73:473-487.
133. Zlotkin T, Farkash Y, Orly J. Cell-specific expression of immunoreactive cholesterol side-chain cleavage cytochrome P-450 during follicular development in the rat ovary. Endocrinology 1986; 119:2809-2820.
134. Goldring NB, Durica JM, Lifka J, Hedin L, Ratoosh SL, Miller WL, Orly J, Richards JS. Cholesterol side-chain cleavage P450 messenger ribonucleic acid: evidence for hormonal regulation in rat ovarian follicles and constitutive expression in corpora lutea. Endocrinology 1987; 120:1942-1950.
135. Goldschmit D, Kraicer P, Orly J. Periovulatory expression of cholesterol side-chain cleavage cytochrome P-450 in cumulus cells. Endocrinology 1989; 124:369-378.
136. Zuber MX, John ME, Okamura T, Simpson ER, Waterman MR. Bovine adrenocortical cytochrome P-450(17 alpha). Regulation of gene expression by ACTH and elucidation of primary sequence. J Biol Chem 1986; 261:2475-2482.
137. Pelletier G, Dupont E, Simard J, Luu-The V, Belanger A, Labrie F. Ontogeny and subcellular localization of 3 beta-hydroxysteroid dehydrogenase (3 beta-HSD) in the human and rat adrenal, ovary and testis. J Steroid Biochem Mol Biol 1992; 43:451-467.
138. Stocco DM. StAR protein and the regulation of steroid hormone biosynthesis. Annu Rev Physiol 2001; 63:193-213.
139. Marsh JM, Savard K. The stimulation of progesterone synthesis in bovine corpora lutea by adenosine 3',5'-monophosphate. Steroids 1966; 8:133-148.
140. Marsh JM. The stimulatory effect of luteinizing hormone on adenyl cyclase in the bovine corpus luteum. J Biol Chem 1970; 245:1596-1603.
141. Leung PC, Steele GL. Intracellular signaling in the gonads. Endocr Rev 1992; 13:476-498.
142. Davis JS. Mechanisms of hormone action: luteinizing hormone receptors and second-messenger pathways. Curr Opin Obstet Gynecol 1994; 6:254-261.
143. Strauss JF, 3rd, Kallen CB, Christenson LK, Watari H, Devoto L, Arakane F, Kiriakidou M, Sugawara T. The steroidogenic acute regulatory protein (StAR): a window into the complexities of intracellular cholesterol trafficking. Recent Prog Horm Res 1999; 54:369-394; discussion 394-365.

144. Clark BJ, Ranganathan V, Combs R. Steroidogenic acute regulatory protein expression is dependent upon post-translational effects of cAMP-dependent protein kinase A. Mol Cell Endocrinol 2001; 173:183-192.
145. Sugawara T, Holt JA, Driscoll D, Strauss JF, 3rd, Lin D, Miller WL, Patterson D, Clancy KP, Hart IM, Clark BJ, et al. Human steroidogenic acute regulatory protein: functional activity in COS-1 cells, tissue-specific expression, and mapping of the structural gene to 8p11.2 and a pseudogene to chromosome 13. Proc Natl Acad Sci U S A 1995; 92:4778-4782.
146. Skalhegg BS, Tasken K. Specificity in the cAMP/PKA signaling pathway. Differential expression,regulation, and subcellular localization of subunits of PKA. Front Biosci 2000; 5:D678-693.
147. Beebe SJ, Oyen O, Sandberg M, Froysa A, Hansson V, Jahnsen T. Molecular cloning of a tissue-specific protein kinase (C gamma) from human testis--representing a third isoform for the catalytic subunit of cAMP-dependent protein kinase. Mol Endocrinol 1990; 4:465-475.
148. Manna PR, Wang XJ, Stocco DM. Involvement of multiple transcription factors in the regulation of steroidogenic acute regulatory protein gene expression. Steroids 2003; 68:1125-1134.
149. Tremblay JJ, Hamel F, Viger RS. Protein kinase A-dependent cooperation between GATA and CCAAT/enhancer-binding protein transcription factors regulates steroidogenic acute regulatory protein promoter activity. Endocrinology 2002; 143:3935-3945.
150. Carr DW, Stofko-Hahn RE, Fraser ID, Cone RD, Scott JD. Localization of the cAMP-dependent protein kinase to the postsynaptic densities by A-kinase anchoring proteins. Characterization of AKAP 79. J Biol Chem 1992; 267:16816-16823.
151. Trendelenburg G, Hummel M, Riecken EO, Hanski C. Molecular characterization of AKAP149, a novel A kinase anchor protein with a KH domain. Biochem Biophys Res Commun 1996; 225:313-319.
152. Feliciello A, Rubin CS, Avvedimento EV, Gottesman ME. Expression of a kinase anchor protein 121 is regulated by hormones in thyroid and testicular germ cells. J Biol Chem 1998; 273:23361-23366.
153. Affaitati A, Cardone L, de Cristofaro T, Carlucci A, Ginsberg MD, Varrone S, Gottesman ME, Avvedimento EV, Feliciello A. Essential role of A-kinase anchor protein 121 for cAMP signaling to mitochondria. J Biol Chem 2003; 278:4286-4294.
154. Ginsberg MD, Feliciello A, Jones JK, Avvedimento EV, Gottesman ME. PKA-dependent binding of mRNA to the mitochondrial AKAP121 protein. J Mol Biol 2003; 327:885-897.
155. Ranganathan G, Pokrovskaya I, Ranganathan S, Kern PA. Role of A kinase anchor proteins in the tissue-specific regulation of lipoprotein lipase. Mol Endocrinol 2005; 19:2527-2534.
156. Livigni A, Scorziello A, Agnese S, Adornetto A, Carlucci A, Garbi C, Castaldo I, Annunziato L, Avvedimento EV, Feliciello A. Mitochondrial AKAP121 links cAMP and src signaling to oxidative metabolism. Mol Biol Cell 2006; 17:263-271.
157. Newhall KJ, Criniti AR, Cheah CS, Smith KC, Kafer KE, Burkart AD, McKnight GS. Dynamic anchoring of PKA is essential during oocyte maturation. Curr Biol 2006; 16:321-327.
158. Dyson MT, Jones JK, Kowalewski MP, Manna PR, Alonso M, Gottesman ME, Stocco DM. Mitochondrial A-kinase anchoring protein 121 binds type II protein kinase A and enhances steroidogenic acute regulatory protein-mediated steroidogenesis in MA-10 mouse leydig tumor cells. Biol Reprod 2008; 78:267-277.
159. Bock P. [Peroxisomes in the mouse ovary]. Z Zellforsch Mikrosk Anat 1972; 133:131-140.
160. Novikoff AB, Novikoff PM. Microperoxisomes. J Histochem Cytochem 1973; 21:963-966.

161. Singh D, Pandey RS. Changes in catalase activity and hydrogen peroxide level in rat ovary during estrous cycle and induction of catalase in rat ovary by estradiol-17 beta. Indian J Exp Biol 1998; 36:421-423.
162. Peterson SL, Stevenson PM. Changes in catalase activity and concentration during ovarian development and differentiation. Biochim Biophys Acta 1992; 1135:207-214.
163. Neill JD, Smith MS. Pituitary-ovarian interrelationships in the rat. Curr Top Exp Endocrinol 1974; 2:73-106.
164. Enders AC, Nelson DM. Pinocytotic activity of the uterus of the rat. Am J Anat 1973; 138:277-299.
165. Behl R, Pandey RS. FSH induced stimulation of catalase activity in goat granulosa cells in vitro. Anim Reprod Sci 2002; 70:215-221.
166. Miller WL, Auchus RJ. The molecular biology, biochemistry, and physiology of human steroidogenesis and its disorders. Endocr Rev 2011; 32:81-151.
167. Hogenboom S, Tuyp JJ, Espeel M, Koster J, Wanders RJ, Waterham HR. Phosphomevalonate kinase is a cytosolic protein in humans. J Lipid Res 2004; 45:697-705.
168. Hogenboom S, Tuyp JJ, Espeel M, Koster J, Wanders RJ, Waterham HR. Mevalonate kinase is a cytosolic enzyme in humans. J Cell Sci 2004; 117:631-639.
169. Gallegos AM, Atshaves BP, Storey SM, Starodub O, Petrescu AD, Huang H, McIntosh AL, Martin GG, Chao H, Kier AB, Schroeder F. Gene structure, intracellular localization, and functional roles of sterol carrier protein-2. Prog Lipid Res 2001; 40:498-563.
170. van Noort M, Rommerts FF, van Amerongen A, Wirtz KW. Intracellular redistribution of SCP2 in Leydig cells after hormonal stimulation may contribute to increased pregnenolone production. Biochem Biophys Res Commun 1988; 154:60-65.
171. Moeller G, Adamski J. Integrated view on 17beta-hydroxysteroid dehydrogenases. Mol Cell Endocrinol 2009; 301:7-19.
172. Moeller G, Adamski J. Multifunctionality of human 17beta-hydroxysteroid dehydrogenases. Mol Cell Endocrinol 2006; 248:47-55.
173. Adamski J, Husen B, Marks F, Jungblut PW. Purification and properties of oestradiol 17 beta-dehydrogenase extracted from cytoplasmic vesicles of porcine endometrial cells. Biochem J 1992; 288 (Pt 2):375-381.
174. Adamski J, Carstensen J, Husen B, Kaufmann M, de Launoit Y, Leenders F, Markus M, Jungblut PW. New 17 beta-hydroxysteroid dehydrogenases. Molecular and cell biology of the type IV porcine and human enzymes. Ann N Y Acad Sci 1996; 784:124-136.
175. Grabenbauer M, Fahimi HD, Baumgart E. Detection of peroxisomal proteins and their mRNAs in serial sections of fetal and newborn mouse organs. J Histochem Cytochem 2001; 49:155-164.
176. Kananen K, Markkula M, Rainio E, Su JG, Hsueh AJ, Huhtaniemi IT. Gonadal tumorigenesis in transgenic mice bearing the mouse inhibin alpha-subunit promoter/simian virus T-antigen fusion gene: characterization of ovarian tumors and establishment of gonadotropin-responsive granulosa cell lines. Mol Endocrinol 1995; 9:616-627.
177. Vijayan V, Baumgart-Vogt E, Naidu S, Qian G, Immenschuh S. Bruton's tyrosine kinase is required for TLR-dependent heme oxygenase-1 gene activation via Nrf2 in macrophages. J Immunol 2011; 187:817-827.
178. Bradford MM. A rapid and sensitive method for the quantitation of microgram quantities of protein utilizing the principle of protein-dye binding. Anal Biochem 1976; 72:248-254.
179. Wang W. A-kinase anchoring proteins AKAP1, -4, -10 and -11 with different subcellular localizations in Sertoli cells and their roles in male fertility. Justus-Liebig-Universität Gießen; 2016.
180. Peters H. The development of the mouse ovary from birth to maturity. Acta Endocrinol (Copenh) 1969; 62:98-116.

181. Havelock JC, Rainey WE, Carr BR. Ovarian granulosa cell lines. Mol Cell Endocrinol 2004; 228:67-78.
182. Terpe K. Overview of tag protein fusions: from molecular and biochemical fundamentals to commercial systems. Appl Microbiol Biotechnol 2003; 60:523-533.
183. Stocco DM, Wells J, Clark BJ. The effects of hydrogen peroxide on steroidogenesis in mouse Leydig tumor cells. Endocrinology 1993; 133:2827-2832.
184. McCord JM, Keele BB, Jr., Fridovich I. An enzyme-based theory of obligate anaerobiosis: the physiological function of superoxide dismutase. Proc Natl Acad Sci U S A 1971; 68:1024-1027.
185. Diemer T, Allen JA, Hales KH, Hales DB. Reactive oxygen disrupts mitochondria in MA-10 tumor Leydig cells and inhibits steroidogenic acute regulatory (StAR) protein and steroidogenesis. Endocrinology 2003; 144:2882-2891.
186. El Mouatassim S, Guerin P, Menezo Y. Expression of genes encoding antioxidant enzymes in human and mouse oocytes during the final stages of maturation. Mol Hum Reprod 1999; 5:720-725.
187. Roels F, K Dherde, Vamecq J, Kerckaert I, Dacremont G. Peroxisomes in oocytes. Histochemistry and Cytochemistry. In: Proceedings of the Xth International Congress,Kyoto, Japan; 1996.
188. Harvey MB, Arcellana-Panlilio MY, Zhang X, Schultz GA, Watson AJ. Expression of genes encoding antioxidant enzymes in preimplantation mouse and cow embryos and primary bovine oviduct cultures employed for embryo coculture. Biol Reprod 1995; 53:532-540.
189. Figueroa C, Kawada ME, Veliz LP, Hidalgo U, Barros C, Gonzalez S, Santos MJ. Peroxisomal proteins in rat gametes. Cell Biochem Biophys 2000; 32 Spring:259-268.
190. Grant P, Ahlemeyer B, Karnati S, Berg T, Stelzig I, Nenicu A, Kuchelmeister K, Crane DI, Baumgart-Vogt E. The biogenesis protein PEX14 is an optimal marker for the identification and localization of peroxisomes in different cell types, tissues, and species in morphological studies. Histochem Cell Biol 2013; 140:423-442.
191. Distler E. Peroxisomen im murinen Ovar. Justus-Liebig-Universität Gießen,Germany.; 2015. Doctor thesis.
192. Agarwal A, Allamaneni SS. Role of free radicals in female reproductive diseases and assisted reproduction. Reprod Biomed Online 2004; 9:338-347.
193. Agarwal A, Aponte-Mellado A, Premkumar BJ, Shaman A, Gupta S. The effects of oxidative stress on female reproduction: a review. Reprod Biol Endocrinol 2012; 10:49.
194. Kumar NM, Gilula NB. The gap junction communication channel. Cell 1996; 84:381-388.
195. Beyer EC. Gap junctions. Int Rev Cytol 1993; 137C:1-37.
196. Eppig JJ. Intercommunication between mammalian oocytes and companion somatic cells. Bioessays 1991; 13:569-574.
197. Taniguchi Ishikawa E, Gonzalez-Nieto D, Ghiaur G, Dunn SK, Ficker AM, Murali B, Madhu M, Gutstein DE, Fishman GI, Barrio LC, Cancelas JA. Connexin-43 prevents hematopoietic stem cell senescence through transfer of reactive oxygen species to bone marrow stromal cells. Proc Natl Acad Sci U S A 2012; 109:9071-9076.
198. Parshad RK, Guraya SS. Changes in catalase activity during follicular growth, atresia and luteinization in rat ovary. Indian J Exp Biol 1993; 31:109-111.
199. Fortune JE. Ovarian follicular growth and development in mammals. Biol Reprod 1994; 50:225-232.
200. Klinken SP, Stevenson PM. Changes in enzyme activities during the artificially stimulated transition from follicular to luteal cell types in rat ovary. Eur J Biochem 1977; 81:327-332.
201. Russo JJ, Black VH. Hormone-dependent changes in peroxisomal enzyme activity in guinea pig adrenal. J Biol Chem 1982; 257:3883-3889.

202. Tuckey RC, Kostadinovic Z, Stevenson PM. Ferredoxin and cytochrome P-450scc concentrations in granulosa cells of porcine ovaries during follicular cell growth and luteinization. J Steroid Biochem 1988; 31:201-205.
203. Sligar SG, Lipscomb JD, Debrunner PG, Gunsalus IC. Superoxide anion production by the autoxidation of cytochrome P450cam. Biochem Biophys Res Commun 1974; 61:290-296.
204. Goda K, Chu J, Kimura T, Schaap AP. Cytochrome c enhancement of singlet molecular oxygen production by the NADPH-dependent adrenodoxin reductase-adrenodoxin system: the role of singlet oxygen in damaging adrenal mitochondrial membranes. Biochem Biophys Res Commun 1973; 52:1300-1306.
205. Weisiger RA, Fridovich I. Mitochondrial superoxide simutase. Site of synthesis and intramitochondrial localization. J Biol Chem 1973; 248:4793-4796.
206. Mills GC. Hemoglobin catabolism. I. Glutathione peroxidase, an erythrocyte enzyme which protects hemoglobin from oxidative breakdown. J Biol Chem 1957; 229:189-197.
207. Meister A, Anderson ME. Glutathione. Annu Rev Biochem 1983; 52:711-760.
208. Combelles CM, Holick EA, Paolella LJ, Walker DC, Wu Q. Profiling of superoxide dismutase isoenzymes in compartments of the developing bovine antral follicles. Reproduction 2010; 139:871-881.
209. El-Shahat KH, Kandil M. Antioxidant capacity of follicular fluid in relation to follicular size and stage of estrous cycle in buffaloes. Theriogenology 2012; 77:1513-1518.
210. Basini G, Simona B, Santini SE, Grasselli F. Reactive oxygen species and anti-oxidant defences in swine follicular fluids. Reprod Fertil Dev 2008; 20:269-274.
211. Sabatini L, Wilson C, Lower A, Al-Shawaf T, Grudzinskas JG. Superoxide dismutase activity in human follicular fluid after controlled ovarian hyperstimulation in women undergoing in vitro fertilization. Fertil Steril 1999; 72:1027-1034.
212. Miyazaki T, Sueoka K, Dharmarajan AM, Atlas SJ, Bulkley GB, Wallach EE. Effect of inhibition of oxygen free radical on ovulation and progesterone production by the in-vitro perfused rabbit ovary. J Reprod Fertil 1991; 91:207-212.
213. Shkolnik K, Tadmor A, Ben-Dor S, Nevo N, Galiani D, Dekel N. Reactive oxygen species are indispensable in ovulation. Proc Natl Acad Sci U S A 2011; 108:1462-1467.
214. Covarrubias L, Hernandez-Garcia D, Schnabel D, Salas-Vidal E, Castro-Obregon S. Function of reactive oxygen species during animal development: passive or active? Dev Biol 2008; 320:1-11.
215. Prates EG, Alves SP, Marques CC, Baptista MC, Horta AE, Bessa RJ, Pereira RM. Fatty acid composition of porcine cumulus oocyte complexes (COC) during maturation: effect of the lipid modulators trans-10, cis-12 conjugated linoleic acid (t10,c12 CLA) and forskolin. In Vitro Cell Dev Biol Anim 2013; 49:335-345.
216. Homa ST, Racowsky C, McGaughey RW. Lipid analysis of immature pig oocytes. J Reprod Fertil 1986; 77:425-434.
217. Nagan N, Zoeller RA. Plasmalogens: biosynthesis and functions. Prog Lipid Res 2001; 40:199-229.
218. McEvoy TG, Coull GD, Broadbent PJ, Hutchinson JS, Speake BK. Fatty acid composition of lipids in immature cattle, pig and sheep oocytes with intact zona pellucida. J Reprod Fertil 2000; 118:163-170.
219. Prates EG, Nunes JT, Pereira RM. A role of lipid metabolism during cumulus-oocyte complex maturation: impact of lipid modulators to improve embryo production. Mediators Inflamm 2014; 2014:692067.
220. Aardema H, Vos PL, Lolicato F, Roelen BA, Knijn HM, Vaandrager AB, Helms JB, Gadella BM. Oleic acid prevents detrimental effects of saturated fatty acids on bovine oocyte developmental competence. Biol Reprod 2011; 85:62-69.
221. Sturmey RG, O'Toole PJ, Leese HJ. Fluorescence resonance energy transfer analysis of mitochondrial:lipid association in the porcine oocyte. Reproduction 2006; 132:829-837.

222. Wu LL, Dunning KR, Yang X, Russell DL, Lane M, Norman RJ, Robker RL. High-fat diet causes lipotoxicity responses in cumulus-oocyte complexes and decreased fertilization rates. Endocrinology 2010; 151:5438-5445.
223. Dunning KR, Russell DL, Robker RL. Lipids and oocyte developmental competence: the role of fatty acids and beta-oxidation. Reproduction 2014; 148:R15-27.
224. Ami D, Mereghetti P, Natalello A, Doglia SM, Zanoni M, Redi CA, Monti M. FTIR spectral signatures of mouse antral oocytes: molecular markers of oocyte maturation and developmental competence. Biochim Biophys Acta 2011; 1813:1220-1229.
225. Dunning KR, Cashman K, Russell DL, Thompson JG, Norman RJ, Robker RL. Beta-oxidation is essential for mouse oocyte developmental competence and early embryo development. Biol Reprod 2010; 83:909-918.
226. Jorritsma R, Cesar ML, Hermans JT, Kruitwagen CL, Vos PL, Kruip TA. Effects of non-esterified fatty acids on bovine granulosa cells and developmental potential of oocytes in vitro. Anim Reprod Sci 2004; 81:225-235.
227. Marei WF, Wathes DC, Fouladi-Nashta AA. The effect of linolenic Acid on bovine oocyte maturation and development. Biol Reprod 2009; 81:1064-1072.
228. Marei WF, Wathes DC, Fouladi-Nashta AA. Impact of linoleic acid on bovine oocyte maturation and embryo development. Reproduction 2010; 139:979-988.
229. Pierce SB, Walsh T, Chisholm KM, Lee MK, Thornton AM, Fiumara A, Opitz JM, Levy-Lahad E, Klevit RE, King MC. Mutations in the DBP-deficiency protein HSD17B4 cause ovarian dysgenesis, hearing loss, and ataxia of Perrault Syndrome. Am J Hum Genet 2010; 87:282-288.
230. Leenders F, Dolez V, Begue A, Moller G, Gloeckner JC, de Launoit Y, Adamski J. Structure of the gene for the human 17beta-hydroxysteroid dehydrogenase type IV. Mamm Genome 1998; 9:1036-1041.
231. van Grunsven EG, van Berkel E, Ijlst L, Vreken P, de Klerk JB, Adamski J, Lemonde H, Clayton PT, Cuebas DA, Wanders RJ. Peroxisomal D-hydroxyacyl-CoA dehydrogenase deficiency: resolution of the enzyme defect and its molecular basis in bifunctional protein deficiency. Proc Natl Acad Sci U S A 1998; 95:2128-2133.
232. Sanders SL, Stouffer RL. Localization of steroidogenic enzymes in macaque luteal tissue during the menstrual cycle and simulated early pregnancy: immunohistochemical evidence supporting the two-cell model for estrogen production in the primate corpus luteum. Biol Reprod 1997; 56:1077-1087.
233. Faust PL, Kovacs WJ. Cholesterol biosynthesis and ER stress in peroxisome deficiency. Biochimie 2014; 98:75-85.
234. Magalhaes MM, Magalhaes MC. Peroxisomes in adrenal steroidogenesis. Microsc Res Tech 1997; 36:493-502.
235. Keller GA, Scallen TJ, Clarke D, Maher PA, Krisans SK, Singer SJ. Subcellular localization of sterol carrier protein-2 in rat hepatocytes: its primary localization to peroxisomes. J Cell Biol 1989; 108:1353-1361.
236. Mendis-Handagama SM, Watkins PA, Gelber SJ, Scallen TJ, Zirkin BR, Ewing LL. Luteinizing hormone causes rapid and transient changes in rat Leydig cell peroxisome volume and intraperoxisomal sterol carrier protein-2 content. Endocrinology 1990; 127:2947-2954.
237. van Amerongen A, van Noort M, van Beckhoven JR, Rommerts FF, Orly J, Wirtz KW. The subcellular distribution of the nonspecific lipid transfer protein (sterol carrier protein 2) in rat liver and adrenal gland. Biochim Biophys Acta 1989; 1001:243-248.
238. Chanderbhan R, Noland BJ, Scallen TJ, Vahouny GV. Sterol carrier protein2. Delivery of cholesterol from adrenal lipid droplets to mitochondria for pregnenolone synthesis. J Biol Chem 1982; 257:8928-8934.
239. Reinhart MP. Intracellular sterol trafficking. Experientia 1990; 46:599-611.
240. Rueckert DG, Schmidt K. Lipid transfer proteins. Chem Phys Lipids 1990; 56:1-20.
241. Vahouny GV, Chanderbhan R, Kharroubi A, Noland BJ, Pastuszyn A, Scallen TJ. Sterol carrier and lipid transfer proteins. Adv Lipid Res 1987; 22:83-113.

242. Wirtz KW, Snoek GT, Gadella TW, van Paridon PA, Somerharju PJ. Properties and possible function of phosphatidylinositol-transfer proteins. Biotechnol Appl Biochem 1990; 12:485-488.
243. Chanderbhan R, Tanaka T, Strauss JF, Irwin D, Noland BJ, Scallen TJ, Vahouny GV. Evidence for sterol carrier protein2-like activity in hepatic, adrenal and ovarian cytosol. Biochem Biophys Res Commun 1983; 117:702-709.
244. Rennert H, Amsterdam A, Billheimer JT, Strauss JF, 3rd. Regulated expression of sterol carrier protein 2 in the ovary: a key role for cyclic AMP. Biochemistry 1991; 30:11280-11285.
245. Trzeciak WH, Simpson ER, Scallen TJ, Vahouny GV, Waterman MR. Studies on the synthesis of sterol carrier protein-2 in rat adrenocortical cells in monolayer culture. Regulation by ACTH and dibutyryl cyclic 3',5'-AMP. J Biol Chem 1987; 262:3713-3717.
246. Magalhaes MC, Magalhaes MM. Ultrastructural alterations produced in rat adrenal by aminoglutethimide. A stereologic and cytochemical study. Endocrinology 1972; 90:444-452.
247. Mazzocchi G, Robba C, Rebuffat P, Belloni AS, Nussdorfer GG. Effects of the hypolipidemic drug nafenopin on the zona fasciculata of the rat adrenal cortex: a correlated biochemical and stereological study. Anat Rec 1982; 204:245-254.
248. Mazzocchi G, Rebuffat P, Belloni AS, Gottardo G, Meneghelli V, Nussdorfer GG. Effects of mevinolin, an inhibitor of cholesterol synthesis, on the morphological and functional responses of rat adrenal zona fasciculata to a prolonged treatment with 4-aminopyrazolo-pyrimidine. Anat Rec 1988; 221:700-706.
249. Hikim AP, Amador AG, Bartke A, Russell LD. Structure/function relationships in active and inactive hamster Leydig cells: a correlative morphometric and endocrine study. Endocrinology 1989; 125:1844-1856.
250. Mendis-Handagama SM, Zirkin BR, Ewing LL. Comparison of components of the testis interstitium with testosterone secretion in hamster, rat, and guinea pig testes perfused in vitro. Am J Anat 1988; 181:12-22.
251. Rapoport R, Sklan D, Wolfenson D, Shaham-Albalancy A, Hanukoglu I. Antioxidant capacity is correlated with steroidogenic status of the corpus luteum during the bovine estrous cycle. Biochim Biophys Acta 1998; 1380:133-140.
252. Black VH, Russo JJ. Stereological analysis of the guinea pig adrenal: effects of dexamethasone and ACTH treatment with emphasis on the inner cortex. Am J Anat 1980; 159:85-120.
253. Chu JW, Kimura T. Studies on adrenal steroid hydroxylases. Complex formation of the hydroxylase components. J Biol Chem 1973; 248:5183-5187.
254. Tuckey RC, Kamin H. The oxyferro complex of adrenal cytochrome P-450scc. Effect of cholesterol and intermediates on its stability and optical characteristics. J Biol Chem 1982; 257:9309-9314.
255. Sugino N, Takiguchi S, Kashida S, Karube A, Nakamura Y, Kato H. Superoxide dismutase expression in the human corpus luteum during the menstrual cycle and in early pregnancy. Mol Hum Reprod 2000; 6:19-25.
256. Keller GA, Warner TG, Steimer KS, Hallewell RA. Cu,Zn superoxide dismutase is a peroxisomal enzyme in human fibroblasts and hepatoma cells. Proc Natl Acad Sci U S A 1991; 88:7381-7385.
257. Singh AK, Dobashi K, Gupta MP, Asayama K, Singh I, Orak JK. Manganese superoxide dismutase in rat liver peroxisomes: biochemical and immunochemical evidence. Mol Cell Biochem 1999; 197:7-12.
258. Karnati S, Luers G, Pfreimer S, Baumgart-Vogt E. Mammalian SOD2 is exclusively located in mitochondria and not present in peroxisomes. Histochem Cell Biol 2013; 140:105-117.
259. Brites P, Motley AM, Gressens P, Mooyer PA, Ploegaert I, Everts V, Evrard P, Carmeliet P, Dewerchin M, Schoonjans L, Duran M, Waterham HR, et al. Impaired

neuronal migration and endochondral ossification in Pex7 knockout mice: a model for rhizomelic chondrodysplasia punctata. Hum Mol Genet 2003; 12:2255-2267.
260. Sheikh FG, Pahan K, Khan M, Barbosa E, Singh I. Abnormality in catalase import into peroxisomes leads to severe neurological disorder. Proc Natl Acad Sci U S A 1998; 95:2961-2966.
261. Baumgart E, Fahimi HD, Steininger H, Grabenbauer M. A review of morphological techniques for detection of peroxisomal (and mitochondrial) proteins and their corresponding mRNAs during ontogenesis in mice: application to the PEX5-knockout mouse with Zellweger syndrome. Microsc Res Tech 2003; 61:121-138.
262. Baumgart E, Vanhorebeek I, Grabenbauer M, Borgers M, Declercq PE, Fahimi HD, Baes M. Mitochondrial alterations caused by defective peroxisomal biogenesis in a mouse model for Zellweger syndrome (PEX5 knockout mouse). Am J Pathol 2001; 159:1477-1494.
263. Scott JD, Stofko RE, McDonald JR, Comer JD, Vitalis EA, Mangili JA. Type II regulatory subunit dimerization determines the subcellular localization of the cAMP-dependent protein kinase. J Biol Chem 1990; 265:21561-21566.
264. Dessauer CW. Adenylyl cyclase--A-kinase anchoring protein complexes: the next dimension in cAMP signaling. Mol Pharmacol 2009; 76:935-941.
265. Carr DW, Stofko-Hahn RE, Fraser ID, Bishop SM, Acott TS, Brennan RG, Scott JD. Interaction of the regulatory subunit (RII) of cAMP-dependent protein kinase with RII-anchoring proteins occurs through an amphipathic helix binding motif. J Biol Chem 1991; 266:14188-14192.
266. Bauman AL, Soughayer J, Nguyen BT, Willoughby D, Carnegie GK, Wong W, Hoshi N, Langeberg LK, Cooper DM, Dessauer CW, Scott JD. Dynamic regulation of cAMP synthesis through anchored PKA-adenylyl cyclase V/VI complexes. Mol Cell 2006; 23:925-931.
267. Smith FD, Reichow SL, Esseltine JL, Shi D, Langeberg LK, Scott JD, Gonen T. Intrinsic disorder within an AKAP-protein kinase A complex guides local substrate phosphorylation. Elife 2013; 2:e01319.
268. Li W, Amri H, Huang H, Wu C, Papadopoulos V. Gene and protein profiling of the response of MA-10 Leydig tumor cells to human chorionic gonadotropin. J Androl 2004; 25:900-913.
269. King SR, Stocco DM. ATP and a mitochondrial electrochemical gradient are required for functional activity of the steroidogenic acute regulatory (StAR) protein in isolated mitochondria. Endocr Res 1996; 22:505-514.
270. Brigelius-Flohe R, Muller C, Menard J, Florian S, Schmehl K, Wingler K. Functions of GI-GPx: lessons from selenium-dependent expression and intracellular localization. Biofactors 2001; 14:101-106.
271. Forman HJ, Torres M. Reactive oxygen species and cell signaling: respiratory burst in macrophage signaling. Am J Respir Crit Care Med 2002; 166:S4-8.
272. Li Q, Sanlioglu S, Li S, Ritchie T, Oberley L, Engelhardt JF. GPx-1 gene delivery modulates NFkappaB activation following diverse environmental injuries through a specific subunit of the IKK complex. Antioxid Redox Signal 2001; 3:415-432.
273. Fridovich I. Superoxide radical and superoxide dismutases. Annu Rev Biochem 1995; 64:97-112.
274. Al-Gubory KH, Fowler PA, Garrel C. The roles of cellular reactive oxygen species, oxidative stress and antioxidants in pregnancy outcomes. Int J Biochem Cell Biol 2010; 42:1634-1650.
275. Agarwal A, Gupta S, Sekhon L, Shah R. Redox considerations in female reproductive function and assisted reproduction: from molecular mechanisms to health implications. Antioxid Redox Signal 2008; 10:1375-1403.
276. Guerin P, El Mouatassim S, Menezo Y. Oxidative stress and protection against reactive oxygen species in the pre-implantation embryo and its surroundings. Hum Reprod Update 2001; 7:175-189.

277. Ruder EH, Hartman TJ, Blumberg J, Goldman MB. Oxidative stress and antioxidants: exposure and impact on female fertility. Hum Reprod Update 2008; 14:345-357.
278. Sabuncu T, Vural H, Harma M, Harma M. Oxidative stress in polycystic ovary syndrome and its contribution to the risk of cardiovascular disease. Clin Biochem 2001; 34:407-413.
279. Behrman HR, Aten RF. Evidence that hydrogen peroxide blocks hormone-sensitive cholesterol transport into mitochondria of rat luteal cells. Endocrinology 1991; 128:2958-2966.
280. Behrman HR, Preston SL. Luteolytic actions of peroxide in rat ovarian cells. Endocrinology 1989; 124:2895-2900.
281. Endo T, Aten RF, Leykin L, Behrman HR. Hydrogen peroxide evokes antisteroidogenic and antigonadotropic actions in human granulosa luteal cells. J Clin Endocrinol Metab 1993; 76:337-342.
282. Tsai SC, Lu CC, Lin CS, Wang PS. Antisteroidogenic actions of hydrogen peroxide on rat Leydig cells. J Cell Biochem 2003; 90:1276-1286.
283. Artemenko IP, Zhao D, Hales DB, Hales KH, Jefcoate CR. Mitochondrial processing of newly synthesized steroidogenic acute regulatory protein (StAR), but not total StAR, mediates cholesterol transfer to cytochrome P450 side chain cleavage enzyme in adrenal cells. J Biol Chem 2001; 276:46583-46596.
284. Arakane F, Kallen CB, Watari H, Stayrook SE, Lewis M, Strauss JF, 3rd. Steroidogenic acute regulatory protein (StAR) acts on the outside of mitochondria to stimulate steroidogenesis. Endocr Res 1998; 24:463-468.
285. Clark BJ, Soo SC, Caron KM, Ikeda Y, Parker KL, Stocco DM. Hormonal and developmental regulation of the steroidogenic acute regulatory protein. Mol Endocrinol 1995; 9:1346-1355.
286. Burton GW, Joyce A, Ingold KU. Is vitamin E the only lipid-soluble, chain-breaking antioxidant in human blood plasma and erythrocyte membranes? Arch Biochem Biophys 1983; 221:281-290.
287. Burton GW. Vitamin E: molecular and biological function. Proc Nutr Soc 1994; 53:251-262.
288. Chow CK. Biological functions and metabolic fate of vitamin E revisited. J Biomed Sci 2004; 11:295-302.
289. Karanth S, Yu WH, Mastronardi CA, McCann SM. Vitamin E stimulates luteinizing hormone-releasing hormone and ascorbic acid release from medial basal hypothalami of adult male rats. Exp Biol Med (Maywood) 2003; 228:779-785.
290. Chen H, Liu J, Luo L, Baig MU, Kim JM, Zirkin BR. Vitamin E, aging and Leydig cell steroidogenesis. Exp Gerontol 2005; 40:728-736.
291. Sen Gupta R, Sen Gupta E, Dhakal BK, Thakur AR, Ahnn J. Vitamin C and vitamin E protect the rat testes from cadmium-induced reactive oxygen species. Mol Cells 2004; 17:132-139.
292. Senthil kumar J, Banudevi S, Sharmila M, Murugesan P, Srinivasan N, Balasubramanian K, Aruldhas MM, Arunakaran J. Effects of Vitamin C and E on PCB (Aroclor 1254) induced oxidative stress, androgen binding protein and lactate in rat Sertoli cells. Reprod Toxicol 2004; 19:201-208.
293. Murugesan P, Muthusamy T, Balasubramanian K, Arunakaran J. Studies on the protective role of vitamin C and E against polychlorinated biphenyl (Aroclor 1254)--induced oxidative damage in Leydig cells. Free Radic Res 2005; 39:1259-1272.

9 Index of abbreviation

ABCD	ATP-binding cassette
ACOX	Acyl-CoA oxidases
ALDP	Adrenoleukodystrophy protein
AGPS	Aalkyldihydroxyacetone phosphate synthase
AKAP	A-kinase anchoring protein
BMP	Bone morphogenetic protein
CREB	cAMP response-element binding protein
CL	Corpus luteum
cAMP	Adenylate cyclase/cyclic-AMP
CoA	coenzyme A
°C	Degree Celcius
DHPAT	Dihydroxyacetone phosphate acyltransferase
DHAP	Dihydroxyacetonephosphate
DHEA	Dehydroepiandrosterone
ER	Endoplasmic reticulum
EGF	Epidermal growth factor
FSH	Follicle-stimulating hormone
FPP	Farnesyl diphosphate
FBS	Fetal bovine serum
GDF-9	Growth differentiation factor-9
GNPAT	Glyceronephosphate O-acyltransferase
GR	Glutathione reductase
g	gram
hCG	Human chorionic gonadotropin
H2O2	Hydrogen peroxide
HMG-CoA	3-hydroxy-3-methylglutaryl coenzyme A reductase
HGF	Hepatocyte growth factor
HDL	High-density lipoprotein
HSD	hydroxysteroid dehydrogenase
h	Hour
IDI1	Isopentenyl diphosphate delta isomerase

IRD	Infantile Refsum disease
IGF-I	Insulin-like growth factor-I
IMM	Inner mitochondrial membrane
IF	immunofluorescence
KL	Kit ligand
KGF	Keratinocyte growth factor
LH	Luteinizing hormone
LDL	Low-density lipoprotein
MFPs	Multifunctional proteins
MVK	Mevalonate kinase
MPD	Mevalonate pyrophosphate decarboxylase
min	minute
NALD	Neonatal adrenoleukodystrophy
·NO	Nitric oxide
OMM	Outer mitochondrial membrane
O2·−	Superoxide anion
·OH	Hydroxyl radical
PMPs	Peroxisome membrane proteins
PTS	Peroxisomal targeting signals
PBD	Peroxisome biogenesis disorder
PFA	Paraformaldehyde
PKA	Protein kinase A
PMVK	Phosphomevalonate kinase
P450scc	cytochrome P450 side chain cleavage
qPCR	Quantitative real time polymerase chain reaction
RNS	Reactive nitrogen species
RCDP	Rhizomelic chondrodysplasia punctate
ROS	Reactive oxygen species
RT	Room temperature
RT-PCR	Semi-quantitative polymerase chain reaction
SCPx	Sterol carrier protein x
SOD	Superoxide dismutase
StAR	Steroidogenic acute regulatory protein

TGF	Transforming growth factor
VLCFAs	Very long chain fatty acids
ZS	Zellweger syndrome

.

10 Acknowledgements

Here, in this section, I would like to thank all the people who helped me during my PhD life in Justus Liebig University Giessen.

First of all, I would like to express my most sincere gratitude to my supervisor, Prof. Dr. Eveline Baumgart-Vogt. I couldn't manage to complete my PhD program without her help. Until now I can still remember how difficult everything was for me when I first came to Germany because my limited knowledge of molecular biology and my poor English. My professor treated me with great patience: she taught me the knowledge of cell biology and molecular biology, guided me to construct the subject of my thesis and helped me to establish my confidence in research and life. I was greatly encouraged and motivated under her help. My English level and scientific research capability were greatly improved during the past four years. Secondly, I would like to thank my post-doc Claudia Colasante. She is always the first person I turned to for help when I came across difficulties in experiments and projects. Dr. Claudia Colasante is always ready to help me without any hesitation. I would like also express my gratitude to my former colleague Lilit Kamalyan, who helped me a lot during my early time in this lab. My lab mates Natalia EI-Merie and Eistine Boateng, I have enjoyed the time spending with you two in the lab and in the spare times. Moreover, I am very grateful to Mrs. Elke Rodenberg-Frank, Mrs. Andrea Textor, PD Dr. Barbara Ahlemeyer, Mrs. Bianca Pfeiffer, Mrs. Petra Hahn-Kohlberger, Mrs. Susanne Pfreimer, Dr. Wieland Stöckmann, Dr. Klaus Peter Valerius and all colleagues in our lab and all staff at the Institute of Anatomy and Cell Biology II for their help and excellent technical assistance. Finally, thanks the China Scholarship Council (CSC) for funding me my PhD study, thanks also goes to PhD program of the Medical Faculty of the Justus Liebig University, Giessen for giving me this great opportunity to be a part of this prestigious educational program.

11 Curriculum Vitae

The curriculum vitae was removed from the electronic version of the paper.